



## AN ABSTRACT OF THE THESIS OF

Hayley A. Corson-Rikert for the degree of Master of Science in Water Resources Science presented on September 5, 2014

Title: Carbon Dynamics in the Hyporheic Zone of a Headwater Mountain Stream in the Cascade Mountains, Oregon

Abstract approved:

---

Steven M. Wondzell

Mary V. Santelmann

---

This study investigated carbon dynamics in the hyporheic zone of a steep, forested catchment in the Cascade Mountains of western Oregon, USA. Water samples were collected monthly from a headwater stream and well network during baseflow conditions from July to December 2013 and again in March 2014. We also sampled during one fall storm event, collecting pre-storm, rising leg, and extended high flow samples. The well network is located at the base of Watershed 1 (WS1) of the H.J. Andrews Experimental Forest and spans the full width of the floodplain (~14 m) along a 29 m reach of stream. We measured pH, temperature, water level, major anions, major cations, DOC, DIC, and total alkalinity. Flow paths, travel time to wells and hydraulic conductivity were available from previous studies.

During baseflow periods, hyporheic DOC decreased with median travel time through the subsurface. DIC concentrations increased with travel time, but the magnitude of this increase in DIC was too large to be explained by metabolism of stream water DOC. This suggests that there are additional sources of DIC and/or

DOC in the subsurface, and that hyporheic DIC concentrations are not well linked to stream-source DOC. The most likely supplemental sources of DIC to hyporheic water are soil CO<sub>2</sub> and microbial respiration of DOC leached from buried particulate organic matter and from overlying soils. Overall, the hyporheic zone appears to be a source of DIC to the stream.

In summer, the hyporheic zone is likely isolated from vertical infiltration or lateral inflow of soil water, and particulate organic carbon is not present in stream water. Thus, spatial patterns in hyporheic zone biogeochemistry must result from underlying spatial patterns in hyporheic flowpaths, groundwater inputs, and buried particulate organic carbon. With the transition to the rainy season throughout the fall and early winter, vertical infiltration and leaching of accumulated solutes from the overlying soil appear to become important sources of carbon that help explain patterns in hyporheic zone biogeochemistry.

During a small November storm event, DOC and nitrate concentrations in the stream displayed clockwise hysteresis. Travel time appeared to be associated with both nitrate and DOC response patterns in the hyporheic zone. In wells with long travel times, DOC and nitrate concentrations showed a clockwise hysteresis pattern that mimicked and even exceeded that observed in the stream. We hypothesize that these solutes were flushed from overlying soils into the hyporheic zone via vertically infiltrating rainwater. In wells with short travel times, we observed only a small peak in DOC and nitrate concentrations during the storm, potentially due to lateral infiltration of stream water later in the event.

Overall, temporal patterns in hyporheic solute chemistry during the November storm differed from patterns we observed in the well network. This suggests that whole-watershed processes that controlled stream water chemistry during this storm event were different than those that controlled solute concentrations in the hyporheic zone. Nonetheless, the hyporheic zone must have been linked to the stream. That measurements in our well network reveal a very different response between the stream and the hyporheic zone suggests that: 1) Our hyporheic zone is not representative of stream-hyporheic riparian processes that occur within the larger watershed, or 2) Hillslope-stream or within-stream processes dominate during storms, and at these times the influence of the hyporheic zone on the stream is much weaker than during baseflow.

During both baseflow and storm periods, the hydrology of the WS1 system is complex – hyporheic exchange flows follow extended, non-linear flow paths through a heterogeneous subsurface and may be augmented by lateral inflows of groundwater and, during storms, vertical infiltration of soil water. Our results from both baseflow and storm sampling suggest that a complex set of physical mechanisms and biogeochemical processes influence carbon transport and transformation within this hyporheic environment.

©Copyright by Hayley A. Corson-Rikert  
September 5, 2014  
All Rights Reserved

Carbon Dynamics in the Hyporheic Zone of a Headwater Mountain Stream  
in the Cascade Mountains, Oregon

by  
Hayley A. Corson-Rikert

A THESIS

submitted to

Oregon State University

in partial fulfillment of  
the requirements for the  
degree of

Master of Science

Presented September 5, 2014  
Commencement June 2015

Master of Science thesis of Hayley A. Corson-Rikert presented on September 5, 2014

APPROVED:

---

Co-Major Professor, representing Water Resources Science

---

Co-Major Professor, representing Water Resources Science

---

Director of the Water Resources Graduate Program

---

Dean of the Graduate School

I understand that my thesis will become part of the permanent collection of Oregon State University libraries. My signature below authorizes release of my thesis to any reader upon request.

---

Hayley A. Corson-Rikert, Author

## ACKNOWLEDGEMENTS

First and foremost, thank you to my advisors Steve Wondzell and Mary Santelmann for helping me to design and implement this project, for providing insight into my analysis of such a complex system, for pushing me to do my best work, and for being so enthusiastic about my data. Thank you, Steve, for introducing me to the H.J. Andrews Forest, for taking me on as a student so late in my first year, for meeting with me on a weekly basis, for being so accessible, and for helping me to become a more thorough and more advanced scientific writer and thinker. Thank you, Mary, for guiding me through the graduate school process from the very start, and for giving me such sound advice every time we met. Thank you to Roy Haggerty for taking the time on numerous occasions to discuss my data, for arranging meetings with visiting scientists, and for being so generous with his lab space and field equipment. Thank you to Lisa Ganio for spending many, many hours helping me to interpret my data and for providing me with invaluable guidance and assistance while I conducted my statistical analysis. I have been incredibly lucky to have such an involved, passionate, and helpful committee.

Thank you to Mark Schulze and Kathy Keable at the H.J. Andrews Experimental Forest for being so kind and for providing crucial field assistance. Thank you to the H.J Andrews research network for data support and for being so responsive to my many inquiries. I am honored to have had the chance to conduct research in such a beautiful setting and as part of a vibrant scientific community.

Thank you to Kathy Motter at the Oregon State University Institute for Water and Watersheds Collaboratory, for training me how to conduct the laboratory

analyses, for answering my endless questions, and for providing so much moral support.

Thank you to Roy Haggerty and Steve Wondzell for providing funding to make this research possible. Thank you to the Water Resources Graduate Program at Oregon State University for the opportunity to study water resources science, and for providing me with facilities in which to study and conduct research. Thank you to the graduate school for awarding me the Provost's Distinguished Fellowship, which allowed me to focus completely on courses and research in my first year. Thank you to the Pacific Northwest Research Station for the opportunity to conduct research at an U.S.F.S. Experimental Forest and Long Term Ecological Research site. Thank you to the Institute for Water and Watersheds for providing support for the IWW Collaboratory, which is an invaluable asset to graduate students at Oregon State University.

Thank you to WaterWorld for your unending support and camaraderie and for making PWOW and PWOTALP happen. Thank you to my family for being so loving and for encouraging me at every step. Thank you to Denis and Anne White for being my family away from home here in Corvallis and for showing so much interest in my research and life.

Most of all, thank you to Nick Dosch for helping me to sample every single time, even when it meant sampling in the rain, in the snow, and in the middle of the night. Thank you, also, for assisting me with lab work, for providing feedback at every stage, and for being incredibly supportive throughout this entire process. I could not have made it here without you.

## Table of Contents

	<u>Page</u>
1 Introduction.....	1
2 Carbon dynamics in the hyporheic zone of a headwater mountain stream in the Cascade Mountains, Oregon .....	4
2.1 Abstract.....	4
2.2 Introduction.....	4
2.3 Study site.....	7
2.4 Methods.....	10
2.4.1 Preparatory methods .....	10
2.4.2 Field methods .....	11
2.4.3 Laboratory methods .....	13
2.4.4 Calculations .....	15
2.4.5 Statistical methods .....	17
2.5 Results.....	19
2.5.1 Consistent biogeochemical patterns .....	19
2.5.2 Seasonal biogeochemical patterns .....	21
2.5.3 Spatial biogeochemical patterns .....	23
2.5.4 Model results .....	26
2.6 Discussion.....	31
2.6.1 Carbon dynamics as a function of median travel times.....	31
2.6.2 Modeled relationships.....	33
2.6.3 System considerations – Hydrologic sources of DOC and DIC.....	36
2.6.4 System considerations – Biogeochemical sources/sinks of DOC and DIC.....	41
2.6.5 System considerations – Drivers and controls on carbon processing.....	43
2.6.6 System considerations – Importance of spatial intermittency .....	49
2.7 Future work.....	50
2.8 Conclusions.....	50
2.9 Acknowledgements.....	52
2.10 References.....	52

## Table of Contents (Continued)

	<u>Page</u>
3 Solute dynamics in a headwater stream and riparian hyporheic zone during a small November storm in the Cascade Mountains, Oregon .....	58
3.1 Abstract .....	58
3.2 Introduction.....	59
3.3 Study site.....	62
3.4 Methods.....	64
3.4.1 Preparatory methods .....	64
3.4.2 Field methods .....	65
3.4.3 Laboratory methods .....	66
3.4.4 Calculations .....	67
3.5 Results.....	68
3.5.1 DOC concentrations .....	68
3.5.2 DIC concentrations .....	71
3.5.3 Nitrate concentrations.....	72
3.5.4 Chloride concentrations.....	74
3.5.5 Ion balance.....	76
3.6 Discussion.....	77
3.6.1 Stream solute dynamics .....	77
3.6.2 Hyporheic solute dynamics .....	81
3.7 Conclusions.....	83
3.8 References.....	85
4 Conclusions.....	88
BIBLIOGRAPHY .....	91

## Table of Contents (Continued)

	<u>Page</u>
APPENDICES .....	98
Appendix A    Complete model lists .....	99
Appendix A.1    Complete list of September DOC models .....	99
Appendix A.2    Complete list of November DOC models .....	100
Appendix A.3    Initial list of September DIC models.....	101
Appendix A.4    Final list of September DIC models.....	102
Appendix A.5    Initial list of November DIC models.....	103
Appendix A.6    Final list of November DIC models .....	104
Appendix B    Detailed field methods.....	105
Appendix C    Detailed laboratory methods .....	107
Appendix C.1    Detailed methods for DIC analysis .....	107
Appendix C.2    Detailed methods for DOC analysis.....	109
Appendix C.3    Detailed methods for anion analysis .....	110
Appendix C.4    Detailed methods for cation analysis.....	112

## LIST OF FIGURES

<u>Figure</u>	<u>Page</u>
Figure 2.1 – Location of the H.J. Andrews Experimental Forest within Oregon ( <i>A</i> ), and location of Watershed 1 and the well network within H.J. Andrews ( <i>B, C</i> ). Note that flow is from right to left in the well network figure. All wells that were sampled are active wells and are labeled. Data sources: The image of the well network site ( <i>D</i> ) was modified from Wondzell (2006); The catchment outlines and stream networks are from the H.J. Andrews Experimental Forest; The Oregon outline is from ESRI and TomTom. ....	8
Figure 2.2 – Timing of sampling runs conducted during 2013 and 2014. Discharge data is from the WS1 gaging station at H.J. Andrews Experimental Forest, Oregon .....	13
Figure 2.3 – Relationships between key variables over the full study period. All of the included observations are from hyporheic wells. Well D7 is excluded due to its distinct hillslope response. The stars in figures <i>A, B</i> , and <i>D</i> indicate stream concentrations.....	20
Figure 2.4 – Seasonal patterns in $\text{Cl}^-$ , $\text{Ca}^{+2}$ , DOC, and DIC concentrations. All of the included observations are from hyporheic wells. Well D7 is excluded due to its distinct hillslope response.....	22
Figure 2.5 – Spatial patterns in carbon concentrations within the well network in September ( <i>A, B</i> ) and November ( <i>D, E</i> ), as well as the spatial distribution of the 1997 median travel times ( <i>C</i> ). Solute concentrations within the subsurface are represented in the contoured grid. Stream concentrations for the same sampling run are shown within the stream outline at the edges of the grid. Well locations are given in the upper left panel, and match the orientation of Figure 2.1. The stream flows from right to left.....	23
Figure 2.6 – Spatial patterns in the depth to water ( <i>A</i> ), pH ( <i>C</i> ), and $\text{PO}_4^{-3}$ ( <i>D</i> ) within the well network in September. Spatial distribution of subsurface temperatures in December ( <i>B</i> ). Dissolved oxygen concentrations in the subsurface as measured in July 2014 ( <i>E</i> ; Serchan, unpublished data, 2014). All data for the subsurface are represented in the contoured grid. Stream values for the same sampling run are shown within the stream outline at the edges of the grid. Well locations are given in the upper left panel, and match the orientation of Figure 2.1. The stream flows from right to left. ....	25
Figure 2.7 – A schematic of observed solute dynamics in the stream and WS1 hyporheic zone. Potential hydrologic and biogeochemical sources and sinks of DOC and DIC to the WS1 hyporheic zone during baseflow periods are shown in light grey boxes. The sources that we expect are the most likely explanation for observed excess DIC concentrations are presented in bold text, while sources that we expect are insignificant are presented in italic text. Potential sources of which we do not know the magnitude or relative importance are presented in standard text.....	39

## LIST OF FIGURES (Continued)

<u>Figure</u>	<u>Page</u>
Figure 3.1 - Location of the H.J. Andrews Experimental Forest within Oregon ( <i>A</i> ), and location of Watershed 1 and the well network within H.J. Andrews ( <i>B, C</i> ). Note that flow is from right to left in the well network figure. For this study wells D5, D6, D7, E4, G1, G2, G3, G5, and G6 were sampled. Data sources: The image of the well network site ( <i>D</i> ) was modified from Wondzell (2006); The catchment outlines and stream networks are from the H.J. Andrews Experimental Forest; The Oregon outline is from ESRI and TomTom. ....	63
Figure 3.2 - Timing of storm sampling within fall 2013 ( <i>A</i> ), and November 2013 ( <i>B</i> ). The period displayed in Figures 3.3 - 3.7 is highlighted in blue. The streamflow data are from the WS1 gaging station at the H.J. Andrews Experimental Forest. ....	66
Figure 3.3 - Stream and hyporheic DOC and nitrate concentrations by discharge. Observations are connected in the order in which they were collected. Concentrations in the stream and in wells where both solutes displayed hysteresis are shown in <i>A</i> and <i>C</i> . Concentrations in wells where neither DOC nor nitrate displayed hysteresis are shown in <i>B</i> and <i>D</i> . Note that nitrate concentrations are on a logarithmic scale. ....	69
Figure 3.4 – Hyporheic and stream DOC concentrations from 11/15/13 to 11/17/13. Discharge is displayed in the background. 1-hour precipitation totals and cumulative precipitation are given in the top panel. Precipitation and discharge data are from the PRIMET meteorological station and WS1 gaging station at the H.J. Andrews Experimental Forest. ....	70
Figure 3.5 – Hyporheic and stream DIC concentrations from 11/15/13 to 11/17/13. Discharge is displayed in the background. 1-hour precipitation totals and cumulative precipitation are given in the top panel. Precipitation and discharge data are from the PRIMET meteorological station and WS1 gaging station at the H.J. Andrews Experimental Forest. ....	72
Figure 3.6 – Hyporheic and stream nitrate concentrations from 11/15/13 to 11/17/13. Note that nitrate concentrations are on a log scale. Discharge is displayed in the background. 1-hour precipitation totals and cumulative precipitation are given in the top panel. Precipitation and discharge data are from the PRIMET meteorological station and WS1 gaging station at the H.J. Andrews Experimental Forest. ....	74
Figure 3.7 – Hyporheic and stream chloride concentrations from 11/15/13 to 11/17/13. Discharge is displayed in the background. 1-hour precipitation totals and cumulative precipitation are given in the top panel. Precipitation and discharge data are from the PRIMET meteorological station and WS1 gaging station at the H.J. Andrews Experimental Forest. ....	75

## LIST OF FIGURES (Continued)

<u>Figure</u>	<u>Page</u>
Figure 3.8 - Hyporheic and stream ion balance from 11/15/13 to 11/17/13. Discharge is displayed in the background. 1-hour precipitation totals and cumulative precipitation are given in the top panel. Precipitation and discharge data are from the PRIMET meteorological station and WS1 gaging station at the H.J. Andrews Experimental Forest.	76

## LIST OF TABLES

<u>Table</u>	<u>Page</u>
Table 2.1 - Sampling information and hydrologic and climatic conditions for each of seven baseflow sampling runs. Climatic data and hydrologic data courtesy of the PRIMET meteorological station and WS1 gaging station at the H.J. Andrews Experimental Forest, Oregon .....	12
Table 2.2 - DOC models for September. Models are ranked based on the associated AIC values. Adjusted $r^2$ are given since the models include three terms. ....	26
Table 2.3 – DOC models for November. Models are ranked based on the associated AIC values. Adjusted $r^2$ are given since the models include three terms. ....	27
Table 2.4 – A matrix of Pearson's correlation coefficients ( $r$ , black text, below diagonal) and coefficients of determination ( $r^2$ , grey text, above diagonal) for major variable pairs in September .....	28
Table 2.5 – A matrix of Pearson's correlation coefficients ( $r$ , black text, below diagonal) and coefficients of determination ( $r^2$ , grey text, above diagonal) for major variable pairs in November.....	28
Table 2.6 – DIC models for September. Models are ranked based on the associated AIC values. $r^2$ cannot be computed for general linear models fit with the 'nlme' package in R. ....	29
Table 2.7 - DIC models for November. Models are ranked based on the associated AIC values. $r^2$ cannot be computed for general linear models fit with the 'nlme' package in R. ....	30
Table 3.1 - Median travel times, and pre-storm depth to water (relative to ground surface) in the selected hyporheic wells. Median travel times from Wondzell, unpublished data, 1997.....	68

## LIST OF APPENDIX TABLES

<u>Table</u>	<u>Page</u>
Table A.1 - A full list of DOC models for September. Models are ranked based on the associated AIC values. Adjusted $r^2$ are given since the models include three terms.....	99
Table A.2 - A full list of DOC models for November. Models are ranked based on the associated AIC values. Adjusted $r^2$ are given since the models include three terms.....	100
Table A.3 – An initial list of DIC models for November, before the stepwise regression was re-done to include a spatial autocorrelation structure. Models are ranked based on the associated AIC values. Adjusted $r^2$ are given since the models include three terms.....	101
Table A.4 – A full list of DIC models for September, with the Gaussian spatial autocorrelation structure. Models are ranked based on the associated AIC values. $r^2$ cannot be computed for general linear models fit with the 'nlme' package in R. ....	102
Table A.5 - An initial list of DIC models for November, before the stepwise regression was re-done to include a spatial autocorrelation structure. Models are ranked based on the associated AIC values. Adjusted $r^2$ are given since the models include three terms.....	103
Table A.6 - A full list of DIC models for September, with the Gaussian spatial autocorrelation structure. Models are ranked based on the associated AIC values. $r^2$ cannot be computed for general linear models fit with the 'nlme' package in R. ....	104

## 1 Introduction

Recent efforts to construct carbon budgets for aquatic ecosystems have estimated that inland waters receive twice as much carbon from terrestrial ecosystems as they export to global oceans (Cole et al., 2007; Aufdenkampe et al., 2011). Oceanic export accounts for only half of the carbon input because streams and rivers transform, evade, and store a significant amount of terrestrially-derived carbon (Benstead and Leigh, 2012).

The link between terrestrial and aquatic ecosystems is strongest in headwater reaches, and terrestrial carbon enters headwater streams through direct inputs such as leaf-fall and throughfall, and through overland and subsurface flow. The carbon that these mechanisms transport is produced and mobilized as a result of numerous processes: soil respiration, leaching, chemical weathering, physical erosion, carbonate precipitation, and root respiration from riparian vegetation (Cole et al., 2007; Aufdenkampe et al., 2011). Once it reaches the stream, this terrestrial carbon is biogeochemically transformed, and microbial communities downstream rely on the transformed carbon as source of energy (Battin et al., 2008).

Headwater reaches play an important role in not only transporting, but in transforming terrestrial carbon because the metabolic performance of streams is higher in headwater reaches than at any other point in the river network (Battin et al., 2008). In high-gradient, small streams, coarse, heterogeneous streambeds allow for frequent exchange between surface and shallow subsurface waters (Kasahara and Wondzell, 2003; Battin et al., 2008; Wondzell, 2011). This exchange, termed hyporheic exchange flow, serves to increase the residence time of organic molecules that are transported by the

water and simultaneously increase their exposure to biofilms and aggregates that dominate microbial communities in the high surface-area environment of the subsurface, while providing a steady stream of oxygen and nutrients (Battin et al., 2008). As a result, organic matter is actively processed and metabolized in hyporheic zones, and large quantities of CO<sub>2</sub> are generated via respiration (Grimm and Fisher, 1984; Findlay et al., 1993; Pusch and Schwoerbel, 1994; Pusch, 1996; Mulholland et al., 1997; Baker et al., 1999; Battin, 1999; Sobczak and Findlay, 2002). Because the flux of water through hyporheic zones is proportionally large relative to total streamflow in headwater reaches, and because these zones are so biologically active, return flows of hyporheic water to headwater stream ecosystems are of sufficiently distinct composition and large enough magnitude to alter the bulk properties of stream water (Battin et al., 2008; Wondzell, 2011).

During dry, baseflow conditions, when flow from hillslopes to streams is limited, studies have observed relatively little movement of carbon from hillslopes to aquatic systems (Buffam et al., 2001). During storm events or snowmelt, however, carbon is flushed out of soils and into stream ecosystems as a result of vertical infiltration and lateral water movement (Hornberger et al., 1994; Hood et al., 2003; Hood et al., 2006; van Verseveld, 2008; Pacific et al., 2010). In many forested catchments, mean stream concentrations of DOC may double or triple with the onset of a storm or during snowmelt (Buffam et al., 2001; McGlynn and McDonnell, 2003; Hood et al., 2006; Raymond and Saiers, 2010; Wilson et al., 2013). Over the course of a storm event, stream water DOC concentrations commonly display clockwise hysteresis, with greater concentrations of DOC on the rising limb than on the receding limb of storm hydrographs (Buffam et al.,

2001; Hood et al., 2003; McGlynn and McDonnell, 2003; Hood et al., 2006; van Verseveld et al., 2008).

Within most catchments, the near-stream riparian zone and the hillslopes of the catchment represent two spatially distinct sources of carbon to the stream. During the rising limb of the storm hydrograph, riparian contribution of DOC is greater than hillslope contribution (Buffam et al., 2001; McGlynn and McDonnell, 2003; Hood et al., 2006; van Verseveld et al., 2008). This trend is reversed on the receding limb (Buffam et al., 2001; McGlynn and McDonnell, 2003; Hood et al., 2006; van Verseveld et al., 2008). This shift in delivery is due to a physical disconnect between riparian and hillslope components. Carbon in riparian areas can be quickly flushed to streams by even small amounts of rainwater infiltration, while carbon that has accumulated in hillslope areas cannot be flushed to the stream until soil water deficits are met and soil macropores are filled, thereby allowing hillslope carbon to be mobilized and upland portions of the watershed to be connected to the stream (Bishop et al., 2003; McGlynn and McDonnell, 2003).

Overall, dynamics of carbon transport to streams and hyporheic zones are highly dependent upon the degree of hydrologic connectivity within the catchment, both laterally and vertically. Once carbon reaches the biologically active hyporheic zone, its transformation is controlled and influenced by numerous physical mechanisms and biogeochemical processes. Understanding the relative influence of such factors on carbon processing requires detailed, high-resolution sampling of hyporheic water over varied hydrologic and climatic conditions.

## 2 Carbon dynamics in the hyporheic zone of a headwater mountain stream in the Cascade Mountains, Oregon

### 2.1 *Abstract*

This study investigated carbon dynamics in the hyporheic zone of a steep, forested catchment in the Cascade Mountains of western Oregon, USA. Water samples were collected monthly from a headwater stream and well network from July to December 2013 and again in March 2014. The well network is located at the base of Watershed 1 (WS1) of the H.J. Andrews Experimental Forest and spans the full width of the floodplain (~14 m) along a 29 m reach of stream. We measured pH, temperature, water level, major anions, major cations, DOC, DIC, and total alkalinity. Flow paths, travel time to wells and hydraulic conductivity were available from previous studies.

During baseflow periods, hyporheic DOC decreased with median travel time through the subsurface. DIC concentrations increased with travel time, but the magnitude of this increase in DIC was too large to be explained by metabolism of stream water DOC. This suggests that there are additional sources of DIC and/or DOC in the subsurface, and that hyporheic DIC concentrations are not well linked to stream-source DOC. The most likely supplemental sources of DIC to hyporheic water are soil CO<sub>2</sub> and microbial respiration of DOC leached from buried particulate organic matter and from overlying soils. Overall, the hyporheic zone appears to be a source of DIC to the stream.

### 2.2 *Introduction*

Aquatic ecosystems transform carbon on timescales that are short in comparison to timescales of carbon production and storage in terrestrial ecosystems (Battin et al.,

2008). As a result, streams and rivers play an active role in global carbon cycling. First- and second- order headwater streams are a particularly important component of aquatic carbon budgets because they make up 75% of total stream length globally and receive large amounts of carbon from adjacent terrestrial ecosystems (Downing et al., 2012). Terrestrial carbon enters headwater streams through direct inputs such as leaf-fall and throughfall, and through overland and subsurface flow. Once it reaches headwater streams, this terrestrial carbon is not only advected to downstream reaches, but is also transformed, evaded, and stored. Recent work has focused on measuring watershed carbon export, and, less commonly, carbon evasion and storage. Little attention has been paid to understanding how and why carbon is transformed in headwater ecosystems. Understanding the physical and biogeochemical controls on carbon transformation is critical, because rates of carbon transformation influence the movement of carbon through a system and determine the form in which it is exported.

Headwater reaches play an important role in not only transporting, but transforming terrestrial carbon because the metabolic performance of streams is higher in headwater reaches than at any other point in the river network (Battin et al., 2008). In high-gradient, small streams, coarse, heterogeneous streambeds allow for frequent exchange between surface and shallow subsurface waters (Kasahara and Wondzell, 2003; Battin et al., 2008; Wondzell, 2011). This exchange, termed hyporheic exchange flow, serves to increase the residence time of organic molecules that are transported by the water and simultaneously increase their exposure to biofilms and aggregates that dominate microbial communities in the high surface area environment of the subsurface, while providing a steady supply of oxygen and nutrients (Battin et al., 2008). As a result,

organic matter is actively processed and metabolized in hyporheic zones, and large quantities of CO<sub>2</sub> are generated via respiration (Grimm and Fisher, 1984; Findlay et al., 1993; Pusch and Schwoerbel, 1994; Pusch, 1996; Mulholland et al., 1997; Baker et al., 1999; Battin, 1999; Sobczak and Findlay, 2002). Because the flux of water through hyporheic zones is proportionally large relative to total streamflow in headwater reaches, and because these zones are so biologically active, return fluxes of hyporheic water to headwater stream ecosystems are of sufficiently distinct composition and large enough magnitude to alter the bulk properties of stream water (Battin et al., 2008; Wondzell, 2011). Hyporheic exchange therefore has the potential to influence carbon cycling in headwater ecosystems.

To date, research into carbon dynamics in hyporheic systems has focused primarily on DOC removal and transport (McDowell 1985; Findlay and Sobczak, 1996; Hinton et al., 1998; Battin, 1999; Chestnut and McDowell, 2000; Buffam et al., 2001; Sobczak and Findlay, 2002; Zarnetske et al., 2011), DOC metabolism (Grimm and Fisher, 1984; Pusch, 1996; Battin, 1999), or DIC or CO<sub>2</sub> production (Hedin 1990; Raymond and Bauer, 2000; Öquist et al., 2009; Crawford et al., 2013; Khadka et al., 2014). Only a handful of studies have investigated both organic and inorganic carbon dynamics simultaneously (Findlay et al., 1993; Schindler and Krabbenhoft, 1998). These studies have helped to establish the functional importance of hyporheic zones, and together support our hypothesis that hyporheic exchange influences carbon cycling in aquatic systems. However, given that organic and inorganic carbon are inextricably linked through metabolism, the lack of concurrent measurements of both organic and inorganic carbon within hyporheic systems hampers our ability to understand how carbon

is transformed in hyporheic environments. The focus of our study was to investigate inorganic and organic carbon dynamics in the hyporheic zone of a headwater catchment in the Western Cascade Mountains of Oregon. We collected water samples from a well network that spanned the full width of the riparian corridor at the base of the catchment during baseflow periods in each of seven months. In our analysis, we sought to evaluate the influence of seasonal, physical, and biogeochemical processes on carbon cycling within this hyporheic environment.

### **2.3 *Study site***

This study was conducted in the lower portion of Watershed 1 (WS1), a study watershed in the H.J. Andrews Experimental Forest, located in the Western Cascades of Oregon, USA ( $44^{\circ} 12' 28.0''$  N,  $122^{\circ} 15' 30.0''$  W; Figure 2.1). Watershed 1 is a steep, forested catchment that is 95.9 ha in size, and ranges in elevation from 450 to 1027 m. The climate is characterized by cool, wet winters and warm, dry summers. At lower elevations, air temperatures range from an average of 1 °C in January to 18°C in July. The 230 cm of annual precipitation falls primarily as rain from November to March. Snow occasionally accumulates, but WS1 lies within the transient snow zone, where snow accumulates during cold winter storms, but melts during warm periods or warmer storms, so that snow packs do not persist for the entire winter. As a result, peak streamflow in WS1 occurs anytime throughout the winter and declines in summer months. Streamflow becomes so low in July, August, and September that surface flow cannot be continuously sustained, and the stream becomes spatially intermittent.

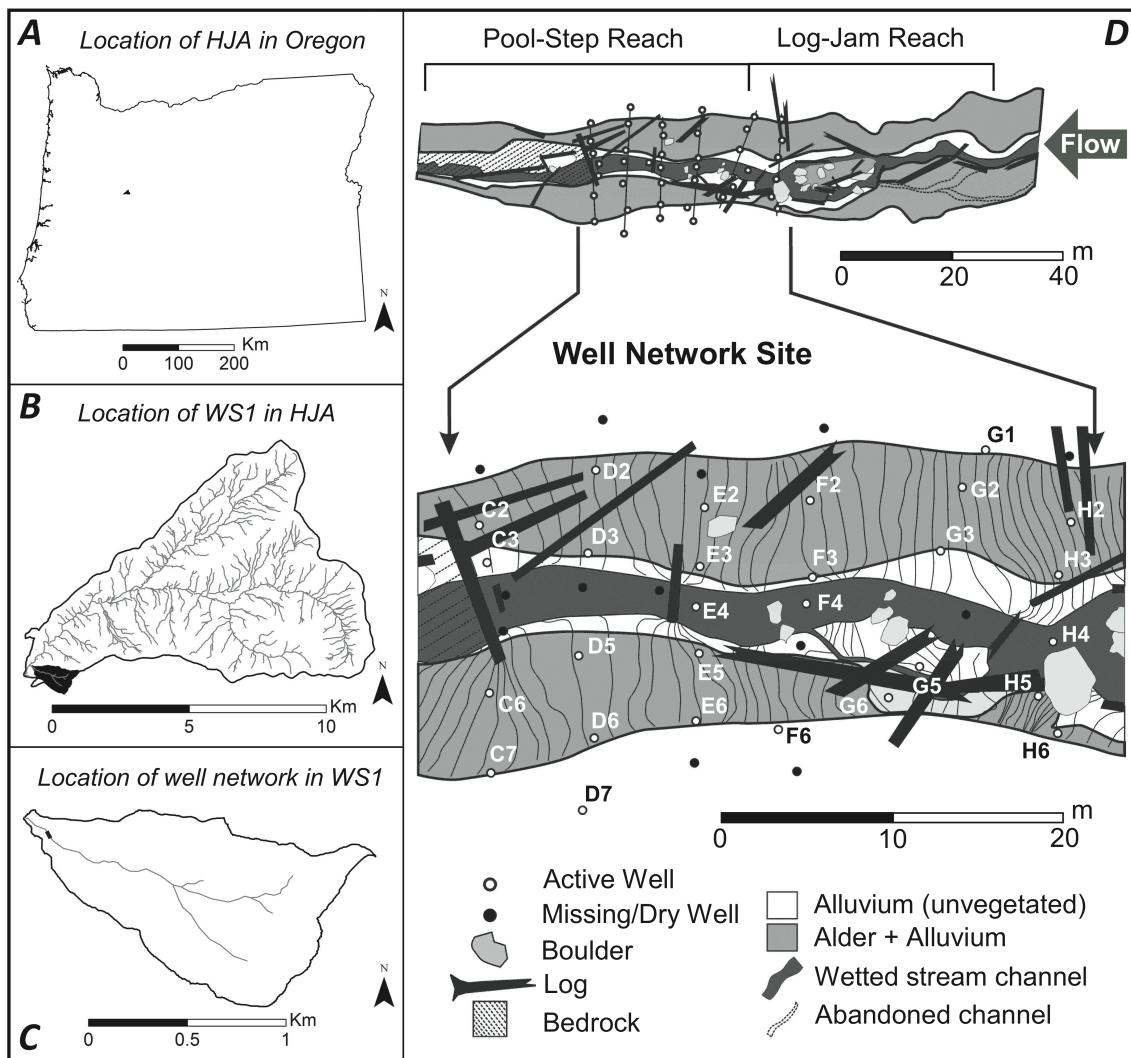


**Figure 2.1** – Location of the H.J. Andrews Experimental Forest within Oregon (*A*), and location of Watershed 1 and the well network within H.J. Andrews (*B, C*). Note that flow is from right to left in the well network figure. All wells that were sampled are active wells and are labeled. Data sources: The image of the well network site (*D*) was modified from Wondzell (2006); The catchment outlines and stream networks are from the H.J. Andrews Experimental Forest; The Oregon outline is from ESRI and TomTom.

Throughout WS1, the soils are gravel clay loam, and tend to be shallow (0.5 – 2 m) and porous, allowing high rates of infiltration (Rothacher et al., 1967; Dyrness, 1969). Tuffs and breccias of the Oligocene to lower Miocene Little Butte Formation underlie the

middle and lower portions of the watershed, while the upper northeast corner is underlain by an andesitic flow (Swanson and James, 1975).

From 1962 to 1966, WS1 was 100% clear-cut using skyline yarding to lift logs clear of the ground and thereby minimize soil disturbance as logs were removed from the watershed. In 1966, the logging debris (slash) was burned (Levno and Rothacher, 1969; Halpern and Franklin, 1990). Today, dense stands of Douglas fir and hemlock dominate on hillslopes. Red alder dominates the riparian zone, although maple, cottonwood, and dogwood are also present (Rothacher et al., 1967; Halpern and Franklin, 1990; Johnson and Jones, 2000). The alders established after the logging operation, and today are being over-topped by Douglas fir. As a result, many have died or fallen in recent years.

The stream channel in WS1 is steep and usually confined. It has been shaped by debris flows, which have scoured the stream to bedrock in places. Reaches where colluvium is deposited are less constrained (Wondzell, 2006). Our study site is located in a zone of colluvial deposition near the base of WS1. The channel remains steep, with an average longitudinal gradient of 14%. The poorly sorted colluvial sediment is up to 2 m thick across the 14 m wide valley floor (Wondzell, 2006). The channel is broken into a series of pools and steps that have formed over logs and boulders (Wondzell, 2006). These steps drive 50% of hyporheic exchange between the stream and subsurface (Kasahara and Wondzell, 2003). During high and low baseflow, down-valley hydraulic gradients along this reach average 1.4 times steeper than cross-valley gradients (Wondzell, 2006). This leads to the development of extended flow paths that are parallel to the stream and to the predominance of long-timescale hyporheic exchange (Wondzell, 2006), with median residence times estimated at 17 hours (Kasahara and Wondzell,

2003). Despite these long residence times, hyporheic water in WS1 is generally oxic (Serchan, unpublished data, 2014)

The well network is located in the 14 m wide riparian zone at the base of WS1, and spans 29 m of stream length (Wondzell, 2006). When it was installed in 1997, it contained 30 shallow (~1 – 1.7 m deep) riparian wells and 7 in-stream piezometers (2006). This study was able to sample 24 wells and 4 piezometers – 9 of the original were cracked, missing, or had gone dry. The wells and piezometers are arrayed in six transects that span the width of the 14 m wide valley floor, perpendicular to the direction of flow (Figure 2.1). Both wells and piezometers are constructed of 3.175 cm (1 1/4 inch) schedule 40 PVC. An array of drilled holes serves as a screen along the bottom 50 cm of the wells and bottom 5 cm of the in-stream piezometers (Wondzell, 2006). The deepest well extends to 1.7 m, but the majority are approximately 1 m deep (Wondzell, 2006). We also sampled one hillslope well, located approximately 150 m up the watershed at the base of a hillslope hollow, which we installed during the summer of 2013.

## 2.4 Methods

### 2.4.1 Preparatory methods

We conducted all preparatory and analytical lab work at the Institute for Water and Watersheds Collaboratory at Oregon State University using operating procedures developed by the Oregon State University and United States Forest Service Cooperative Chemical Analytical Laboratory (CCAL). Prior to fieldwork, we acid washed all equipment for field sample collection and lab analysis in a 10% v/v HCl acid bath according to the CCAL quality assurance plan (CCAL, unpublished, 2013). This

equipment included 40 mL borosilicate vials, 250 mL Nalgene HDPE bottles, VWR 60 mL syringes with BD Luer-Lok tips, Cole-Parmer polycarbonate stopcocks with Luer connections, a 4.7 cm filter apparatus, and 0.635 cm (1/4 inch) sample tubing. In addition, we baked the 40 mL borosilicate vials that were allocated for DOC analysis at 550 °C for three hours (CCAL, unpublished, 2013). We rinsed the 140 mL syringes and 0.635 cm tubing used for purging the wells in DI water and dried them in a low-temperature oven between sampling runs. We prepared Whatman 4.7 cm grade GF/F glass microfiber filters by rinsing them with 1 L of DI water, drying them, and baking them in a muffle furnace at 500 °C for 3 hours (CCAL, unpublished, 2013). We stored prepared filters in clean, individual foil packets. Note that the use of trade or firm names in this publication is for reader information and does not imply endorsement by the US Department of Agriculture of any product or service.

#### *2.4.2 Field methods*

We conducted all fieldwork in Watershed 1 at the H.J. Andrews Experimental Forest. In order to prepare the well network for sampling, we cleared all wells of accumulated sediment by flushing them once with pressurized stream water. We cleaned one half of the network in early June 2013 in preparation for a partial sampling run, and washed the remaining wells in mid-July 2013. In each case, the cleaning was performed at least a week in advance of sample collection so that water chemistry would recover and thus reflect in-situ hyporheic conditions.

On the afternoon prior to each sampling run, we recorded the pH and temperature of each well and the stream using an YSI 60 probe. We also determined the depth to

water in each well using a tape measure and wet-erase marker. Following this, we removed 700 mL from each of the wells using the designated purge syringes and tubing.

The following morning (on the date given for each sampling run in Table 2.1), we sampled each of the 28 wells, the stream, and the hillslope well, collecting one field duplicate for every ten samples.

**Table 2.1** - Sampling information and hydrologic and climatic conditions for each of seven baseflow sampling runs. Climatic data and hydrologic data courtesy of the PRIMET meteorological station and WS1 gaging station at the H.J. Andrews Experimental Forest, Oregon

Run	Date	No. Wells Sampled	Avg. Air T °C	Avg. EC µS/cm	Avg. Stream T °C	Avg. Q L/s	5-day ppt total mm	21-day ppt total mm
B	7/25/13	16	29.9	52.7	15.6	1.3	0.0	0.0
C	8/22/13	25	27.1	56.7	15.5	0.5	0.0	10.9
D	9/19/13	28	20.9	53.5	12.8	1.0	4.1	37.9
E	10/28/13	28	7.6	45.2	8.7	4.1	8.9	20.0
F	11/15/13	28	5.3	42.9	8.0	7.7	2.9	94.3
G	12/8/13	28	-6.0	34.6	1.5	18.0	11.2	149.1
H	3/16/14	28	13.1	35.4	8.3	34.2	0.4	291.9

We extracted water from the wells using the acid washed 60 mL syringes, stopcocks, and 0.635 cm sample tubing. Prior to sample collection, we rinsed the sample tubing and syringes three times with approximately 180 mL of well water. We used an additional 60 mL of water to rinse the prepared GFF filters and the acid washed HDPE bottles. We then collected 250 mL of water for DOC, anion, cation, and alkalinity analysis, which we filtered in the field through the prepared glass microfiber filters into the HDPE bottles. We sampled stream water using this same technique. On a few occasions, 250 mL of unfiltered stream and well water were collected for TOC analysis. We collected sample aliquots for DIC analysis last so as to minimize exposure of the

water to the atmosphere, and preserved each sample in an individual, locked, airtight syringe. We transported all samples back to the lab on ice and kept them in cold storage until analysis.

We sampled the WS1 well network at monthly intervals from July to December 2013 and then again in March 2014, focusing our sampling during baseflow or near-baseflow periods after relatively dry antecedent conditions (Figure 2.2; Table 2.1). We obtained discharge, stream temperature, and stream conductivity data from the WS1 gaging station, located approximately 50 m below the well network. We used precipitation and temperature data recorded at the PRIMET meteorological station at the H.J. Andrews headquarters, located approximately 0.6 km from the WS1 gaging station.

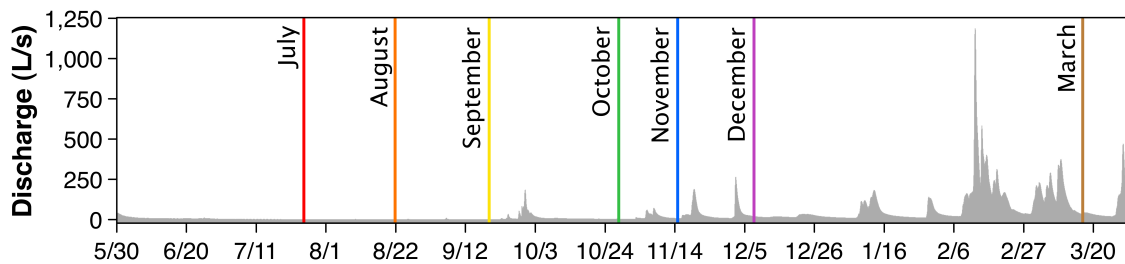


**Figure 2.2** – Timing of sampling runs conducted during 2013 and 2014. Discharge data is from the WS1 gaging station at H.J. Andrews Experimental Forest, Oregon

#### 2.4.3 Laboratory methods

We performed all analytical work in the IWW Collaboratory at Oregon State University. Methods for these analyses are presented below. CCAL standard operating procedures are developed primarily from the cited APHA methods, but comparable EPA methods are noted for reference. The format of all methods citations is as follows: (CCAL standard operating procedure, APHA method, EPA method, method detection limit).

Immediately prior to analysis, we filtered the DIC sample aliquots through 25 mm diameter VWR 0.45  $\mu\text{m}$  nylon syringe filters with polypropylene housing into acid washed 40 mL borosilicate vials. We filled the vials at an angle and capped them as soon as an inverted meniscus was formed, so as to limit atmospheric exposure. We analyzed the filtered samples on a Shimadzu TOC-VSCH Combustion Carbon Analyzer within 72 hours (CCAL 21A.0, n/a, n/a, 0.05 mg/L). We modified the procedure slightly in order to account for higher concentrations of DIC in hyporheic water by using ten standards ranging in concentration from 0 to 20 ppm and including both 1 and 10 ppm check standards.

We used aliquots of the field-filtered 250 mL sample for DOC, anion, cation, and alkalinity analysis. We used the unfiltered stream and well water, when it was collected, to analyze TOC content. We determined concentrations of DOC and TOC using a Shimadzu TOC-VSCH Combustion Carbon Analyzer (CCAL 20A.2, APHA 5310B, EPA 415.1, 0.05 mg C L<sup>-1</sup>). We measured major cations K<sup>+</sup>, Na<sup>+</sup>, Mg<sup>+2</sup>, and Ca<sup>+2</sup> on a Perkin-Elmer Atomic Absorption Spectrometer, a Perkin-Elmer AAnalyst-100 (CCAL 60B.1, APHA 3111, EPA 7000B, K<sup>+</sup>: 0.03 mg L<sup>-1</sup>, Na<sup>+</sup>: 0.01 mg L<sup>-1</sup>, Mg<sup>+2</sup>: 0.02 mg L<sup>-1</sup>, Ca<sup>+2</sup>: 0.06 mg L<sup>-1</sup>). We determined concentrations of major anions NO<sub>3</sub><sup>-</sup>, SO<sub>4</sub><sup>-2</sup>, Cl<sup>-</sup>, and PO<sub>4</sub><sup>-3</sup> on a Dionex 1500 Ion Chromatograph (CCAL 50B.1, APHA 4110B, EPA 9056A, 0.01 mg L<sup>-1</sup>). We measured total alkalinity by titrating all samples to a pH of 4.5 on a Radiometer TIM840 AutoTitrator (CCAL 10C.0, APHA method 2320 - modifications: use 0.02N Na<sub>2</sub>CO<sub>3</sub> and 0.02N H<sub>2</sub>SO<sub>4</sub>, no EPA method, 0.2 mg CaCO<sub>3</sub> L<sup>-1</sup>).

#### 2.4.4 Calculations

In order to calculate concentrations of the major carbonate species, we calculated appropriate  $K_{a1}$  and  $K_{a2}$  for each sample using the observed field temperatures. To do so, we followed the method used by the USGS software CO2calc (Robbins et al., 2010). This software uses the equations developed by Millero (2006) to determine  $pK_1$  and  $pK_2$  for the carbonate system, as they allow for a wide range of salinity (0 – 40) and are valid within a temperature range of 0 to 35 °C. As our samples were all fresh water, we used the equations given to estimate  $pK_1^°$  and  $pK_2^°$ , which represent the values of  $pK_1$  and  $pK_2$  in pure water, where salinity (S) is zero (Millero et al., 2006):

$$pK_1^° = -126.3405 + 6320.81/T + 19.568 \ln T \quad \text{Eq. 2.1}$$

$$pK_2^° = -90.1833 + 5143.69/T + 14.613 \ln T \quad \text{Eq. 2.2}$$

We used these constants to calculate  $K_{a1}$  and  $K_{a2}$ , ( $K_{a1} = 10^{-pK_1^°}$ ,  $K_{a2} = 10^{-pK_2^°}$ ), and then computed the alpha terms  $\alpha_0$ ,  $\alpha_1$ , and  $\alpha_2$  (Benjamin, 2010):

$$\alpha_0 = \left( 1 + \frac{K_{a1}}{[H^+]} + \frac{K_{a1} \cdot K_{a2}}{[H^+]^2} \right)^{-1} \quad \text{Eq. 2.3}$$

$$\alpha_1 = \left( \frac{[H^+]}{K_{a1}} + 1 + \frac{K_{a2}}{[H^+]} \right)^{-1} \quad \text{Eq. 2.4}$$

$$\alpha_2 = \left( \frac{[H^+]^2}{K_{a1} \cdot K_{a2}} + \frac{[H^+]}{K_{a2}} + 1 \right)^{-1} \quad \text{Eq. 2.5}$$

We used the alpha terms to calculate the concentrations of the carbonate species, using our measured DIC concentration as TOTCO<sub>3</sub> (Benjamin, 2010):

$$[H_2CO_3] = \alpha_0 \cdot TOTCO_3 \quad \text{Eq. 2.6}$$

$$[HCO_3^-] = \alpha_1 \cdot TOTCO_3 \quad \text{Eq. 2.7}$$

$$[CO_3^{2-}] = \alpha_2 \cdot TOTCO_3 \quad \text{Eq. 2.8}$$

In order to calculate  $[OH^-]$ , we computed the value of the equilibrium constant  $K_W$  at each temperature. We used the Van't Hoff equation, where  $T_1$  is the standard reference temperature (298 K), and  $T_2$  is the observed field temperature, in K (Benjamin, 2010):

$$\ln \frac{K_W|_{T_2}}{K_W|_{T_1}} = \frac{\Delta H_r^o}{R} \cdot \left( \frac{1}{T_1} - \frac{1}{T_2} \right) \quad \text{Eq. 2.9}$$

For each sample,  $[OH^-]$  was calculated from pH and  $K_W$ :

$$[OH^-] = \frac{K_W|_{T_2}}{[H^+]} \quad \text{Eq. 2.10}$$

After calculating the concentrations of the carbonate species and hydroxide, we computed the anion deficit:

$$\text{AnionDeficit} = \sum[\text{Cations}] - \sum[\text{Anions}] \quad \text{Eq. 2.11}$$

We also calculated the Ion Balance, as a percent:

$$\left( \frac{\sum[\text{Cations}] - \sum[\text{Anions}]}{\sum[\text{Cations}] + \sum[\text{Anions}]} \right) \cdot 100 \quad \text{Eq. 2.12}$$

For both equations:

$$\sum[\text{Cations}] = \sum([H^+] + [Ca^{+2}] + [Mg^{+2}] + [Na^+] + [K^+]) \quad \text{Eq. 2.13}$$

$$\sum[\text{Anions}] = \sum([OH^-] + [HCO_3^-] + [CO_3^{2-}] + [PO_4^{-3}] + [SO_4^{-2}] + [Cl^-] + [NO_3^-]) \quad \text{Eq. 2.14}$$

All cation and anion concentrations are in meq L<sup>-1</sup>

We calculated the amount of excess DIC that could not be explained by the conversion of stream DOC to DIC as follows:

$$\text{ExcessDIC} = \left( \text{DIC}_{\text{Hyp}} - \text{DIC}_{\text{Stream}} \right) - \Delta \text{DOC} \quad \text{Eq. 2.15}$$

where  $\Delta \text{DOC}$  is the slope from a regression of DOC vs. travel time for each sampling run. Travel times for all wells in the well network had previously been calculated using EC breakthrough curves from a five-day continuous salt tracer test of the WS1 well network conducted in 1997, the results of which are discussed in Wondzell (2006). Travel time is defined as the time (in hours) for observed EC in each well to reach one-half of the final observed plateau concentration.

#### *2.4.5 Statistical methods*

We conducted an exploratory statistical analysis in order to identify potential models that could explain DIC and DOC concentrations within the well network. Our dataset included repeated measures, and displayed unequal variance from month to month. In addition, the distribution of wells in space led to spatial autocorrelation in certain variables. This spatial correlation was not consistent for all terms in all months. Building a statistically valid model of the entire study period would therefore have required including a temporal autocorrelation structure, a spatial autocorrelation structure, and numerous interaction terms. As such, we chose to simplify our analysis by restricting our exploratory model analysis to individual months, eliminating the need to consider the temporal autocorrelation and unequal variance. We selected September to represent the dry summer period and November to represent the wet fall months. We eliminated data from the stream and hillslope well in order to only consider patterns in

DIC and DOC within the hyporheic zone. We also excluded all observations from well D7 (figure 2.1), as data from a separate study of a storm event indicated that it behaved similarly to the hillslope well, likely because of its location at the base of a small hillslope hollow (Corson-Rikert, unpublished data, 2013).

We used R and MATLAB software to perform manual stepwise regressions for each response variable (DIC and DOC) in each of the selected months for a total of four stepwise regressions. Since the analysis was exploratory, and not intended to produce predictive models, we adapted the traditional stepwise approach by manually following every statistically significant path, using  $\alpha = 0.05$  as the cut-off p-value to add or remove a term from the model. Due to sample size limitations, we were limited to three-variable models. For DOC our list of potential explanatory variables was as follows: depth to water, sampling depth, pH, temperature, total alkalinity,  $\text{PO}_4^{3-}$ ,  $\text{NO}_3^-$ ,  $\text{SO}_4^{2-}$ ,  $\text{Cl}^-$ ,  $\text{Mg}^{+2}$ ,  $\text{Ca}^{+2}$ ,  $\text{Na}^+$ ,  $\text{K}^+$ , anion deficit, travel time, distance from stream, and  $\ln K_{\text{sat}}$ . For DIC, this list also included DOC as a potential explanatory variable. Anion and cation concentrations, anion deficit, and total alkalinity were in meq L<sup>-1</sup>, and DOC and DIC concentrations were in mM.

After we produced a list of significant models for each response variable within each month, we evaluated each model for spatial autocorrelation. If spatial autocorrelation was present in more than a few models and if a spatial autocorrelation structure significantly improved the Akaike Information Criterion (AIC) of those models, we redid the manual stepwise regression for that response variable in that month, including a Gaussian spatial autocorrelation structure at every step. In order to include the Gaussian spatial autocorrelation structure we used the ‘nlme’ package in R and the

restricted maximum likelihood method (REML) to fit general linear models. Once we obtained a final list of models for each response variable in each month, we ranked the list using AIC to evaluate the degree of support in the data for that model.

## 2.5 Results

### 2.5.1 Consistent biogeochemical patterns

The temperature of hyporheic water was relatively constant with travel time during six of the seven sampling runs (figure 2.3A). December sampling occurred during a very cold spell, when stream temperature decreased to 0.89 °C overnight. Our data show that cold water infiltrated into the subsurface, lowering temperatures in wells with travel times of less than 30 hours (Figure 2.3A). The temperature signal did not propagate further into the well network.

Concentrations of DOC in hyporheic wells decreased with increasing travel time in all sampling months (Figure 2.3B). This indicates that DOC is lost as hyporheic water moves through the subsurface. Observed increases in DIC concentrations with median travel time complement the observed loss of DOC from hyporheic water (Figure 2.3D). This is expected if DOC is being metabolized by subsurface microbial communities and respired as CO<sub>2</sub>. DIC concentrations over the full study period are positively related to hyporheic water temperature – more DIC is produced in the warmer months of July, August and September than in the cooler months of October, November, and December (Figure 2.3C). Hyporheic DIC concentrations are not closely correlated with subsurface water temperatures within summer months, but are more tightly related to temperature within fall and winter months (Figure 2.3C; Tables 2.4, 2.5).

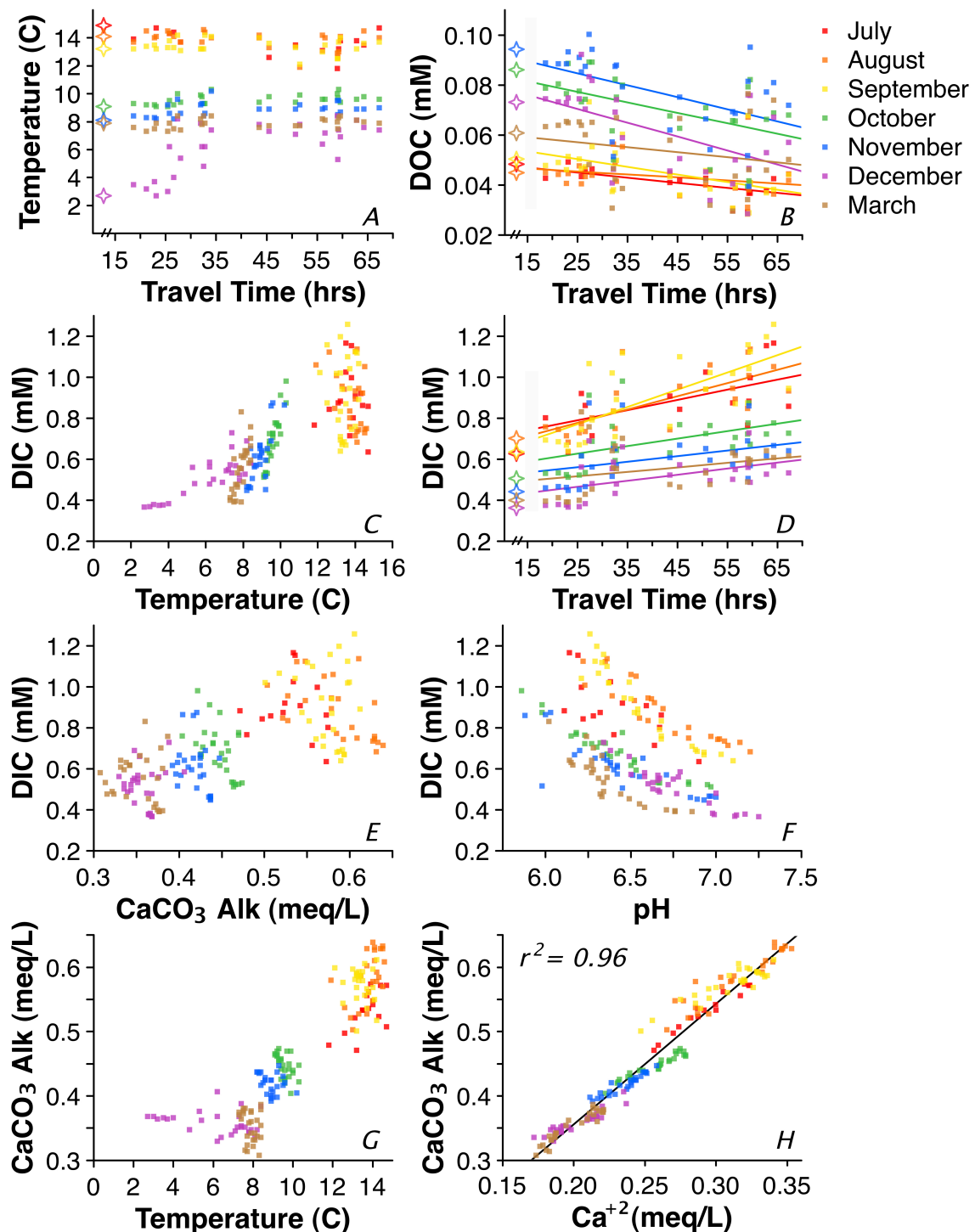


**Figure 2.3** – Relationships between key variables over the full study period. All of the included observations are from hyporheic wells. Well D7 is excluded due to its distinct hillslope response. The stars in figures A, B, and D indicate stream concentrations.

DIC and total alkalinity are positively related over the full study period (Figure 2.3E), likely because of the influence of carbonate speciation on total alkalinity (Stumm and Morgan, 1996). DIC and hyporheic pH are negatively related over the full sampling period. (Figure 2.3F). This relationship is even stronger within individual months (Figure 2.3F; Tables 2.4, 2.5). This is expected if the primary input of DIC to this system is respiration CO<sub>2</sub>, because an addition of CO<sub>2</sub> would simultaneously lower pH and increase DIC (Stumm and Morgan, 1996; Benjamin, 2010). Total alkalinity is also related to temperature, likely because of the correlation between DIC and temperature (Figures 2.3C, 2.3G). Total alkalinity is well correlated with Ca<sup>+2</sup> (Figure 2.3H;  $r^2 = 0.96$ ) and other cation species, which is expected given that using charge balance equations, total alkalinity can also be defined as acid neutralizing capacity (Stumm and Morgan, 1996).

### 2.5.2 Seasonal biogeochemical patterns

We observed a seasonal shift in chloride concentrations within hyporheic water (Figure 2.4A). Chloride concentrations were markedly higher in the wet fall and winter months of October, November, December, and March, potentially reflecting an increased input of chloride to hyporheic flow paths via vertical infiltration of surface soils. Chloride may be accumulated in soils during summer months and leached downward in the fall.

Ca<sup>+2</sup> showed a strong seasonal shift, with lower concentrations of Ca<sup>+2</sup> in hyporheic water during fall and winter months than in summer months (Figure 2.4C). As with chloride, this likely represents an increased input of soil water due to vertical infiltration through the soil profile in the rainy season. Such inputs would be expected to have low concentrations of major cations, as soils within the H.J. Andrews are developed

from highly weathered volcanic parent materials (Rothacher et al., 1967).  $Mg^{+2}$ ,  $Na^+$ ,  $K^+$ , and total alkalinity showed the same seasonal shift.

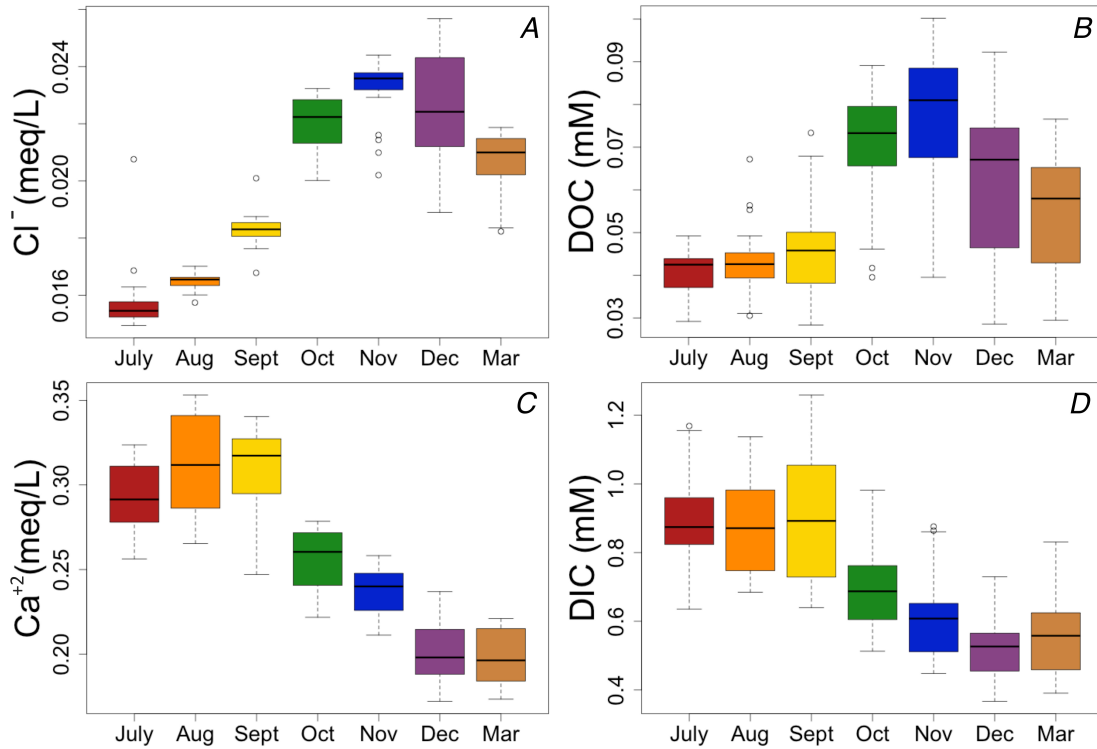


**Figure 2.4** – Seasonal patterns in  $Cl^-$ ,  $Ca^{+2}$ , DOC, and DIC concentrations. All of the included observations are from hyporheic wells. Well D7 is excluded due to its distinct hillslope response.

DOC and DIC concentrations within the well network showed distinct seasonal trends (Figures 2.4B, 2.4D). We observed greater variation in DOC concentrations and higher peak DOC concentrations during fall and winter months, particularly October and November (Figure 2.4B). We expect that in fall and winter months, DOC leached from fallen leaf litter and soil organic matter is mobilized and transported into hyporheic flow paths via vertical infiltration through the overlying soil. This hypothesis is consistent with the seasonal trends in cations and chloride described above. Observed DIC concentrations were highest in summer months, likely because microbial respiration is accelerated at

warmer temperatures during summer baseflow and when the stream is spatially intermittent (Figure 2.4D).

### 2.5.3 Spatial biogeochemical patterns

The seasonal shift in DOC concentrations (Figure 2.4B) is visible when concentrations of the solute are viewed spatially (Figures 2.5A, 2.5D). DOC concentrations in both September and November were highest within, beneath, and alongside the stream corridor, although pockets of elevated DOC were visible within the riparian zone, particularly in November (Figures 2.5A, 2.5D). DOC concentrations were lowest along the base of the adjacent hillslopes (Figures 2.5A, 2.5D).

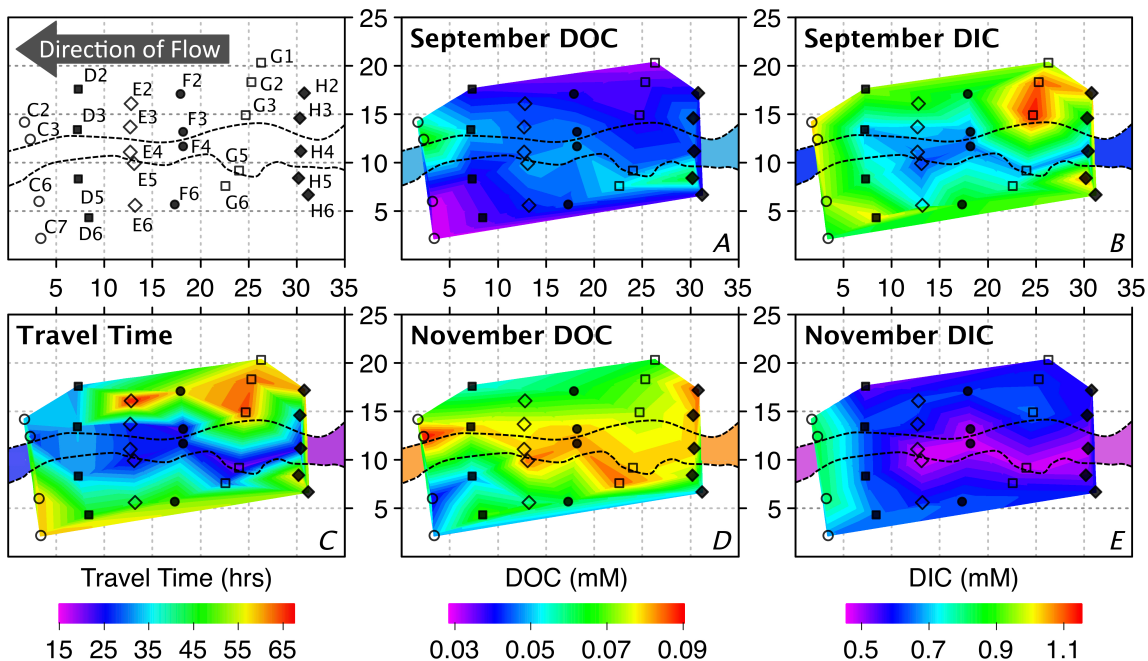


**Figure 2.5** – Spatial patterns in carbon concentrations within the well network in September (A, B) and November (D, E), as well as the spatial distribution of the 1997 median travel times (C). Solute concentrations within the subsurface are represented in the contoured grid. Stream concentrations for the same sampling run are shown within the stream outline at the edges of the grid. Well locations are given in the upper left panel, and match the orientation of Figure 2.1. The stream flows from right to left.

Although concentrations of DIC were lower in November than in September (Figure 2.4D), some spatial patterns were consistent between seasons (Figures 2.5B, 2.5E). DIC concentrations were lowest alongside and beneath the stream as well as within the stream water itself, and hotspots of high DIC concentrations were visible in both months (e.g., well G3 in September; Figures 2.5B, 2.5E).

Within the hyporheic network, spatial patterns in water table depth were consistent throughout the full sampling period, and are shown here using data from the September sampling run (Figure 2.6A). The depth to the water table was generally greatest in wells that were located at the edge of the riparian zone, and least in wells located along the stream bank (Figure 2.6A).

Spatial patterns in the pH of hyporheic water within the WS1 subsurface were also consistent throughout our study period. As shown in September, the water within the stream itself had high pH in all months (Figure 2.6C). Wells with comparatively low pH values were generally located further from the stream, although the pH of hyporheic water was also low in wells such as G3, which is near to the stream yet has a long median travel time (Figure 2.6C). This pattern was markedly similar to that shown by the infiltration of cold water in December (Figure 2.6B).

Phosphate ( $\text{PO}_4^{3-}$ ) concentrations varied three-fold within the subsurface of the WS1 riparian zone (Figure 2.6D). The spatial distribution of  $\text{PO}_4^{3-}$  concentrations was consistent during all sampling runs, with the highest  $\text{PO}_4^{3-}$  concentrations observed in wells located at the base of the hillslopes, as shown in September (Figure 2.6D).

We were unable to measure dissolved oxygen concentrations in the hyporheic zone during the course of this study. However, using recent data provided by new

research initiatives (Serchan, unpublished data, 2014), we can see that in July 2014, dissolved oxygen concentrations ranged from 2 – 8 mg L<sup>-1</sup> within the subsurface (Figure 2.6E). As expected, given the porous substrate and high rates of hyporheic exchange, no anoxic regions were found (Figure 2.6E). This is consistent with a handful of discrete measurements made in November 2013 (Corson-Rikert, unpublished data, 2013). However, year-round concentrations of dissolved oxygen within the subsurface are unknown. Additionally, we cannot rule out the possibility that anoxic micro-sites occur.

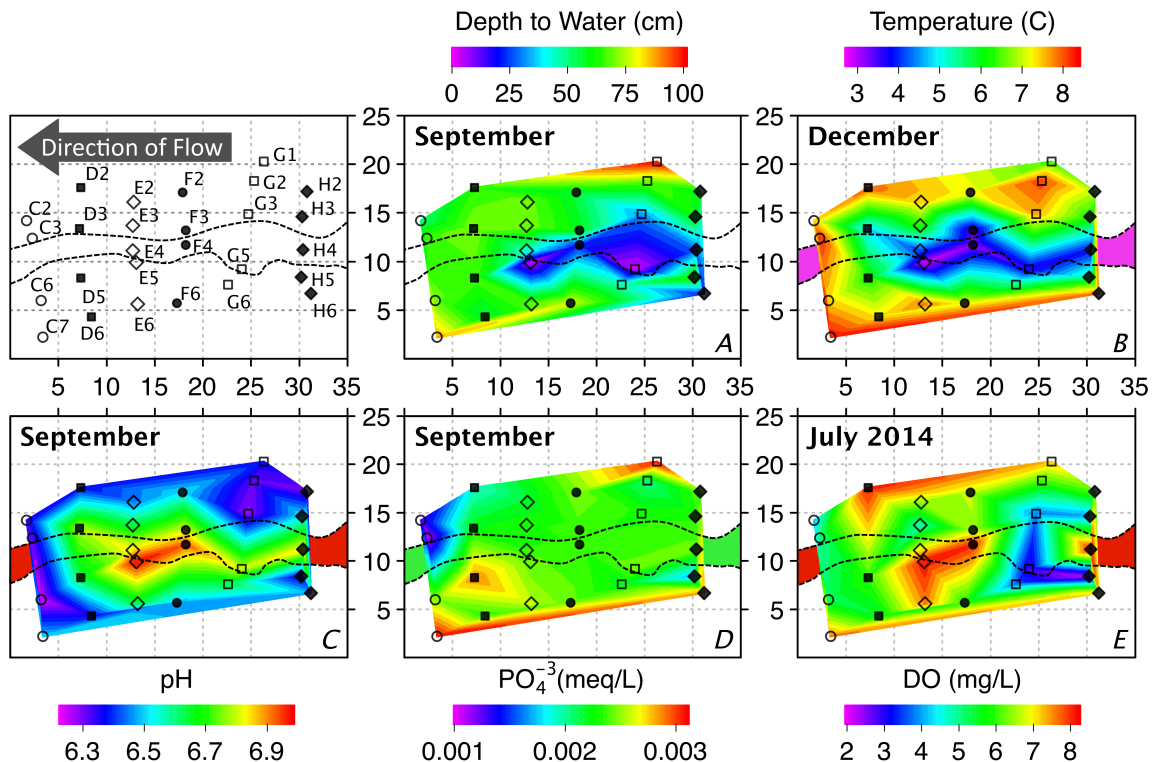


**Figure 2.6** – Spatial patterns in the depth to water (A), pH (C), and PO<sub>4</sub><sup>-3</sup> (D) within the well network in September. Spatial distribution of subsurface temperatures in December (B). Dissolved oxygen concentrations in the subsurface as measured in July 2014 (E; Serchan, unpublished data, 2014). All data for the subsurface are represented in the contoured grid. Stream values for the same sampling run are shown within the stream outline at the edges of the grid. Well locations are given in the upper left panel, and match the orientation of Figure 2.1. The stream flows from right to left.

### 2.5.4 Model results

The manual stepwise regression generated 16 three-term models for DOC in September and 25 three-term models for DOC in November. Spatial autocorrelation was not present for DOC models in either month. The initial DIC models that we generated for September and November showed spatial autocorrelation, so we redid the manual stepwise regression with a Gaussian spatial autocorrelation structure. This resulted in 48 models for DIC in September and 16 models for DIC in November. We present a selection of models here, highlighting key variables and the relative ranking of models for each month (Tables 2.2, 2.3, 2.6, 2.7). A full list of all models can be found in Corson-Rikert (2014), Appendix A.

**Table 2.2** - DOC models for September. Models are ranked based on the associated AIC values. Adjusted  $r^2$  are given since the models include three terms.

September DOC Models				
16 Models	Rank	Variables	AIC	$r^2a$
Top 5 models	1	PO <sub>4</sub> <sup>-3</sup> , pH, Ca <sup>+2</sup>	-202.2	0.769
	2	PO <sub>4</sub> <sup>-3</sup> , Total Alkalinity, Mg <sup>+2</sup>	-201.1	0.760
	3	PO <sub>4</sub> <sup>-3</sup> , Ca <sup>+2</sup> , Travel Time	-200.6	0.756
	4	PO <sub>4</sub> <sup>-3</sup> , Ca <sup>+2</sup> , Mg <sup>+2</sup>	-200.3	0.753
	5	PO <sub>4</sub> <sup>-3</sup> , Ca <sup>+2</sup> , NO <sub>3</sub> <sup>-</sup>	-199.8	0.747
Other PO <sub>4</sub> <sup>-3</sup> models	6	PO <sub>4</sub> <sup>-3</sup> , Distance from stream, NO <sub>3</sub> <sup>-</sup>	-199.7	0.747
	10	PO <sub>4</sub> <sup>-3</sup> , Travel Time, Total Alkalinity	-197.8	0.729
Additional Models	11	NO <sub>3</sub> <sup>-</sup> , Distance from stream, SO <sub>4</sub> <sup>-2</sup>	-189.7	0.633
	12	NO <sub>3</sub> <sup>-</sup> , Temperature, Distance from stream	-187.1	0.596
	13	Travel Time, SO <sub>4</sub> <sup>-2</sup> , Ca <sup>+2</sup>	-185.5	0.572
	14	K <sup>+</sup> , Total Alkalinity, Mg <sup>+2</sup>	-183.8	0.544

We included AIC and an adjusted  $r^2$  value for the DOC models, which did not include spatial autocorrelation structures (Tables 2.2, 2.3). For the DIC models, we only present AIC values, as  $r^2$  cannot be computed for the generalized linear models that were used at each step of the manual stepwise regression to fit the Gaussian spatial correlation structure (Tables 2.6, 2.7). We have included matrices of Pearson's correlation coefficients and coefficients of determination for major variable pairs in November and September (Tables 2.4, 2.5)

**Table 2.3** – DOC models for November. Models are ranked based on the associated AIC values. Adjusted  $r^2$  are given since the models include three terms.

November DOC Models					
25 Models	Rank	Variables	AIC	$r^2a$	
Top 5 models	1	Temperature, $\text{Cl}^-$ , $\text{K}^+$	-171.2	0.7447	
	2	Temperature, $\text{K}^+$ , Anion Deficit	-170.9	0.742	
	3	Temperature, $\text{PO}_4^{3-}$ , Distance from stream	-170.3	0.7356	
	4	$\text{K}^+$ , $\text{SO}_4^{2-}$ , $\text{Cl}^-$	-169.5	0.7276	
	5	$\text{PO}_4^{3-}$ , $\text{SO}_4^{2-}$ , $\text{K}^+$	-168.8	0.7199	
Other $\text{PO}_4^{3-}$ models	8	$\text{PO}_4^{3-}$ , $\text{NO}_3^-$ , $\text{SO}_4^{2-}$	-166.2	0.6905	
	10	pH, $\text{PO}_4^{3-}$ , $\text{NO}_3^-$	-165.4	0.6808	
Additional Models	4	$\text{K}^+$ , $\text{SO}_4^{2-}$ , $\text{Cl}^-$	-169.5	0.7276	
	6	pH, $\text{Cl}^-$ , $\text{K}^+$	-168.4	0.7157	
	11	$\text{Cl}^-$ , Anion Deficit, $\text{K}^+$	-165.3	0.6795	

In September,  $\text{PO}_4^{3-}$  appeared in all of the best-supported models for DOC, and  $\text{Ca}^{+2}$  was often present (Table 2.2). Other cation species, total alkalinity, travel time, distance from the stream, and the nutrients  $\text{NO}_3^-$  and  $\text{SO}_4^{2-}$  were also significant explanatory variables. Concentrations of  $\text{Ca}^{+2}$  and total alkalinity were highly correlated in September ( $r = 0.91$ ,  $r^2 = 0.83$ ), and appear to be interchangeable (Tables 2.2, 2.4).

Travel time and distance from the stream were also interchangeable, as both provide spatial information and the two terms are moderately correlated ( $r = 0.65$ ,  $r^2 = 0.42$ ; Tables 2.2, 2.4).

**Table 2.4** – A matrix of Pearson's correlation coefficients ( $r$ , black text, below diagonal) and coefficients of determination ( $r^2$ , grey text, above diagonal) for major variable pairs in September

September Correlation Matrix															
	DOC	DIC	Alk	An Def	Ca <sup>+2</sup>	Cl <sup>-</sup>	Dist	K <sup>+</sup>	Mg <sup>+2</sup>	NO <sub>3</sub> <sup>-</sup>	pH	PO <sub>4</sub> <sup>-3</sup>	SO <sub>4</sub> <sup>-2</sup>	Temp	T T
<b>DOC</b>	0.01	0.00	0.05	0.00	0.10	0.38	0.40	0.04	0.37	0.04	0.58	0.12	0.05	0.21	
<b>DIC</b>	<b>-0.12</b>	0.03	0.01	<b>0.20</b>	<b>0.01</b>	<b>0.18</b>	<b>0.03</b>	<b>0.27</b>	<b>0.04</b>	<b>0.88</b>	<b>0.11</b>	<b>0.52</b>	<b>0.00</b>	<b>0.52</b>	
Alk	<b>-0.04</b>	<b>-0.17</b>	0.17	0.83	0.00	0.10	0.29	0.31	0.00	0.10	0.14	0.32	0.02	0.00	
An Def	<b>-0.23</b>	<b>0.08</b>	0.41	0.19	0.00	0.01	0.09	0.16	0.05	0.04	0.05	0.03	0.07	0.10	
Ca <sup>+2</sup>	<b>0.00</b>	<b>-0.45</b>	0.91	0.44	0.00	0.13	0.37	0.06	0.00	0.29	0.19	0.52	0.02	0.01	
Cl <sup>-</sup>	<b>0.32</b>	<b>-0.10</b>	0.05	0.07	<b>0.01</b>	0.08	0.09	0.01	0.00	0.01	0.09	0.00	0.29	0.06	
Dist	<b>-0.62</b>	<b>0.43</b>	-0.31	0.12	-0.36	<b>-0.29</b>	0.05	0.07	0.14	0.30	0.11	0.04	0.05	0.42	
K <sup>+</sup>	<b>-0.63</b>	<b>-0.16</b>	0.54	0.30	0.61	<b>-0.30</b>	<b>0.23</b>	0.05	0.37	0.03	0.64	0.40	0.04	0.10	
Mg <sup>+2</sup>	<b>-0.19</b>	<b>0.52</b>	0.56	0.40	0.25	0.10	0.26	<b>0.22</b>	0.00	0.17	0.00	0.01	0.00	0.31	
NO <sub>3</sub> <sup>-</sup>	<b>-0.61</b>	<b>0.19</b>	0.01	0.23	0.03	-0.01	0.38	0.61	0.05	0.08	0.20	0.04	0.11	0.21	
pH	<b>0.20</b>	<b>-0.94</b>	0.32	-0.19	0.54	0.08	-0.55	0.16	-0.41	-0.28	0.07	0.49	0.02	0.53	
PO <sub>4</sub> <sup>-3</sup>	<b>-0.76</b>	<b>-0.33</b>	0.38	0.22	0.44	-0.30	0.33	0.80	0.06	0.45	0.27	0.05	0.08	0.03	
SO <sub>4</sub> <sup>-2</sup>	<b>-0.34</b>	<b>-0.72</b>	0.57	0.17	0.72	0.06	-0.19	0.63	-0.11	0.19	0.70	<b>0.75</b>	0.03	0.08	
Temp	<b>0.22</b>	<b>0.05</b>	-0.13	0.26	-0.13	0.54	-0.23	-0.20	0.01	0.33	-0.14	-0.43	-0.23	0.03	
T T	<b>-0.46</b>	<b>0.72</b>	0.06	0.32	-0.12	-0.24	0.65	0.32	0.56	0.46	-0.73	0.18	-0.28	-0.16	

Pearson's Correlations ( $r$ )

Coefficient of Determination ( $r^2$ )

**Table 2.5** – A matrix of Pearson's correlation coefficients ( $r$ , black text, below diagonal) and coefficients of determination ( $r^2$ , grey text, above diagonal) for major variable pairs in November.

November Correlation Matrix															
	DOC	DIC	Alk	An Def	Ca <sup>+2</sup>	Cl <sup>-</sup>	Dist	K <sup>+</sup>	Mg <sup>+2</sup>	NO <sub>3</sub> <sup>-</sup>	pH	PO <sub>4</sub> <sup>-3</sup>	SO <sub>4</sub> <sup>-2</sup>	Temp	T T
<b>DOC</b>	0.10	0.03	0.34	0.00	<b>0.52</b>	<b>0.42</b>	<b>0.23</b>	<b>0.14</b>	<b>0.38</b>	<b>0.31</b>	<b>0.24</b>	<b>0.15</b>	<b>0.28</b>	<b>0.22</b>	
<b>DIC</b>	<b>-0.32</b>	0.09	0.24	0.12	<b>0.06</b>	<b>0.06</b>	<b>0.11</b>	<b>0.30</b>	<b>0.16</b>	<b>0.66</b>	<b>0.12</b>	<b>0.62</b>	<b>0.71</b>	<b>0.10</b>	
Alk	<b>0.16</b>	<b>-0.30</b>	0.03	0.90	0.03	0.26	0.02	0.00	0.03	0.66	0.12	0.19	0.14	0.41	
An Def	<b>-0.58</b>	<b>0.49</b>	-0.17	0.05	0.18	0.23	0.01	0.44	0.18	0.69	0.01	0.50	0.46	0.05	
Ca <sup>+2</sup>	<b>0.07</b>	<b>-0.34</b>	0.95	-0.22	0.00	0.18	0.12	0.01	0.06	0.27	0.12	0.31	0.18	0.23	
Cl <sup>-</sup>	<b>0.72</b>	<b>-0.25</b>	0.18	-0.42	<b>0.03</b>	0.22	0.20	0.00	0.10	0.14	0.26	0.04	0.10	0.15	
Dist	<b>-0.65</b>	<b>0.25</b>	-0.51	0.48	-0.43	<b>-0.47</b>	0.09	0.13	0.31	0.31	0.03	0.21	0.22	0.40	
K <sup>+</sup>	<b>-0.48</b>	<b>-0.33</b>	0.15	-0.11	0.35	<b>-0.45</b>	<b>0.30</b>	0.06	0.11	0.05	0.67	0.21	0.08	0.18	
Mg <sup>+2</sup>	<b>-0.37</b>	<b>0.55</b>	0.05	0.66	-0.12	-0.04	0.36	<b>-0.24</b>	0.29	0.35	0.07	0.56	0.53	0.00	
NO <sub>3</sub> <sup>-</sup>	<b>-0.62</b>	<b>0.40</b>	0.17	0.42	0.24	-0.31	<b>0.56</b>	<b>0.33</b>	<b>0.54</b>	0.18	0.03	0.14	0.20	0.11	
pH	<b>0.56</b>	<b>-0.81</b>	-0.81	-0.83	0.52	0.38	-0.56	0.22	-0.59	-0.42	0.02	0.76	0.74	0.22	
PO <sub>4</sub> <sup>-3</sup>	<b>-0.49</b>	<b>-0.34</b>	-0.34	0.08	0.35	-0.51	0.18	0.82	-0.27	0.17	0.13	0.18	0.07	0.13	
SO <sub>4</sub> <sup>-2</sup>	<b>0.39</b>	<b>-0.79</b>	0.44	0.71	0.56	0.21	-0.46	0.46	-0.75	-0.38	0.87	<b>0.42</b>	0.79	0.07	
Temp	<b>-0.53</b>	<b>0.84</b>	-0.37	0.68	-0.43	-0.32	0.47	-0.28	0.73	0.45	-0.86	-0.27	<b>-0.89</b>	0.12	
T T	<b>-0.47</b>	<b>0.32</b>	-0.64	0.22	-0.48	-0.39	0.63	0.42	-0.01	0.33	-0.47	0.36	-0.27	0.34	

Pearson's Correlations ( $r$ )

Coefficient of Determination ( $r^2$ )

The variable  $\text{PO}_4^{3-}$  remained an important explanatory variable for DOC in November, but temperature,  $\text{K}^+$ , and  $\text{SO}_4^{2-}$  also appeared more often within the top five models (Table 2.3). The variables  $\text{Ca}^{+2}$  and total alkalinity no longer showed up as significant explanatory variables. The increased appearance of  $\text{Cl}^-$  and the correlation between DOC and  $\text{Cl}^-$  in November ( $r = 0.72$ ,  $r^2 = 0.52$ ) suggest that  $\text{Cl}^-$  concentrations may be associated with a seasonal driver of hyporheic DOC concentrations (Table 2.3). In November, pH was strongly correlated with  $\text{SO}_4^{2-}$  ( $r = 0.87$ ,  $r^2 = 0.76$ ) and anion deficit ( $r = -0.83$ ,  $r^2 = 0.69$ ) and appeared interchangeably with both in several models (Tables 2.3, 2.5).

**Table 2.6** – DIC models for September. Models are ranked based on the associated AIC values.  $r^2$  cannot be computed for general linear models fit with the 'nlme' package in R.

September DIC Models			
(with Gaussian spatial autocorrelation structure)			
48 Models	Rank	Variables	AIC
Top 5 models	1	pH, $\text{Mg}^{+2}$ , $\text{SO}_4^{-2}$	-73.9
	2	pH, $\text{Mg}^{+2}$ , $\text{PO}_4^{-3}$	-73.0
	3	$\text{SO}_4^{-2}$ , Total Alkalinity, pH	-72.7
	4	pH, Anion Deficit, Total Alkalinity	-67.9
	5	pH, $\text{Mg}^{+2}$ , Anion Deficit	-66.3
Other pH models	6	$\text{Ca}^{+2}$ , Total Alkalinity, pH	-64.2
	9	pH, Depth to Water, $\text{SO}_4^{-2}$	-58.4
Other $\text{SO}_4^{-2}$ models	8	$\text{SO}_4^{-2}$ , DOC, $\text{Cl}^-$	-62.0
	11	$\text{SO}_4^{-2}$ , Total Alkalinity, DOC	-57.2
Other $\text{PO}_4^{-3}$ models	12	$\text{PO}_4^{-3}$ , Travel Time, pH	-55.1
	22	$\text{PO}_4^{-3}$ , $\text{NO}_3^-$ , $\text{Mg}^{+2}$	-47.1
Additional Models	32	$\text{Mg}^{+2}$ , $\text{Na}^+$ , $\text{K}^+$	-38.0
	37	$\text{Mg}^{+2}$ , $\text{Na}^+$ , DOC	-32.9
	44	$\text{Ca}^{+2}$ , Total Alkalinity, Anion Deficit	-27.0

The variable pH appeared in almost all of the top models for DIC in both September and November (Tables 2.6, 2.7). DIC was highly correlated with pH in September ( $r = -0.94$ ,  $r^2 = 0.88$ ), and November ( $r = -0.81$ ,  $r^2 = 0.66$ ), just as it was over

the full study period (Tables 2.4, 2.5; Figure 2.3F). If CO<sub>2</sub> produced via respiration is the primary source of DIC to hyporheic waters, its production would both increase DIC and decrease pH, leading to the observed negative relationship between DIC and pH. In September, Mg<sup>+2</sup>, total alkalinity, anion deficit, and SO<sub>4</sub><sup>-2</sup> were also important explanatory variables for DIC (Table 2.6). The variables PO<sub>4</sub><sup>-3</sup>, DOC, lnK<sub>sat</sub>, depth to water, and Ca<sup>+2</sup> also appeared in models with lower AIC rankings.

**Table 2.7** - DIC models for November. Models are ranked based on the associated AIC values.  $r^2$  cannot be computed for general linear models fit with the ‘nlme’ package in R.

<b>November DIC models</b>			
(with Gaussian spatial autocorrelation structure)			
<b>16 Models</b>	<b>Rank</b>	<b>Variables</b>	<b>AIC</b>
Top 5 Models	1	SO <sub>4</sub> <sup>-2</sup> , Mg <sup>+2</sup> , Cl <sup>-</sup>	-74.8
	2	pH, Anion Deficit, Total Alkalinity	-68.3
	3	SO <sub>4</sub> <sup>-2</sup> , Mg <sup>+2</sup> , Temperature	-64.8
	4	pH, Anion Deficit, Distance from stream	-61.5
	5	pH, Temperature, Anion Deficit	-56.3
Other pH models	7	pH, Temperature, Mg <sup>+2</sup>	-53.7
	15	pH, Temperature, Distance from stream	-42.6
Cl <sup>-</sup> Models	6	K <sup>+</sup> , Cl <sup>-</sup> , lnK <sub>sat</sub>	-55.2
	8	K <sup>+</sup> , Cl <sup>-</sup> , Travel Time	-53.6
Additional Models	10	K <sup>+</sup> , Travel Time, DOC	-49.5
	12	Total Alkalinity, Distance from stream, SO <sub>4</sub> <sup>-2</sup>	-47.8

In November, the high correlation between SO<sub>4</sub><sup>-2</sup> and pH ( $r = 0.87$ ,  $r^2 = 0.76$ ) led SO<sub>4</sub><sup>-2</sup> to replace pH in several of the top models for DIC (Tables 2.5, 2.7). As with DOC, temperature and Cl<sup>-</sup> appeared as explanatory variables for DIC in November (Table 2.7). The correlation between DIC and temperature was strong ( $r = 0.84$ ,  $r^2 = 0.71$ ) in November in comparison to the very weak correlation ( $r = 0.05$ ,  $r^2 = 0.0$ ) in September (Tables 2.4, 2.5). Total alkalinity appeared to be less important than in September (Table 2.7). Travel time, K<sup>+</sup>, lnK<sub>sat</sub>, and distance from stream appeared in less supported models.

## 2.6 Discussion

### 2.6.1 Carbon dynamics as a function of median travel times

As an initial tool for understanding the dynamics of carbon processing within the WS1 hyporheic zone, we investigated the degree to which median travel time explained concentrations of DIC and DOC throughout the well network (Figures 2.3B, 2.3D). This decision was motivated by previous research on gravel bar hyporheic systems in Drift Creek, Oregon (Zarnetske et al., 2011) and Dutchess County, New York (Findlay et al., 1993). These studies demonstrated that source-sink nitrate dynamics (Zarnetske et al., 2011) and patterns of carbon metabolism (Findlay et al., 1993) within the hyporheic zone were a function of median residence time. In our system, DOC was converted and/or removed with increasing travel time and DIC concomitantly increased, likely as a result of microbial respiration of DOC (Figures 2.3B, 2.3D; Findlay et al., 1993). However, the increase in DIC with residence time was approximately ten times larger than the decrease in DOC, far too large to be explained by the conversion of stream DOC (Figure 2.3D). This suggests that there are additional sources of DIC and/or DOC in the subsurface, and that hyporheic DIC concentrations are not well linked to stream-source DOC. Using concurrent measurements of dissolved oxygen, Findlay et al. (1993) concluded that microbial DIC production in the gravel bar was due in equal parts to metabolism of stream water and metabolism of sediment particulate organic matter. The only other potential sources of DIC identified by Findlay et al. (1993) were carbonate dissolution and anaerobic respiration.

In an effort to quantify the unexplained DIC observed in the WS1 hyporheic zone, we computed “excess” DIC as the difference between the magnitude of DIC gained in the subsurface and the magnitude of DOC lost, with stream concentrations of DOC and DIC representing initial end members. The resulting values, when regressed against travel time, do not show any clear pattern. Thus, although “excess” DIC is clearly present, its presence is not well related to travel time, suggesting that additional factors other than subsurface residence time are influencing DIC concentrations within the WS1 hyporheic zone. Perhaps this should be expected given the complexity of this system and the heterogeneity of the subsurface environment in WS1.

The research conducted by Zarnetske et al. (2011) was markedly different from ours in that their hyporheic zone was in an unvegetated gravel bar deposit inset into a channel that was incised into a clay layer, which prevented inputs of groundwater and lateral inputs of soil water. Further, their study was conducted during summer baseflow conditions only, no precipitation occurred during the study period, and all hyporheic zone flow paths originated at the head of a single riffle. Under these conditions hyporheic flow paths were clearly defined, and did not mix with either water leached vertically through the soil profile or lateral inputs of soil water, or with long-residence time groundwater. This allowed relationships between residence times and reduction-oxidation reactions to be clearly arranged along hyporheic flow paths. The hyporheic system studied by Findlay et al. (1993) was also hydrologically simple, and was sampled only during July, August, and September. Our study occurred under more varied hydrologic and climatic conditions in a much more complex environment, and was conducted over a nine-month period. It is

therefore reasonable to expect that a significantly different set of mechanisms and processes would influence geochemical relationships within the WS1 hyporheic zone.

### 2.6.2 Modeled relationships

In order to explore potential indicators and drivers of carbon dynamics within the WS1 hyporheic zone, we performed manual stepwise regressions in R and MATLAB and identified statistically significant models that explained concentrations of DOC and DIC in September and November. In both months, the models for DIC that were best supported by our data (e.g., had the lowest AIC values) represented relationships between DIC and measured variables that we expected, given geochemical processes or known correlations. For example, pH appeared in nearly all of the best-supported models for DIC in both months, likely because CO<sub>2</sub> inputs increase DIC and lower the pH of hyporheic water in the WS1 network (Tables 2.6, 2.7). This is evident in September, when we observed low pH values in wells that had the highest concentrations of DIC (Figures 2.5B, 2.6C). In November, SO<sub>4</sub><sup>-2</sup> stood in place of pH in many models, likely because of the high correlation between the two terms (Table 2.7). These results suggest that CO<sub>2</sub> exerts strong influence over carbonate geochemistry in this system, but they do not provide any information about what mechanisms or processes may be associated with CO<sub>2</sub> (and therefore DIC) production.

For DOC, the picture is even less clear. In September, the strongest ten DOC models all include PO<sub>4</sub><sup>-3</sup> as an explanatory variable, and in November, while PO<sub>4</sub><sup>-3</sup> appears less consistently within the top five models, it is present in all but a handful of the remaining 20 models. Concentrations of PO<sub>4</sub><sup>-3</sup> are negatively correlated with DOC

concentrations (and DIC concentrations) in both months (Tables 2.4, 2.5). It is possible that  $\text{PO}_4^{3-}$  is released as POM is processed or is released through the reduction of iron and manganese oxides, but we are not confident in either of these hypotheses. Individual regressions of DOC vs.  $\text{PO}_4^{3-}$  in both September and November suggest that a handful of outliers may be distorting this relationship. In September, locally high and low values of  $\text{PO}_4^{3-}$  are clearly visible within the well network (Figure 2.6). These high  $\text{PO}_4^{3-}$  concentrations occur along the hillslope boundary, and the geochemistry of at least one such toe-slope well (D7) appears to be influenced by groundwater inputs. While these inflows are too small to influence subsurface flow paths (Wondzell 2006; Wondzell et al., 2009), they may influence water chemistry through inputs of high  $\text{PO}_4^{3-}$  and low DOC water.

The models do indicate important seasonal differences for both DOC and DIC dynamics within the WS1 hyporheic zone. In November, a number of top models for DOC and DIC include temperature. This is a bit puzzling, as temperature ranges by only two degrees over the well network (Figure 2.3A), but suggests that the processes influencing carbon metabolism and respiration in November are sensitive to temperature fluctuations within this range. Alternatively, temperature may be correlated with some other controlling variable, such as water source, that we were unable to measure. The model results also indicate that DOC concentrations are associated with high  $\text{Cl}^-$  concentrations, suggesting that soil DOC may be mobilized and transported into hyporheic waters as a result of vertical infiltration of precipitation. We did observe similar seasonal patterns in DOC and  $\text{Cl}^-$  and a strong correlation between DOC and  $\text{Cl}^-$  in November (Figures 2.3A, 2.3B; Table 2.5).

If we consider less supported models for DOC and DIC, some consistent patterns emerge. Terms that relate information regarding the length of flow paths (e.g. median travel time, and distance from stream) appeared amongst DOC and DIC models with lower AIC values in both months. Together with direct correlations (Tables 2.6, 2.7), this suggests that DOC metabolism and DIC production scale with residence time. Rates of water movement and water table height appear to be less important than we expected, as saturated hydraulic conductivity, sampling depth, and depth to water appear only occasionally in significant models, and only for DIC models (Tables 2.6, 2.7). The variables  $\text{PO}_4^{3-}$ ,  $\text{SO}_4^{2-}$ ,  $\text{Mg}^{+2}$ , and  $\text{K}^+$  appear often within models for both response variables in September and November (Tables 2.2, 2.3, 2.6, 2.7). However, we have no explanation for why variations in the concentration of these anions and cations would account for carbon dynamics within the WS1 subsurface, particularly given that these species are present in relatively low concentrations. It is difficult to know if the magnitude and range of observed concentrations are in fact geochemically significant or if the terms are statistically significant solely because of sample variation.

Ultimately, while the model analysis did bring to light some expected and unexpected (and unexplained) relationships, it produced no clear mechanistic explanation for observed carbon dynamics within the WS1 hyporheic zone. The only exception is additional indication that vertical infiltration may be an important source of DOC to the hyporheic zone during the rainy season, even during baseflow periods between storms. However, the model analysis does provide some general insight into the functioning of this hyporheic system. As we noted in the analysis using median travel times, hyporheic DOC and DIC dynamics are less coupled than we expected. This suggests that although

inorganic and organic carbon dynamics are linked through metabolism, additional processes and mechanisms may be influencing concentrations of DOC and DIC in hyporheic water. In order to better understand hyporheic carbon dynamics within WS1, we must therefore consider multiple sources and sinks of organic and inorganic carbon to hyporheic waters and potential controls on and drivers of carbon processing within this complex subsurface environment.

### *2.6.3 System considerations – Hydrologic sources of DOC and DIC*

#### *2.6.3.1 Groundwater inputs*

The magnitude of groundwater inputs to subsurface flow within the Watershed 1 well network remains poorly understood. Attempts to model hyporheic exchange during baseflow periods using MODFLOW have achieved good results by assigning no-flow conditions along the hillslope boundary and the bedrock-colluvium interface beneath the well network (Kasahara & Wondzell, 2003; Wondzell et al., 2009). The insensitivity of these models to groundwater inputs in Watershed 1 suggests that such inputs, if present, are relatively small. However, during the summer baseflow period in which we sampled, water temperatures in five wells located along the toe slope of adjacent hills were substantially lower than concurrent temperatures in the stream and most of the stream network. Additionally, we observed localized zones of high  $\text{PO}_4^{3-}$  and low DOC hyporheic water along the margins of the well network that persisted throughout the study period (Figures 2.5A, 2.5D, 2.6D). Previous work has shown that diel fluctuations in stream temperature do not propagate into the well network and that in hyporheic

locations with residence times greater than 12 – 15 hours, water temperatures are equivalent to stream temperatures averaged over the preceding several days (Wondzell, 2012). Consequently, low temperatures in these wells most likely result from inputs of colder groundwater. Based on simple mixing, we can estimate what percentage of all flow past a given well would need to be comprised of groundwater in order to explain the observed temperatures:

$$T_H = T_S \cdot Q_s + T_{gw} \cdot Q_{gw} \quad \text{Eq. 2.16}$$

Where  $Q_s$  is the portion of hyporheic flow that originates from the stream,  $Q_{gw}$  is the portion of hyporheic flow that originates from groundwater,  $T_H$  is the temperature of the hyporheic water,  $T_S$  is the temperature of the stream, and  $T_{gw}$  is the temperature of the groundwater.

To use this approach, we must assume that hyporheic water is composed entirely of stream- and ground- water and that during baseflow periods, groundwater temperatures equal the mean annual air temperature, which from 1996 to 2014 averaged 8.1 °C at lower elevations in the H.J. Andrews. We also must ignore conduction from overlying sediment and heat exchange between hyporheic water and sediment within the hyporheic zone. Given that the well network is well shaded, we expect that conduction of heat from overlying sediment will be small, particularly in comparison to advective heat transfer. Heat exchange within the saturated sediment is important, but over a longer period with more or less stable air temperatures, subsurface soil and water temperatures would be expected to converge toward multi-week average temperatures. If these assumptions

hold, then persistent cold-temperature anomalies during the late summer baseflow period should indicate groundwater intrusion.

If we treat  $Q_S$  and  $Q_{gw}$  as proportions that sum to 1, then  $Q_S = 1 - Q_{gw}$ , so that:

$$T_H = T_S \cdot Q_S + T_{gw} \cdot Q_{gw} \quad \text{Eq. 2.17}$$

$$Q_{gw} = \frac{T_H - T_S}{T_{gw} - T_S} \quad \text{Eq. 2.18}$$

Calculated percentages of groundwater in the five wells ranged from 30% - 60% during August and September. This suggests that groundwater may be strongly influencing temperature and water chemistry at these wells, particularly if solute chemistry is significantly different from stream and hyporheic water. These percentages are surprising, given previous success in modeling hyporheic flow and head gradients in WS1 with no groundwater input (Wondzell et al., 2009). However, further efforts to model solute transport found that models that best predicted head values within the well network poorly fitted observed travel times from the 1997 tracer test (Wondzell et al., 2009). No models were developed that could accurately predict solute transport in more than a portion of the well network (Wondzell et al., 2009). Additionally, estimates of  $Q_{HEF}$  varied widely amongst all final models (Wondzell et al., 2009). Although the lack of fit may have resulted from an insufficiency of hydraulic and geomorphic data, these results, together with the observed temperature discrepancies in summer 2013 and geochemical patterns throughout the study period, suggest that groundwater inflows, even if they are small and do not re-arrange the subsurface flow net, may be sufficiently large to augment flow and influence rates of solute transport within the WS1 hyporheic zone. If this is the case, characterizing the chemistry of deep groundwater and identifying local

zones of groundwater inflow will be a crucial step in further constraining the dynamics of geochemical processes within this hyporheic environment (Figure 2.7).

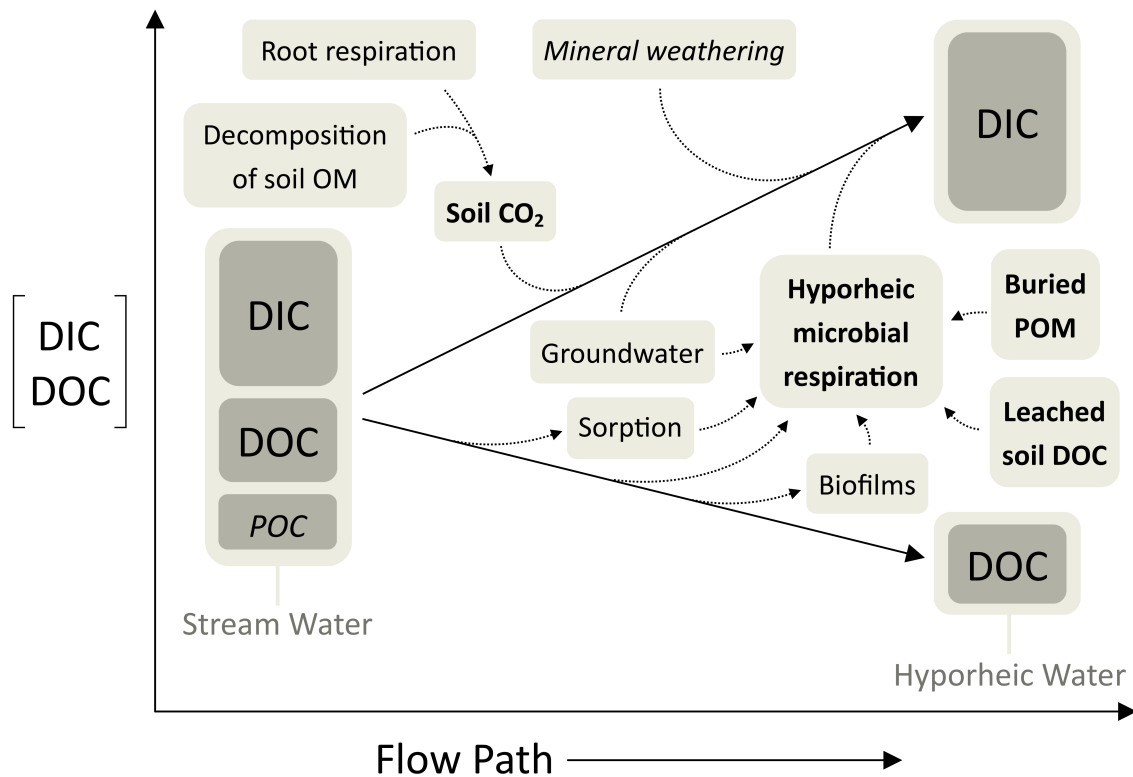


**Figure 2.7** – A schematic of observed solute dynamics in the stream and WS1 hyporheic zone. Potential hydrologic and biogeochemical sources and sinks of DOC and DIC to the WS1 hyporheic zone during baseflow periods are shown in light grey boxes. The sources that we expect are the most likely explanation for observed excess DIC concentrations are presented in bold text, while sources that we expect are insignificant are presented in italic text. Potential sources of which we do not know the magnitude or relative importance are presented in standard text.

#### 2.6.3.2 Hillslope inputs

The importance of hillslope connectivity and the impact of lateral inflows on hyporheic exchange flow within any specific study period is dependent upon antecedent precipitation, soil moisture deficits, and the extent of hillslope area that drains to the stream reach in question (Wondzell, 2006; Jensco et al., 2010). Research during storm

events indicates that hillslopes in WS1 are not hydrologically connected to riparian zones unless soil moisture deficits in hillslope soils are satisfied (Hood et al., 2006). As a result of this work, we do not expect hillslope water to strongly influence hyporheic exchange flows or biogeochemical cycling during baseflow periods.

#### 2.6.3.3 *Vertical infiltration of precipitation*

Increased concentrations of  $\text{Cl}^-$  during fall and winter months suggest that either rainwater percolates to the hyporheic zone in sufficient quantities to alter hyporheic water chemistry or that the infiltrating water flushes soils of salts that accumulated during the summer dry period (Figure 2.4A). In either case, vertical infiltration would represent an important pathway for solute delivery to the riparian hyporheic zone during these months. Lower concentrations of major cations during the wet season would support this hypothesis, as the weathered soils of WS1 would be expected to produce a low flux of cation species in comparison to deeper groundwater sources (Figure 2.4C). We did observe higher concentrations of DOC during this same period and a strong positive correlation ( $r = 0.72$ ,  $r^2 = 0.52$ ) between DOC and  $\text{Cl}^-$  (Figure 2.4B; Table 2.5). Modeling results for November indicated increased association between DOC and DIC concentrations and  $\text{Cl}^-$  (Tables 2.3, 2.7). Seasonal flushing of accumulated DOC from soil horizons by infiltrating rainwater may be an important mechanism for DOC delivery to WS1 hyporheic waters (Figure 2.7). This flushing hypothesis is supported by observed peaks in DOC and  $\text{Cl}^-$  during November, and lower concentrations of both solutes in December and March (Figures 2.4A, 2.4B). This late-season reduction in DOC could also be linked to colder soil temperatures and decreased rates of soil metabolic processes.

#### *2.6.4 System considerations – Biogeochemical sources/sinks of DOC and DIC*

Microbial respiration in hyporheic sediments under aerobic and anaerobic conditions has long been recognized as an important contributor to community respiration in stream ecosystems (Grimm and Fisher, 1984; Findlay et al., 1993; Pusch, 1996; Mulholland et al., 1997; Boulton et al., 1998; Battin et al., 2003). We expect that it is extremely important in WS1, and that the high concentrations of DIC in hyporheic waters in WS1 result from microbial respiration of DOC (Figure 2.7). However, this is an open system, and both soil and root respiration may be important contributors of DIC to the WS1 hyporheic system (Figure 2.7; Butman and Raymond, 2011; Tsyplkin and Macpherson, 2012). We do not currently have any way to quantify respiration by riparian vegetation or estimate rates of diffusion of CO<sub>2</sub> from the atmosphere of unsaturated soils into hyporheic zone water.

Another potential source of DIC to the hyporheic zone is the production of bicarbonate through mineral weathering of carbonates and aluminosilicates (Findlay et al., 1993). No carbonates are present in regional bedrock, thus hydrolysis of carbonate minerals is not a plausible source of DIC (Swanson and James, 1975). Soils in WS1 are developed from highly weathered breccias and tuffs and basalt flows, and thus do not contain significant quantities of aluminosilicates (Swanson and James, 1975). As such, we do not expect that aluminosilicate mineral weathering is a source of bicarbonate to the WS1 hyporheic zone (Figure 2.7; Rothacher et al., 1967; Swanson and James, 1975). This conclusion is supported by strong correlations between DIC and pH in all sampling months, which indicate that CO<sub>2</sub> is the primary source of DIC to WS1 hyporheic waters.

Adsorption of DOC to clays and iron and aluminum oxides has been recognized as a potentially important mechanism for DOC removal from water moving through soils (McDowell, 1985; Findlay et al., 1993; Liu et al., 2014). Adsorption is greater under oxic conditions and at low pH (Liu et al., 2014). We did not measure iron or aluminum concentrations, but the pH of hyporheic water ranges from 6-7 and point measurements indicate that hyporheic water is generally oxic (Serchan, unpublished data, 2014). In addition, WS1 soils are classified as gravel clay loam (Rothacher et al., 1967).

Adsorption may therefore be a mechanism for DOC removal in the hyporheic zone of WS1 (Figure 2.7). However, desorption of adsorbed DOC would reverse this process, and could in turn represent a source of DOC to hyporheic microbes. DOC may also be removed and stored in subsurface biofilms (Figure 2.7; Battin, 1999). Eventually, this stored DOC may be metabolized, producing DIC. It is difficult to constrain the magnitude and timescale of these DOC removal processes. However, the observed accumulation of DIC along subsurface flow paths within WS1 may indicate that the loss of DOC via adsorption or storage is unimportant in comparison to biotic consumption of DOC (Findlay et al., 1993). We may also be underestimating the amount of “excess” DIC if all stream-source DOC is adsorbed, but the error introduced by this would be small given that stream DOC concentrations are an order of magnitude smaller than observed DIC concentrations.

In small headwater mountain streams like WS1, inputs of terrestrial allochthonous material are the primary source of organic material to aquatic ecosystems. While stream water may transport significant quantities of particulate organic matter into the hyporheic zone during storm events, point measurements of particulate organic carbon (POC) in

WS1 stream water during baseflow periods indicate that POC is below detection limits or present only in very small amounts (Figure 2.7; Corson-Rikert, unpublished data, 2013). However, even if the stream does not transport POC into the hyporheic zone during baseflow conditions, buried pockets of organic matter, such as leaves or logs, likely exist in the subsurface, and roots are certainly present. If conditions are oxic, microbial conditioning of buried POC could be an important source of DOC to WS1 hyporheic waters (Figure 2.7; Findlay et al., 1993). Research in other forested ecosystems has shown that soil organic matter is a source of DOC to hyporheic waters and drives respiration in hyporheic sediments (Hedin, 1990; Findlay et al., 1993; Gurwick et al., 2008; Crocker and Meyer, 2014).

### *2.6.5 System considerations – Drivers and controls on carbon processing*

The influence of hyporheic biogeochemical processes on the function of a stream ecosystem depends upon three factors: 1) The proportion of total streamflow that is routed through the subsurface via hyporheic exchange flows ( $Q_{HEF}:Q_{Stream}$ ) 2) the residence-time distribution of hyporheic water within the subsurface, and 3) the time-scale of the reactions that are occurring within the subsurface environment (Findlay, 1995; Battin et al., 2008; Wondzell, 2011).

#### 2.6.5.1 Rates of hyporheic exchange

In Watershed 1, the well network is situated in a stream reach that is unconstrained in comparison to reaches immediately above and below. As a result, hyporheic exchange occurs at a range of timescales and extends through a broad area, and may be influenced by changes in discharge, inflows from adjacent hillslopes, and lateral

inputs of soil- (hillslope-) and ground- water. Hydrologic studies focused on Watershed 1 have used conservative tracers, groundwater flow models, and direct well observations and sampled both baseflow and storm periods in an effort to understand and simulate hyporheic exchange flow (HEF) within the study reach (Kasahara & Wondzell, 2003; Wondzell, 2006; Wondzell et al., 2009; Voltz et al., 2013; Ward et al., 2013).

Groundwater flow models estimate that during baseflow periods, 76% of streamflow passes through the hyporheic zone along a 100 m reach of Watershed 1 (Kasahara and Wondzell, 2003). Consequently, hyporheic flows in Watershed 1 are sufficiently large to change the bulk properties of stream water. Nonetheless, if the magnitude of both  $Q_{HEF}$  and  $Q_{Stream}$  changes seasonally and during storms, this would change  $Q_{HEF}:Q_{Stream}$  and the relative influence of hyporheic zone biogeochemical processes on whole-stream chemistry.

As stream stage increased from low to high baseflow discharge, Wondzell (2006) found no statistically significant difference in water table elevations or lateral hydraulic gradients from hillslopes to the stream, despite significant increases in horizontal hydraulic gradients through stream banks (Wondzell, 2006). Steep down-valley hydraulic gradients also persist across the range of studied discharges and are present even during storm events (Wondzell, 2006; Voltz et al., 2013; Ward et al., 2013). Based on this work, rates and patterns of hyporheic flow within the Watershed 1 well network do not appear to be substantially affected by seasonal or storm-related changes in discharge. Even if  $Q_{HEF}$  is consistent through the year, however,  $Q_{Stream}$  changes seasonally. As a result, hyporheic exchange in Watershed 1 is proportionally less significant and has less

potential to alter the bulk properties of stream water in winter or during storms, when discharge is elevated.

#### 2.6.5.2 Residence time of WS1 hyporheic water

The residence time distribution of hyporheic water within the Watershed 1 well network is moderately well constrained. Conservative tracer experiments were conducted over five-day periods in late summer 1997, and early summer 1998, capturing low and high baseflow discharges, respectively (Wondzell, 2006). The electro-conductivity (EC) data from the wells and the stream that were collected during these tracer injections indicate that median travel times (defined as the time to reach one half of the plateau EC concentration) range from 18 – 68 hours within the well network (Wondzell, unpublished data, 1997). The data are not corrected for in-stream travel times, which may introduce uncertainty into the travel times computed for near-stream wells.

The morphology of the stream channel has been altered by large storm events between 1997 and today, and these changes would be expected to impact rates of exchange to near-stream wells. To a degree, the pattern of infiltration of cold stream water into the WS1 hyporheic zone in December was consistent with the 1997 median travel times for a handful of low travel time wells (Figure 2.3A), but when viewed spatially, the data also indicate that the travel time of other wells may have changed (Figures 2.5C, 2.6B). For example, wells C2 and C3 had low median travel times in 1997 (Figure 2.5C), but remain warm in December (Figure 2.6B). We expect that median travel times to these wells have increased since 1997, as a log located between wells C3 and C6 (Figure 2.1) has breached since that time. The 40 cm of sediment that had

accumulated behind the log washed away after it was breached, and the stream is currently scoured to bedrock at this point. We expect that today, without the log step to drive hyporheic flow into the region around wells C2 and C3, the hyporheic water that reaches these wells follows long residence-time down-valley flow paths. Current research efforts are focused on rebuilding the well network and conducting new tests to determine current median travel times at a range of baseflow discharges.

#### 2.6.5.3 Timescales of subsurface reactions

It is difficult to pinpoint any one “reaction rate” for subsurface processes that influence carbon dynamics, as there are many different “reactions” of interest that occur throughout the subsurface, including microbial decomposition of organic matter, sorption, biofilm production, and thermal cooling. Furthermore, what we are truly interested in is how these reactions and their rates interact with the two factors discussed above,  $Q_{HEF}$ : $Q_{Stream}$  and residence time, and how such interactions may influence the timescale on which these reactions change the bulk properties of hyporheic water (Findlay, 1995; Wondzell, 2011).

If  $Q_{HEF}$  does vary, increased  $Q_{HEF}$  could increase the supply of both nutrients and DOC to the hyporheic zone, accelerating microbial decomposition and respiration. Alternatively, the increased flux of stream water could effectively dilute concentrations of reactants or products of in-situ biogeochemical reactions (for example microbial respiration), lessening the proportional effects of hyporheic reactions. This dilution may be most influential along short residence-time flow paths and at the proximal, near-stream end of longer hyporheic flow paths (Findlay et al., 1993). At longer residence

times, the influence of dilution is less and the products of subsurface processes may gradually accumulate along flow paths. In this case, hyporheic water that has a long residence time may be the most altered, and may exert the most influence upon stream water chemistry upon return to the stream channel (Poole et al., 2008).

An additional factor is water temperature, which we expect to determine the kinetic rate of subsurface reactions. The temperature of hyporheic exchange flows may vary both seasonally, in response to shifts in air temperature, and through space, given the potential for subsurface transport and groundwater inflows to alter the temperature of hyporheic water. In general, subsurface water temperatures varied little throughout the well network within a given sampling period (Figure 2.2A). The exception was December, when cold stream water infiltrated into near stream wells with short median travel times (Figures 2.2A, 2.6B). Water temperatures in wells with long median travel times remained constant (Figures 2.2A, 2.6B). This is consistent with previous research on hyporheic temperature fluctuations in WS3 of the H.J. Andrews, where a diurnal temperature signal in the stream was progressively damped as residence time in the subsurface increased, such that the diurnal signal was not observed in long-residence time ( $\sim > 24$  hour) wells (Wondzell, 2012). Given the relatively small range in hyporheic water temperatures within individual sampling periods, we would not expect temperature to alter rates of hyporheic processes on short timescales. In contrast, over longer periods, we would expect that seasonal shifts in subsurface temperatures would influence subsurface carbon metabolism, and could explain observed high DIC production in warm summer months (Figure 2.4D; Pusch and Schwoerbel, 1994; Yvon-Durocher et al., 2012). Nonetheless, model results for November (Tables 2.3, 2.7) indicate that within a

single sampling run, observed carbon dynamics may be strongly associated with fluctuations in subsurface water temperatures of even 2 °C.

An important component of, and potential control on, subsurface metabolic processes are concentrations of dissolved oxygen (Findlay et al., 1993). We were unable to measure dissolved oxygen concentrations during our study due to instrument limitations, but a small set of measurements indicated that bulk hyporheic waters in WS1 were oxic (Corson-Rikert, unpublished data, 2013). These measurements are consistent with recent measurements of the full well network (Serchan, unpublished data, 2014). However, there was relatively high spatial variation in dissolved oxygen concentrations (Figure 2.6E), which suggests that oxygen may play an important role in regulating aerobic respiration in the WS1 subsurface. Consistent relationships among DOC, DIC,  $\text{NO}_3^-$  (and maybe  $\text{PO}_4^{3-}$ ) suggest that redox reactions, mediated by the presence of dissolved  $\text{O}_2$ , could be shaping observed spatial patterns in hyporheic zone water chemistry. If anoxic micro-sites do occur, anoxic metabolism of DOC leached from buried particulate organic matter could deplete subsurface  $\text{NO}_3^-$  concentrations. Reducing conditions in these micro-sites could also release  $\text{PO}_4^{3-}$  adsorbed to particulate organic matter and metal oxides.

Rates of biogeochemical processes could also be limited by the supply of nutrients to subsurface microbial communities. Numerous processes and mechanisms are expected to influence this supply: rates of vertical infiltration through overlying soils; proximity to individual alder trees (alder fixes N); rates of biological activity along proximal ends of hyporheic flow paths; nutrient demands of riparian vegetation; the height of the water table; as well as saturated hydraulic conductivity, which regulates the

delivery of nutrients and organic matter to the subsurface (Findlay, 1995; Battin, 2000; Poole et al., 2008). Once nutrients are supplied to a given location, nutrient concentrations may be altered by in-situ assimilatory and dissimilatory metabolism, rates of which are dependent upon oxygen concentrations and the density and activity of subsurface biofilms (Findlay, 1995; Battin, 2000; Sobczak and Findlay, 2002). It is difficult to know which of these processes are reflected in associated DOC and DIC concentrations. Models for both September and November did indicate that nutrients were linked to DOC and DIC dynamics in both months (Tables 2.2, 2.3, 2.6, 2.7), but interpreting these relationships is difficult because DIC and DOC concentrations are positively correlated with some nutrients and negatively correlated with others, and the signs of some of these correlations change seasonally (Tables 2.4, 2.5).

#### *2.6.6 System considerations – Importance of spatial intermittency*

During the dry, summer months of July, August, and September, baseflow discharge in WS1 diminishes and the stream becomes spatially intermittent. This spatial intermittency is an important physical control on water movement in WS1 during these months, and integrates the three drivers of carbon processing discussed above. When the stream becomes spatially discontinuous,  $Q_{HEF}:Q_{Stream}$  is maximized, the residence time of water within the catchment is increased, and all stream water and solutes pass through the subsurface and are exposed to microbial communities. Approximately 125 m above the well network, surface flow becomes discontinuous, and the stream flows through the subsurface until it re-emerges roughly 75 m above the well network. We believe that this and other discontinuities amplify the influence of subsurface carbon processing on stream

water chemistry and lead surface water that reaches the well network to be enriched in DIC. Overall, we suggest that spatial intermittency is an important seasonal driver of carbon processing in WS1, and may in part explain the elevated stream and hyporheic DIC concentrations observed in summer months.

### **2.7 *Future work***

From the data gathered over the course of this study, it is difficult to isolate and quantify the influence of specific processes or subsurface characteristics on rates and patterns of carbon metabolism in the hyporheic zone of WS1. Future work, through conservative tracer injections, reactive transport modeling, additional instrumentation of the well network, and continued monthly sampling, will seek to better understand how carbon is delivered to and transported through the well network, and will identify the biogeochemical processes that drive the consumption of DOC and production of DIC in this hyporheic environment.

### **2.8 *Conclusions***

We investigated carbon dynamics during baseflow periods in the hyporheic zone of a headwater mountain stream located within the H.J. Andrews Experimental Forest. We studied this system over a nine-month period, capturing a seasonal shift from dry summer conditions to the wet fall and winter months. The hydrology of this system is complex – hyporheic exchange flows follow extended, non-linear flow paths through a heterogeneous subsurface and may be augmented by lateral inflows of groundwater and vertical infiltration of soil water. As a result, the dynamics of carbon processing that we observed within the well network are difficult to interpret. Each observed concentration is

the sum of numerous biogeochemical processes – which may amplify or negate one another – as well as physical processes – which lead water from a variety of sources to mix in unknown portions and control the rate at which water moves through the subsurface. At the network scale, the end result is a composite signal, the layers of which are difficult to tease apart.

Despite the physical complexity of our site and the temporal span of our investigation, some patterns in carbon dynamics did emerge:

During baseflow periods, hyporheic DOC decreased with median travel time through the subsurface. DIC concentrations increased with travel time, but the magnitude of this increase in DIC was too large to be explained by metabolism of stream water DOC. This suggests that there are additional sources of DIC and/or DOC in the subsurface, and that hyporheic DIC concentrations are not well linked to stream-source DOC. The most likely supplemental sources of DIC to hyporheic water are soil CO<sub>2</sub> and microbial respiration of DOC leached from buried particulate organic matter and from overlying soils. Overall, the hyporheic zone appears to be a source of DIC to the stream.

In summer, the hyporheic zone is likely isolated from vertical infiltration or lateral inflow of soil water, and particulate organic carbon is not present in stream water. Thus, spatial patterns in hyporheic zone biogeochemistry must result from underlying spatial patterns in hyporheic flowpaths, groundwater inputs, and buried particulate organic carbon. With the transition to the rainy season throughout the fall and early winter, vertical infiltration and leaching of accumulated solutes from the overlying soil appear to become important sources of carbon that help explain patterns in hyporheic zone biogeochemistry.

## 2.9 Acknowledgements

Following publication, all data will be made available through the H.J. Andrews Experimental Forest data catalog, which can be accessed via the following url:  
<http://andrewsforest.oregonstate.edu/lter/data.cfm?frameURL=8>. Thank you to the H.J. Andrews staff and the LTER research network for data and field support. Data and facilities were provided by the H.J. Andrews Experimental Forest research program, which is funded by the National Science Foundation's Long-Term Ecological Research Program (DEB 0823380), the U.S. Forest Service Pacific Northwest Research Station, and Oregon State University.

Thank you to the U.S. Forest Service Pacific Northwest Research Station, the Water Resources Graduate Program, and the Oregon State University Provost's Distinguished Fellowship for providing funding and support for this research. Thank you to the IWW Collaboratory for laboratory equipment and training, as well as technical support. Thank you to Nick Dosch for help with fieldwork.

## 2.10 References

- Aufdenkampe, A. K., E. Mayorga, P. A. Raymond, J. M. Melack, S. C. Doney, S. R. Alin, R. E. Aalto, and K. Yoo (2011), Riverine coupling of biogeochemical cycles between land, oceans, and atmosphere, *Frontiers in Ecology and the Environment*, 9(1), 53–60, doi:10.1890/100014.
- Baker, M. A., C. N. Dahm, and H. M. Valett (1999), Acetate retention and metabolism in the hyporheic zone of a mountain stream, *Limnology and Oceanography*, 44(6), 1530–1539, doi:10.4319/lo.1999.44.6.1530.
- Battin, T. J. (1999), Hydrologic flow paths control dissolved organic carbon fluxes and metabolism in an alpine stream hyporheic zone, *Water Resources Research*, 35(10), 3159–3169.

- Battin, T. J. (2000), Hydrodynamics is a major determinant of streambed biofilm activity : From the sediment to the reach scale, *Limnology and Oceanography*, 45(6), 1308–1319.
- Battin, T. J., L. A. Kaplan, D. J. Newbold, and S. P. Hendricks (2003), A mixing model analysis of stream solute dynamics and the contribution of a hyporheic zone to ecosystem function, *Freshwater Biology*, 48, 995–1014.
- Battin, T. J., L. A. Kaplan, S. Findlay, C. S. Hopkinson, E. Marti, A. I. Packman, J. D. Newbold, and F. Sabater (2008), Biophysical controls on organic carbon fluxes in fluvial networks, *Nature Geoscience*, 1, 95–100, doi:10.1038/ngeo602.
- Benjamin, M. M. (2010) *Water Chemistry*. Waveland, Long Grove, IL.
- Benstead, J. P., and D. S. Leigh (2012), An expanded role for river networks, *Nature Geoscience*, 5, 678–679, doi:10.1038/ngeo1593.
- Boulton, A. J., and J. G. Foster (1998), Effects of buried leaf litter and vertical hydrologic exchange on hyporheic water chemistry and fauna in a gravel-bed river in northern New South Wales, Australia, *Freshwater Biology*, (40), 229–243.
- Buffam, I., J. N. Galloway, L. K. Blum, and K. J. McGlathery (2001), A stormflow / baseflow comparison of dissolved organic matter concentrations and bioavailability in an Appalachian stream, *Biogeochemistry*, 53, 269–306.
- Butman, D., and P. A. Raymond (2011), Significant efflux of carbon dioxide from streams and rivers in the United States, *Nature Geoscience*, 4, 839–842, doi:10.1038/ngeo1294.
- CCAL (2013) CCAL Water Analysis Laboratory Quality Assurance Plan. Oregon State University and United States Forest Service Cooperative Chemical Analytical Laboratory.  
<http://www.ccal.oregonstate.edu/sites/ccal/files/pdf/QAP%20Rev%203%202013.pdf>
- Chestnut, T. J., and W. H. McDowell (2000), C and N dynamics in the riparian and hyporheic zones of a tropical stream, Luquillo Mountains, Puerto Rico, *Journal of the North American Benthological Society*, 19(2), 199–214.
- Cole, J. J., Y. T. Prairie, N. F. Caraco, W. H. McDowell, L. J. Tranvik, R. G. Striegl, C. M. Duarte, P. Kortelainen, J. A. Downing, J. J. Middelburg, and J. Melack (2007), Plumbing the Global Carbon Cycle: Integrating Inland Waters into the Terrestrial Carbon Budget, *Ecosystems*, 10, 171–184, doi:10.1007/s10021-006-9013-8.

- Corson-Rikert, H. A. (2014), Carbon dynamics in the hyporheic zone of a headwater mountain stream in the Cascade Mountains, Oregon. M.S. Thesis. Oregon State University.
- Crawford, J. T., R. G. Striegl, K. P. Wickland, M. M. Dornblaser, and E. H. Stanley (2013), Emissions of carbon dioxide and methane from a headwater stream network of interior Alaska, *Journal of Geophysical Research: Biogeosciences*, 118(2), 482–494, doi:10.1002/jgrg.20034.
- Crocker, M. T., and J. L. Meyer (2014), Stream Interstitial dissolved organic carbon in sediments of a southern Appalachian headwater stream, *Journal of the North American Benthological Society*, 6(3), 159–167.
- Downing, J., J. J. Cole, C. M. Duarte, J. J. Middelburg, J. M. Melack, Y. T. Prairie, P. Kortelainen, R. G. Striegl, W. H. McDowell, and L. J. Tranvik (2012), Global abundance and size distribution of streams and rivers, *Inland Waters*, 2, 229–236, doi:10.5268/IW-2.4.502.
- Dyrness, C. T. (1969), Hydrologic properties of soils on three small watersheds in the western Cascades of Oregon, PNW-111, 17 pp., Pacific Northwest Forest and Range Experiment Station, U.S.D.A. Forest Service, Corvallis, Oregon.
- Findlay, S. (1995), Importance of surface-subsurface exchange in stream exchange ecosystems: The hyporheic zone, *Limnology and Oceanography*, 40(1), 159–164.
- Findlay, S., and W. V Sobczak (1996), Variability in removal of dissolved organic carbon in hyporheic sediments, *Journal of the North American Benthological Society*, 15(1), 35–41.
- Findlay, S., D. Strayer, C. Goumbala, and K. Gould (1993), Metabolism of streamwater dissolved organic carbon in the shallow hyporheic zone, *Limnology and Oceanography*, 38(7), 1493–1499, doi:10.4319/lo.1993.38.7.1493.
- Grimm, N. B., and S. G. Fisher (1984), Exchange between interstitial and surface water : Implications for stream metabolism and nutrient cycling, *Hydrobiologia*, 111, 219–228.
- Gurwick, N. P., D. M. McCorkle, P. M. Groffman, A. J. Gold, D. Q. Kellogg, and P. Seitz-Rundlett (2008), Mineralization of ancient carbon in the subsurface of riparian forests, *Journal of Geophysical Research*, 113, G02021, doi:10.1029/2007JG000482.
- Halpern, C. B., and J. F. Franklin (1990), Physiognomic development of *Pseudotsuga* forests in relation to initial structure and disturbance intensity, *Journal of Vegetation Science*, 1, 475–482.

- Hedin, L. O. (1990), Factors controlling sediment community respiration in woodland stream ecosystems, *Oikos*, 57, 94–105.
- Hinton, M. J., S. L. Schiff, and M. C. English (1998), Sources and flowpaths of dissolved organic carbon during storms in two forested watersheds of the Precambrian Shield, *Biogeochemistry*, 41, 175–197.
- Hood, E., M. N. Gooseff, and S. L. Johnson (2006), Changes in the character of stream water dissolved organic carbon during flushing in three small watersheds, Oregon, *Journal of Geophysical Research*, 111, G01007, doi:10.1029/2005JG000082.
- Jencso, K. G., B. L. McGlynn, M. N. Gooseff, K. E. Bencala, and S. M. Wondzell (2010), Hillslope hydrologic connectivity controls riparian groundwater turnover: Implications of catchment structure for riparian buffering and stream water sources, *Water Resources Research*, 46(10), doi:10.1029/2009WR008818.
- Johnson, S. L., and J. A. Jones (2000), Stream temperature responses to forest harvest and debris flows in western Cascades, Oregon, *Canadian Journal of Fisheries and Aquatic Sciences*, 57(S2), 30–39, doi:10.1139/cjfas-57-S2-30.
- Kasahara, T., and S. M. Wondzell (2003), Geomorphic controls on hyporheic exchange flow in mountain streams, *Water Resources Research*, 39(1), 1–14, doi:10.1029/2002WR001386.
- Khadka, M. B., J. B. Martin, and J. Jin (2014), Transport of dissolved carbon and CO<sub>2</sub> degassing from a river system in a mixed silicate and carbonate catchment, *Journal of Hydrology*, 513, 391–402, doi:10.1016/j.jhydrol.2014.03.070.
- Levno, A., and J. Rothacher (1969), Increases in maximum stream temperatures after slash burning in a small experimental watershed, PNW-11, 7 pp., Pacific Northwest Forest and Range Experiment Station, U.S.D.A. Forest Service, Corvallis, Oregon.
- Liu, W., X. Xu, N. M. McGoff, J. M. Eaton, P. Leahy, N. Foley, and G. Kiely (2014), Spatial and Seasonal Variation of dissolved organic carbon (DOC) concentrations in Irish streams: importance of soil and topography characteristics., *Environmental management*, 53(5), 959–67, doi:10.1007/s00267-014-0259-1.
- McDowell, W. H. (1985), Kinetics and Mechanisms of Dissolved Organic Carbon Retention in a Headwater Stream, *Biogeochemistry*, 1(4), 329–352.
- Millero, F. J., T. B. Graham, F. Huang, H. Bustos-Serrano, and D. Pierrot (2006), Dissociation constants of carbonic acid in seawater as a function of salinity and temperature, *Marine Chemistry*, 100, 80–94, doi:10.1016/j.marchem.2005.12.001.

- Mulholland, P. J., E. R. Marzolf, J. R. Webster, D. R. Hart, and S. P. Hendricks (1997), Evidence that hyporheic zones increase heterotrophic metabolism and phosphorus uptake in forest streams, *Limnology and Oceanography*, 42(3), 443–451.
- Öquist, M. G., M. Wallin, J. Seibert, K. Bishop, and H. Laudon (2009), Dissolved inorganic carbon export across the soil/stream interface and its fate in a boreal headwater stream., *Environmental science & technology*, 43(19), 7364–9.
- Poole, G. C., S. J. O'Daniel, K. L. Jones, W. W. Woessner, E. S. Bernhardt, A. M. Helton, J. A. Stanford, B. R. Boer, and T. J. Beechie (2008), Hydrologic spiralling: the role of multiple interactive flow paths in stream ecosystems, *River research and applications*, 14 pp, doi:10.1002/rra.1099.
- Pusch, M. (1996), The metabolism of organic matter in the hyporheic zone of a mountain stream , and its spatial distribution, *Hydrobiologia*, 107–118.
- Pusch, M., and J. Schwoerbel (1994), Community respiration in hyporheic sediments of a mountain stream (Steina, Black Forest), *Archiv fur Hydrobiologie*, 130(1), 35–52.
- Raymond, P. A., and J. E. Bauer (2001), Riverine export of aged terrestrial organic matter to the North Atlantic Ocean., *Nature*, 409, 497–500.
- Robbins, L. L., M. E. Hansen, J. A. Kleypas, and S. C. Meylan (2010), *CO2calc: A User-Friendly Seawater Carbon Calculator for Windows, Mac OS X, and iOS (iPhone)*.
- Rothacher, J., C. T. Dyrness, and R.L. Fredriksen (1967), Hydrologic and related characteristics of three small watersheds in the Oregon Cascades, report, 54 pp., Pacific Northwest Forest and Range Experiment Station, U.S.D.A. Forest Service, Corvallis, Oregon.
- Schindler, J. E., and D. P. Krabbenhoft (1998), The hyporheic zone as a source of dissolved organic carbon and carbon gases to a temperate forested stream, *Biogeochemistry*, 43(2), 157–174.
- Sobczak, W. V., and S. Findlay (2002), Variation in bioavailability of dissolved organic carbon among stream hyporheic flowpaths, *Ecology*, 83(11), 3194–3209.
- Stumm, W., and J. J. Morgan (1996), *Aquatic Chemistry, Chemical Equilibria and Rates in Natural Waters*, 3rd ed., John Wiley, New York.
- Swanson, F.J., and M.E. James (1975), Geology and geomorphology of the H.J. Andrews Experimental Forest, Western Cascades, Oregon, PNW-188, 15 pp., Pacific Northwest Forest and Range Experiment Station, U.S.D.A. Forest Service, Corvallis, Oregon.

- Tsyplkin, M., and G. L. Macpherson (2012), The effect of precipitation events on inorganic carbon in soil and shallow groundwater, Konza Prairie LTER Site, NE Kansas, USA, *Applied Geochemistry*, 27, 2356–2369, doi:10.1016/j.apgeochem.2012.07.008.
- Voltz, T., M. Gooseff, A. S. Ward, K. Singha, M. Fitzgerald, and T. Wagener (2013), Riparian hydraulic gradient and stream-groundwater exchange dynamics in steep headwater valleys, *Journal of Geophysical Research: Earth Surface*, 118(2), 953–969, doi:10.1002/jgrf.20074.
- Ward, A. S., M. Fitzgerald, M. N. Gooseff, T. J. Voltz, A. M. Binley, and K. Singha (2012), Hydrologic and geomorphic controls on hyporheic exchange during base flow recession in a headwater mountain stream, *Water Resources Research*, 48(4), n/a–n/a, doi:10.1029/2011WR011461.
- Wondzell, S. M. (2006), Effect of morphology and discharge on hyporheic exchange flows in two small streams in the Cascade Mountains of Oregon, USA, *Hydrological Processes*, 20(2), 267–287, doi:10.1002/hyp.5902.
- Wondzell, S. M. (2011), The role of the hyporheic zone across stream networks, *Hydrological Processes*, 25(22), 3525–3532, doi:10.1002/hyp.8119.
- Wondzell, S. M. (2012), Hyporheic Zones in Mountain Streams: Physical Processes and Ecosystem Functions, *Rocky Mountain Research Station - Stream Notes*.
- Wondzell, S. M., J. LaNier, and R. Haggerty (2009), Evaluation of alternative groundwater flow models for simulating hyporheic exchange in a small mountain stream, *Journal of Hydrology*, 364(1-2), 142–151, doi:10.1016/j.jhydrol.2008.10.011.
- Yvon-Durocher, G., J. M. Caffrey, A. Cescatti, M. Dossena, P. del Giorgio, J. M. Gasol, J. M. Montoya, J. Pumpanen, P. A. Staehr, M. Trimmer, G. Woodward, and A. P. Allen (2012), Reconciling the temperature dependence of respiration across timescales and ecosystem types., *Nature Letters*, 487(7408), 472–6, doi:10.1038/nature11205.
- Zarnetske, J. P., R. Haggerty, S. M. Wondzell, and M. A. Baker (2011), Dynamics of nitrate production and removal as a function of residence time in the hyporheic zone, *Journal of Geophysical Research*, 116, G01025, doi:10.1029/2010JG001356.

### **3 Solute dynamics in a headwater stream and riparian hyporheic zone during a small November storm in the Cascade Mountains, Oregon**

#### **3.1 Abstract**

We sampled a small headwater stream, a hillslope well, and nine hyporheic wells during a small November storm event in the Western Cascades of Oregon. In the stream, DOC and nitrate concentrations displayed clockwise hysteresis, and we observed a decrease in DIC concentrations and a steady increase in chloride concentrations. DOC concentrations in the hyporheic zone were lower than those observed in the stream, while nitrate and DIC concentrations in the hyporheic zone were higher than those observed in the stream.

Travel time appeared to be associated with both nitrate and DOC response patterns in the hyporheic zone. In wells with long travel times, DOC and nitrate concentrations showed a clockwise hysteresis pattern that mimicked and even exceeded that observed in the stream. We hypothesize that these solutes were flushed from overlying soils into the hyporheic zone via vertically infiltrating rainwater. In wells with short travel times, we observed only a small peak in DOC and nitrate concentrations during the storm, potentially due to lateral infiltration of stream water later in the event.

The DIC response in the hyporheic zone was not as clearly associated with travel time, although in wells with very short travel times, DIC concentrations decreased throughout the storm event, as in the stream. In the majority of the hyporheic wells we observed a decrease in and then slight recovery of DIC concentrations that coincided with

a modest reduction in precipitation and streamflow. In two hyporheic wells, this recovery continued even after additional precipitation caused streamflow to again increase.

During this small November storm event, temporal patterns in stream water chemistry differed from patterns we observed in the well network. This suggests that whole-watershed processes that controlled stream water chemistry during this storm event were different than those that controlled solute concentrations in the hyporheic zone. Nonetheless, the hyporheic zone must have been linked to the stream. That measurements in our well network reveal a very different response between the stream and the hyporheic zone suggests that: 1) Our hyporheic zone is not representative of stream-hyporheic riparian processes that occur within the larger watershed, or 2) Hillslope-stream or within-stream processes dominate during storms, and at these times the influence of the hyporheic zone on the stream is much weaker than during baseflow.

### ***3.2 Introduction***

The link between terrestrial and aquatic ecosystems is strongest in headwater reaches. Terrestrial carbon enters headwater streams through direct inputs such as leaf-fall and throughfall, and through overland and subsurface flow. In mountainous, forested watersheds with highly porous soils, high rates of infiltration prevent overland flow and cause lateral and vertical flow through soils (Rothacher et al., 1967; Harr, 1976; Jones, 2000; van Verseveld et al., 2008). This flux of water represents an important mechanism for carbon transport from terrestrial environments into forested stream ecosystems. The flux of organic matter from forested landscapes to headwater streams varies seasonally, largely due to seasonal changes in the hydrology of mountainous watersheds.

During dry, baseflow conditions, when flow from hillslopes to streams is limited, studies have observed relatively little movement of carbon from hillslopes to aquatic systems (Buffam et al., 2001). During storm events or snowmelt, however, carbon is flushed out of soils and into stream ecosystems as a result of vertical infiltration and lateral water movement (Hornberger et al., 1994; Hood et al., 2003; Hood et al., 2006; van Verseveld, 2008; Pacific et al., 2010). In many forested catchments, mean stream concentrations of DOC may double or triple with the onset of a storm or during snowmelt (Buffam et al., 2001; McGlynn and McDonnell, 2003; Hood et al., 2006; Raymond and Saiers, 2010; Wilson et al., 2013). Over the course of a storm event, stream water DOC concentrations commonly display clockwise hysteresis, with greater concentrations of DOC on the rising limb than on the receding limb of storm hydrographs (Buffam et al., 2001; Hood et al., 2003; McGlynn and McDonnell, 2003; Hood et al., 2006; van Verseveld et al., 2008).

Within most catchments, the near-stream riparian zone and the hillslopes of the catchment represent two spatially distinct sources of carbon to the stream. During the rising limb of the storm hydrograph, riparian contribution of DOC is greater than hillslope contribution (Buffam et al., 2001; McGlynn and McDonnell, 2003; Hood et al., 2006; van Verseveld et al., 2008). This trend is reversed on the receding limb (Buffam et al., 2001; McGlynn and McDonnell, 2003; Hood et al., 2006; van Verseveld et al., 2008). This shift in delivery is due to a physical disconnect between riparian and hillslope components. Carbon in riparian areas can be quickly flushed to streams by even small amounts of rainwater infiltration, while carbon that has accumulated in hillslope areas cannot be flushed to the stream until soil water deficits are met and soil macropores are

filled, thereby allowing hillslope carbon to be mobilized and upland portions of the watershed to be connected to the stream (Bishop et al., 2003; McGlynn and McDonnell, 2003).

Some studies have suggested that the relative dominance of riparian vs. hillslope delivery of DOC to streams during storm events depends upon the depth at which riparian subsurface flow paths intersect with soil horizons. If flow paths intersect with organic-rich horizons (such as A and upper B horizons) then riparian contribution may be significant, but if the pathways are instead through lower, less organic-rich horizons (such as C horizons), DOC contribution from these zones may not be greater than DOC input from hillslopes (Hinton et al., 1998; Bishop et al., 2003). The height of these flow paths is determined by the height of the water table within the riparian area (Hinton et al., 1998). However, vertical infiltration through unsaturated and saturated soils (van Verseveld et al., 2008) presumably links A horizons with lower, DOC-poor horizons, and may mask or amplify the water table signal depending on the conditions.

Dynamics of DOC transport to streams are highly dependent upon the degree of hydrologic connectivity within the catchment (Pacific et al., 2010). If riparian zones and hillslopes are only coupled when storm events cause significant infiltration, then stream DOC concentrations should show a strong contribution from riparian sources early in the storm hydrograph and should display hysteresis over the full storm event (Boyer et al., 1997; Buffam et al., 2001; McGlynn and McDonnell, 2003; Hood et al., 2006). If connectivity is consistent and high, however, or riparian zones are limited, such patterns may not be apparent (Pacific et al., 2010). Given their dependence on the hydrologic connectivity of the catchment, mechanisms and patterns of carbon transport to a stream

cannot be accurately evaluated without knowledge of subsurface flow paths and the degree of connectivity between landscape components such as riparian zones and hillslopes.

In order to observe organic and inorganic carbon and nitrate dynamics during a storm event, we sampled a small headwater stream, a hillslope well, and nine hyporheic wells during a small November storm event in the western Cascades of Oregon.

### ***3.3 Study site***

This study was conducted in the lower portion of Watershed 1 (WS1), a study watershed in the H.J. Andrews Experimental Forest, located in the Western Cascades of Oregon, USA ( $44^{\circ} 12' 28.0''$  N,  $122^{\circ} 15' 30.0''$  W; Figure 3.1). Watershed 1 is a steep, forested catchment that is 95.9 ha in size, and ranges in elevation from 450 to 1027 m. The climate is characterized by cool, wet winters and warm, dry summers. At lower elevations, air temperatures range from an average of 1 °C in January to 18°C in July. The 230 cm of annual precipitation falls primarily as rain from November to March. Snow occasionally accumulates, but WS1 lies within the transient snow zone, where snow accumulates during cold winter storms, but melts during warm periods or warmer storms, so that snow packs do not persist for the entire winter. As a result, peak streamflow in WS1 occurs anytime throughout the winter and declines in summer months.

Throughout WS1, the soils are gravel clay loam and tend to be shallow (0.5 – 2 m) and porous, allowing high rates of infiltration (Rothacher et al., 1967; Dyrness, 1969). Dense stands of Douglas fir and hemlock dominate on hillslopes, while red alder dominates the riparian zone (Rothacher et al., 1967; Halpern and Franklin, 1990; Johnson

and Jones, 2000). The alders are being over-topped by Douglas fir, and many have died or fallen in recent years.

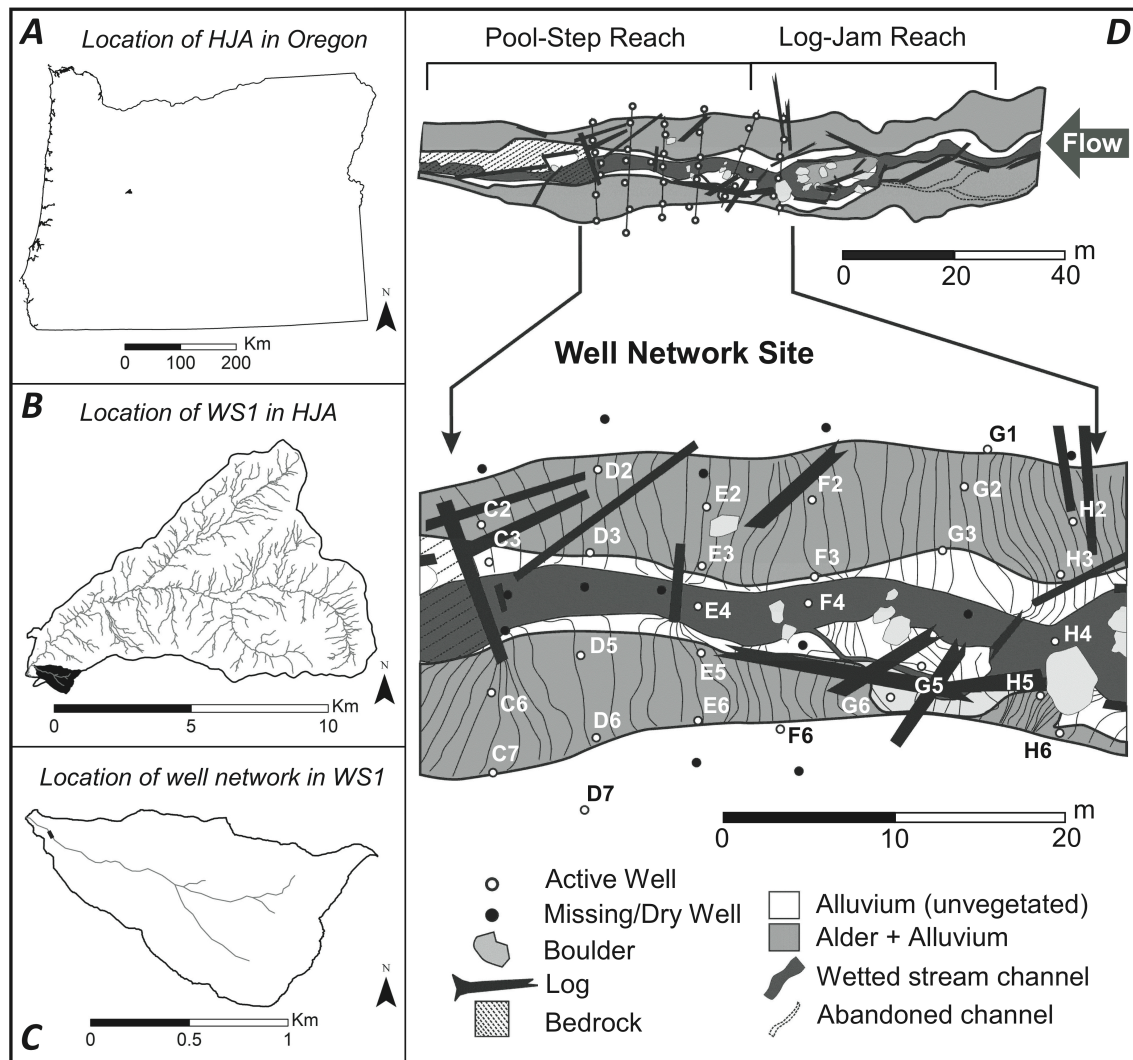


**Figure 3.1** - Location of the H.J. Andrews Experimental Forest within Oregon (*A*), and location of Watershed 1 and the well network within H.J. Andrews (*B, C*). Note that flow is from right to left in the well network figure. For this study wells D5, D6, D7, E4, G1, G2, G3, G5, and G6 were sampled. Data sources: The image of the well network site (*D*) was modified from Wondzell (2006); The catchment outlines and stream networks are from the H.J. Andrews Experimental Forest; The Oregon outline is from ESRI and TomTom.

The stream channel in WS1 is steep and usually confined. Debris flows have scoured the stream to bedrock in constrained reaches, while colluvium has been deposited in less constrained reaches, forming narrow riparian zones. The well network is located in a 14 m wide riparian zone at the base of WS1, and spans 29 m of stream length (Wondzell, 2006; Figure 3.1). Along this reach, the channel remains steep, with an average longitudinal gradient of 14% (Wondzell, 2006).

The wells and piezometers were installed in 1997, and are arrayed in six transects that span the width of the 14 m wide valley floor, perpendicular to the direction of flow (Figure 3.1). Both wells and piezometers are constructed of 3.175 cm (1 1/4 inch) schedule 40 PVC. An array of drilled holes serves as a screen along the bottom 50 cm of the wells and bottom 5 cm of the in-stream piezometers (Wondzell, 2006). The deepest well extends to 1.7 m, but the majority are approximately 1m deep (Wondzell, 2006). This study sampled 7 wells and 2 piezometers, as well as one hillslope well located 150 m up the watershed at the base of a hillslope hollow, which we installed during the summer of 2013.

### **3.4 Methods**

#### *3.4.1 Preparatory methods*

We prepared all equipment and filters for fieldwork at the Institute for Water and Watersheds Collaboratory at Oregon State University using operating procedures developed by the Oregon State University and United States Forest Service Cooperative Chemical Analytical Laboratory (CCAL). This equipment included 40 mL borosilicate vials, 250 mL Nalgene HDPE bottles, VWR 60 mL syringes with BD Luer-Lok tips,

Cole-Parmer polycarbonate stopcocks with Luer connections, 4.7 cm Whatman grade GF/F glass microfiber filters, a 4.7 cm filter apparatus, and 0.635 cm (1/4 inch) sample tubing. All syringes, bottles, vials, tubing, and stopcocks were acid washed in 10 % v/v HCl acid bath, and vials for DOC analysis were also baked in a muffle furnace at 550 °C for three hours. The GF/F filters were rinsed, dried, and baked in a muffle furnace at 500 °C for three hours (CCAL, unpublished, 2013). Note that the use of trade or firm names in this publication is for reader information and does not imply endorsement by the US Department of Agriculture of any product or service.

### 3.4.2 *Field methods*

We conducted all fieldwork in Watershed 1 at the H.J. Andrews Experimental Forest. Our sampling was conducted from November 15<sup>th</sup> – 18<sup>th</sup> (Figure 3.2). On the afternoon of November 14<sup>th</sup>, 2013, we recorded the pH and temperature of each well and the stream using an YSI 60 probe. We then removed 700 mL from each of the wells using the designated purge syringes and tubing. On the morning of the 15<sup>th</sup>, when the storm had not yet begun and the system was still at a baseflow discharge (Figure 3.2), we sampled wells D5, D6, D7, E4, G1, G2, G3, G5, G6 and the hillslope well, collecting one field duplicate. We sampled the stream at both the beginning and end of the sampling run. We collected all samples according to the method outlined in Corson-Rikert (2014).

After the initial pre-storm sampling run on the morning of the 15<sup>th</sup>, we used real-time discharge data from the WS1 gaging station (located approximately 50 m below the well network) and precipitation data from the PRIMET meteorological station (located approximately 0.6 km from the gaging station) in order to mark the onset of the storm

and track the progression of the stream response. We conducted our second sampling run at the tail end of the rising leg early in the morning of November 16<sup>th</sup> (Figure 3.2). We sampled for a third time during an initial peak in the WS1 hydrograph on the afternoon of the 16<sup>th</sup> (Figure 3.2). We performed the final sampling run after a sustained period of high flow, during the afternoon of November 17<sup>th</sup> (Figure 3.2). We used the same procedure and sampled the same wells during all four sampling runs.

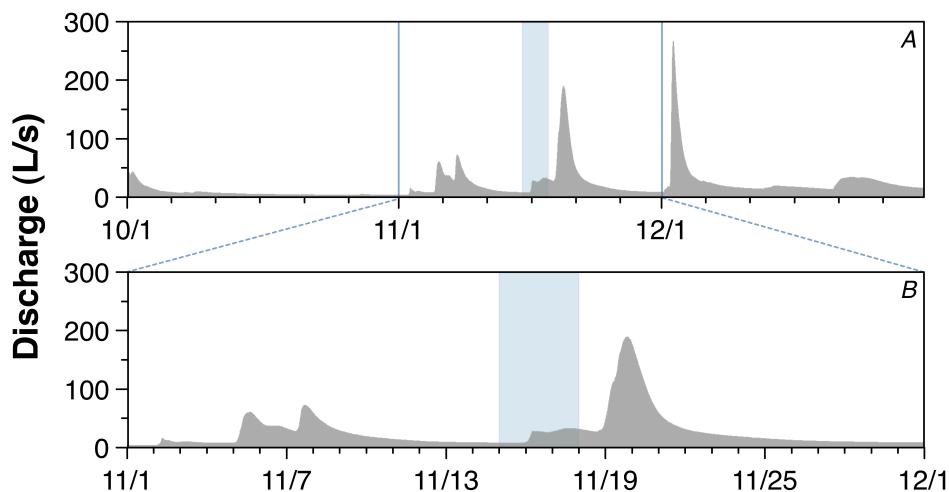


**Figure 3.2** - Timing of storm sampling within fall 2013 (A), and November 2013 (B). The period displayed in Figures 3.3 - 3.7 is highlighted in blue. The streamflow data are from the WS1 gaging station at the H.J. Andrews Experimental Forest.

### 3.4.3 Laboratory methods

We conducted all analytical work in the IWW Collaboratory at Oregon State University. We measured concentrations of DOC and DIC on a Shimadzu TOC-VSCH Combustion Carbon Analyzer. We determined concentrations of major anions on a Dionex 1500 Ion Chromatograph and concentrations of major cations on a Perkin-Elmer AAnalyst-100 Atomic Absorption Spectrometer. We measured total alkalinity by titrating all samples to a pH of 4.5 on a Radiometer TIM840 AutoTitrator. We performed all

analyses according to standard operating procedures that were developed primarily from APHA methods by the Oregon State University and United States Forest Service Cooperative Chemical Analytical Laboratory, as outlined in Corson-Rikert (2014).

### 3.4.4 Calculations

In order to perform an ion balance, we calculated concentrations of the major carbonate species and OH<sup>-</sup> using temperature-corrected equilibrium constants. For the carbonate system, we adjusted  $K_{a1}$  and  $K_{a2}$  for each sample using the observed field temperatures and the equations developed by Millero (2006) to estimate  $pK_1^0$  and  $pK_2^0$ , which represent the values of  $pK_1$  and  $pK_2$  in pure water, where salinity (S) is zero (Millero et al., 2006). We then computed alpha terms and used these terms to calculate the concentrations of the individual carbonate species, using our measured DIC concentrations as TOTCO<sub>3</sub> (Benjamin, 2010). We used the Van't Hoff equation and observed temperatures to adjust the equilibrium constants for water, and then calculated concentrations of OH<sup>-</sup> using the corrected constants and field pH (Benjamin, 2010). The exact equations used are outlined in Corson-Rikert (2014). After calculating the concentrations of the carbonate species and hydroxide (meq L<sup>-1</sup>), we computed the ion balance, as a percent:

$$\left( \frac{\sum[\text{Cations}] - \sum[\text{Anions}]}{\sum[\text{Cations}] + \sum[\text{Anions}]} \right) \cdot 100 \quad \text{Eq. 3.1}$$

where:

$$\sum[\text{Cations}] = \sum([H^+] + [Ca^{+2}] + [Mg^{+2}] + [Na^+] + [K^+]) \quad \text{Eq. 3.2}$$

$$\sum[\text{Anions}] = \sum([OH^-] + [HCO_3^-] + [CO_3^{2-}] + [PO_4^{3-}] + [SO_4^{2-}] + [Cl^-] + [NO_3^-]) \quad \text{Eq. 3.3}$$

Travel times for all wells in the well network had previously been calculated using EC breakthrough curves from a five-day continuous salt tracer test of the WS1 well network conducted in 1997, the results of which are discussed in Wondzell (2006).

Travel time is defined as the time (in hours) for observed EC in each well to reach one-half of the final observed plateau concentration. Travel times for the wells sampled during the storm event range from 18 to 64 hours (Table 3.1).

**Table 3.1** - Median travel times, and pre-storm depth to water (relative to ground surface) in the selected hyporheic wells. Median travel times from Wondzell, unpublished data, 1997.

Well	Travel Time	Pre-storm Depth
	hours	cm
D5	32.2	74.7
D6	45.5	54.1
D7	50.4	159.7
E4	26.6	52.5
G1	56.1	110
G2	62.8	72
G3	64.2	34.5
G5	18.6	-1.6
G6	28.0	52

### 3.5 Results

#### 3.5.1 DOC concentrations

The hydrology of the storm event, with an initial peak in discharge, followed by an extended period of high flow (Figures 3.2, 3.4), prevented observed solute patterns from forming a complete clockwise concentration-discharge hysteresis loop. Nonetheless, DOC concentrations in the stream displayed hysteresis, with higher concentrations on the rising leg than later in the storm event (Figure 3.3). Eight hours after the onset of the

storm, stream DOC concentrations had increased by 260% relative to pre-storm concentrations (Figure 3.4). Ten hours after the storm began stream DOC concentrations had reached 290% of pre-storm values. Under continued high-flow conditions, stream DOC then dropped to 205-210% of pre-storm conditions twenty hours into the storm, and fell to 180% of pre-storm concentrations by 43 hours into the storm.

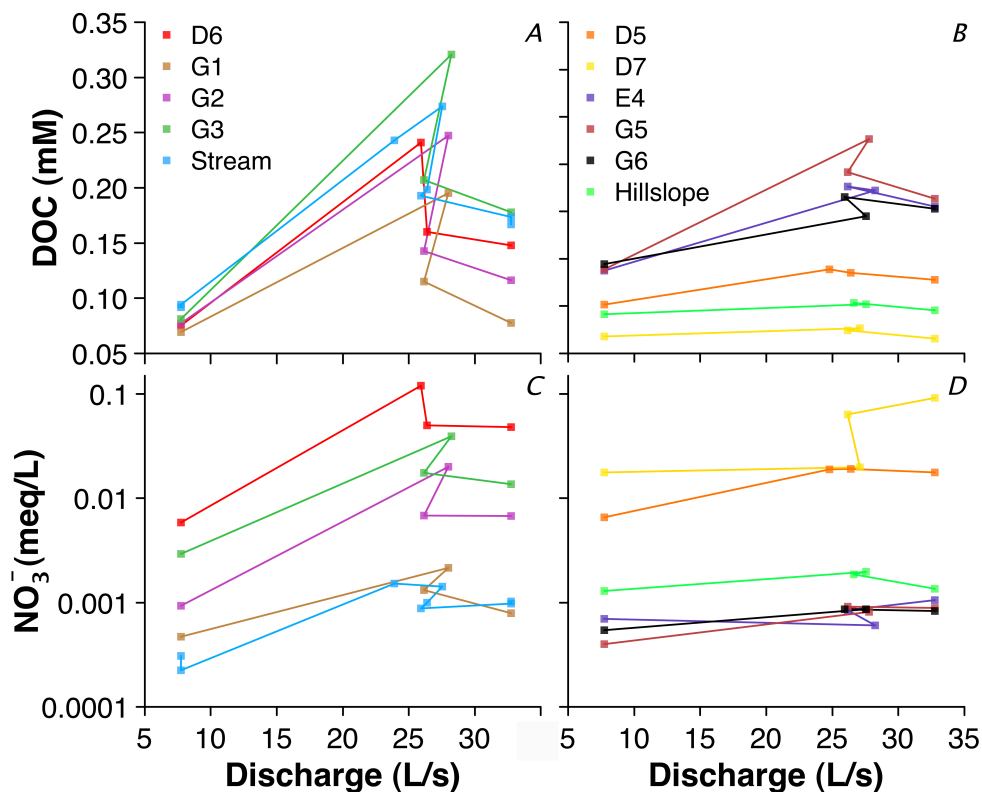


**Figure 3.3** - Stream and hyporheic DOC and nitrate concentrations by discharge. Observations are connected in the order in which they were collected. Concentrations in the stream and in wells where both solutes displayed hysteresis are shown in *A* and *C*. Concentrations in wells where neither DOC nor nitrate displayed hysteresis are shown in *B* and *D*. Note that nitrate concentrations are on a logarithmic scale.

While we did see evidence of a pulse of DOC in the hyporheic zone, the response varied considerably (Figure 3.4). We saw a large peak in DOC concentrations on the rising leg of the hydrograph in four of the hyporheic wells – G1, G2, G3, and D6. DOC

concentrations in these wells at this time had increased by 250-400% relative to pre-storm conditions (Figure 3.4). DOC concentrations then fell to 165-250% and later 110-220% of pre-storm concentrations during the third and fourth sampling runs, respectively. This pattern matched that displayed in the stream (Figure 3.4).

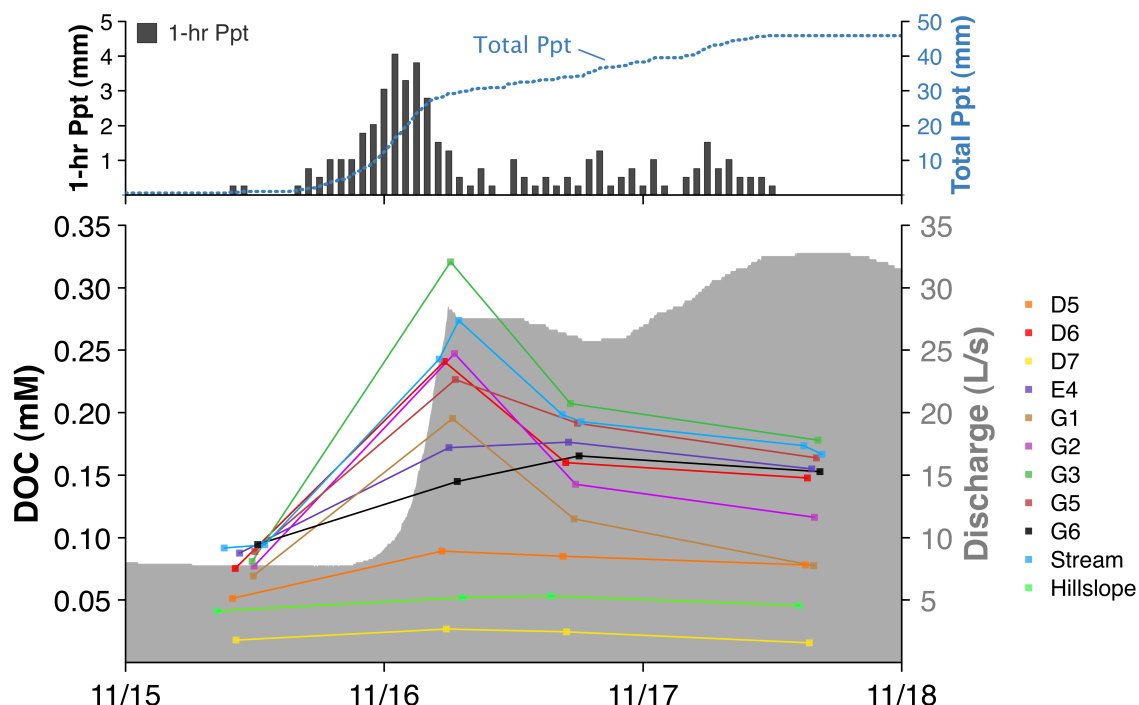


**Figure 3.4** – Hyporheic and stream DOC concentrations from 11/15/13 to 11/17/13. Discharge is displayed in the background. 1-hour precipitation totals and cumulative precipitation are given in the top panel. Precipitation and discharge data are from the PRIMET meteorological station and WS1 gaging station at the H.J. Andrews Experimental Forest.

In well G5, DOC concentrations displayed a weak clockwise hysteresis loop. Wells D5, E4, and G6 displayed a slower response (Figure 3.4). DOC concentrations in these wells had increased moderately (150-200%) by the second sampling run, and remained high through the third sampling run, even after an extended period of sustained high flow. After this point, DOC concentrations in these wells decreased (Figure 3.4).

Overall, the highest DOC concentrations were observed in well G3, and the second highest in the stream itself.

In the hillslope well, we observed very little change in DOC concentrations throughout the storm event (Figure 3.4). During the second sampling period, at the end of the rising leg, DOC concentrations had increased to 125% of pre-storm concentrations, but remained low in comparison to DOC concentrations in the stream and riparian wells. By the third sampling period, DOC concentrations had reached 129% of pre-storm concentrations, but then fell to 110% of pre-storm concentrations by the final sampling run. Well D7, at the edge of the well network (Figure 3.1), behaved much like the hillslope well. DOC concentrations in this well were even lower than those observed in the hillslope well. The concentration of DOC in well D7 did increase slightly to 150% of pre-storm concentrations, but then fell to 135% and 87% of pre-storm concentrations during the two final sampling runs (Figure 3.4).

### *3.5.2 DIC concentrations*

DIC concentrations in the well network and in the stream displayed a markedly different response than DOC (Figure 3.5). In the stream, DIC concentrations decreased over the course of the storm (Figure 3.5). We observed a similar response in wells E4, G5, G6 and the hillslope well (Figure 3.5).

In wells D5, D6, D7 and G3, DIC concentrations decreased between the first and second sampling runs, but then recovered slightly by the time of the third sampling run (Figure 3.5). This recovery followed a slight reduction in precipitation and recession in the storm hydrograph. When streamflow increased again, leading up to the fourth

sampling run, DIC concentrations in these wells had again decreased. DIC concentrations in well G2 decreased through the third sampling run, but had recovered to the pre-storm level by the fourth sampling run (Figure 3.5). In well G1, the recovery was more pronounced, and began after the second sampling run. DIC concentrations were equivalent to pre-storm concentrations in well G1 by the third sampling run, and reached 113% of pre-storm concentrations by the fourth sampling run (Figure 3.5).

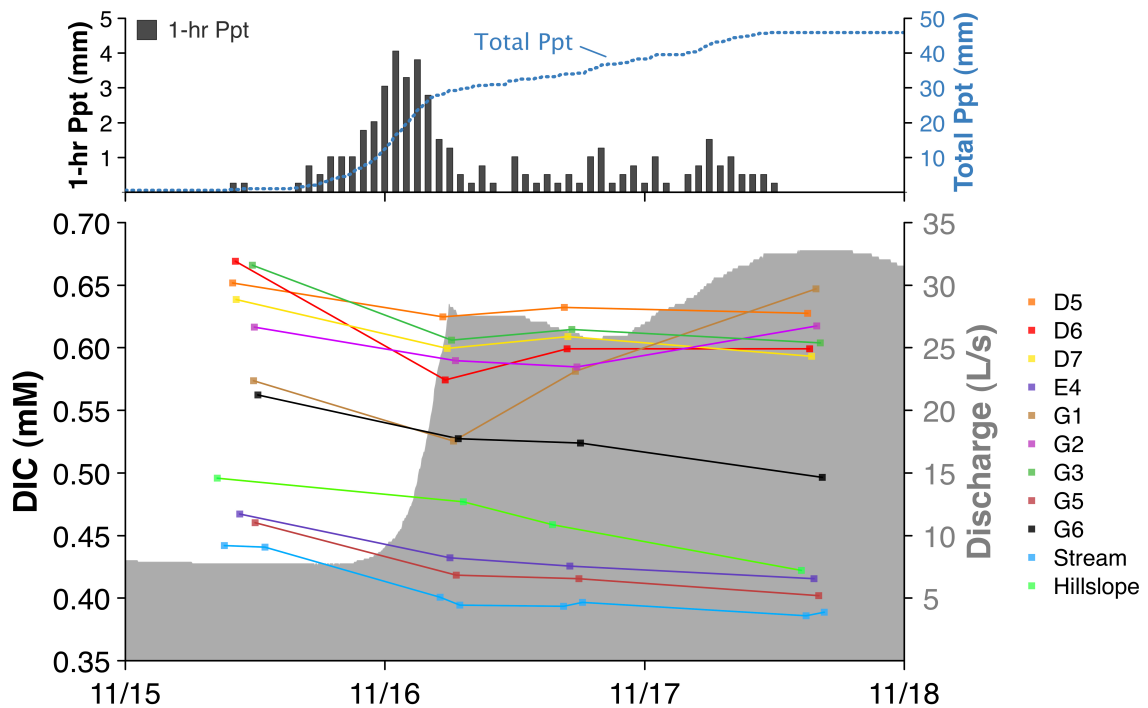


**Figure 3.5** – Hyporheic and stream DIC concentrations from 11/15/13 to 11/17/13. Discharge is displayed in the background. 1-hour precipitation totals and cumulative precipitation are given in the top panel. Precipitation and discharge data are from the PRIMET meteorological station and WS1 gaging station at the H.J. Andrews Experimental Forest.

### 3.5.3 Nitrate concentrations

We observed high stream nitrate concentrations on the rising leg of the storm and lower nitrate concentrations after an extended period of high flow, approximating a

clockwise concentration-discharge hysteresis loop (Figure 3.3). At the start of the second sampling run, the stream nitrate concentration was 678% higher than the pre-storm concentration (Figure 3.6). By the end of the second sampling run, stream nitrate was 634% of the initial concentration (Figure 3.6). During the third and fourth sampling runs, the stream nitrate concentration was ~400% and 440% of the pre-storm concentration. A similar pattern was observed in wells D6, G1, G2, and G3 (Figure 3.6). In well G1, the nitrate concentration increased 500% between the first and second sampling run. The peak was even more extreme in wells G2, G3, and D6, where the increase between the first and second runs was 2150%, 1350%, and 2050%, respectively, and nitrate concentrations were much higher than in well G1 or the stream. In all four of these wells, the nitrate concentration decreased between the second and third sampling run, and then remained relatively constant through the fourth sampling run (Figure 3.6).

Although well D7 also had a high concentration of nitrate during the pre-storm sampling period, it did not display the same pattern – the concentration increased only slightly between the first and second sampling periods, then jumped to 360% and then 520% of the pre-storm concentration during the third and fourth sampling runs (Figures 3.3, 3.6). The hillslope well, in contrast, showed only a very slight increase in nitrate during the second and third sampling runs (Figure 3.6).

Nitrate concentrations in wells D5, G5, and G6 increased moderately (160-290%) between the first and second sampling runs, and then remained steady through the remainder of the storm (Figure 3.6). Overall, concentrations of nitrate in D5 were much higher than in wells G5 and G6 (Figure 3.6). In well E4, nitrate concentrations initially fell, and then increased after the second sampling run (Figure 3.6).

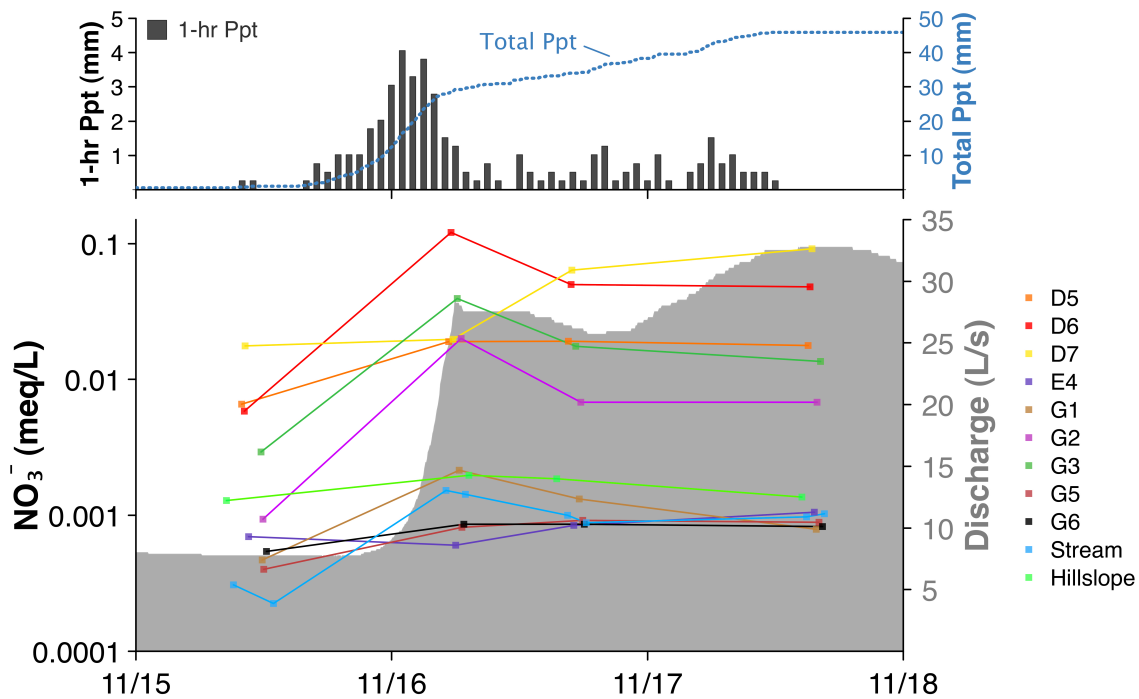


**Figure 3.6** – Hyporheic and stream nitrate concentrations from 11/15/13 to 11/17/13. Note that nitrate concentrations are on a log scale. Discharge is displayed in the background. 1-hour precipitation totals and cumulative precipitation are given in the top panel. Precipitation and discharge data are from the PRIMET meteorological station and WS1 gaging station at the H.J. Andrews Experimental Forest.

### 3.5.4 Chloride concentrations

The chloride concentration of the WS1 stream water increased steadily over the course of the storm event, and by the end of the storm was 120% of the pre-storm concentration (Figure 3.7). Wells E4 and G5 displayed a similar response (Figure 3.7).

Chloride concentrations in wells D5 and G3 increased only slightly, to just 105–108% of pre-storm concentrations (Figure 3.7). The chloride concentration in well G6 was steady through the third sampling run, and then increased to 120% of the pre-storm concentration by the fourth sampling run (Figure 3.7). Chloride concentrations in the stream were higher than in all of the hyporheic wells except D6. In well D6, chloride

concentrations increased sharply between the first and second sampling runs then fell by the third sampling run. Chloride concentrations in wells G1 and G2 increased slightly to~108% of pre-storm concentrations by the second sampling run and then fell. Chloride concentrations in the hillslope well and in D7 were very low before and during the storm. In the hillslope well, the chloride concentration remained constant throughout the event, while in D7, the chloride concentration was slightly elevated during the second and third sampling runs.

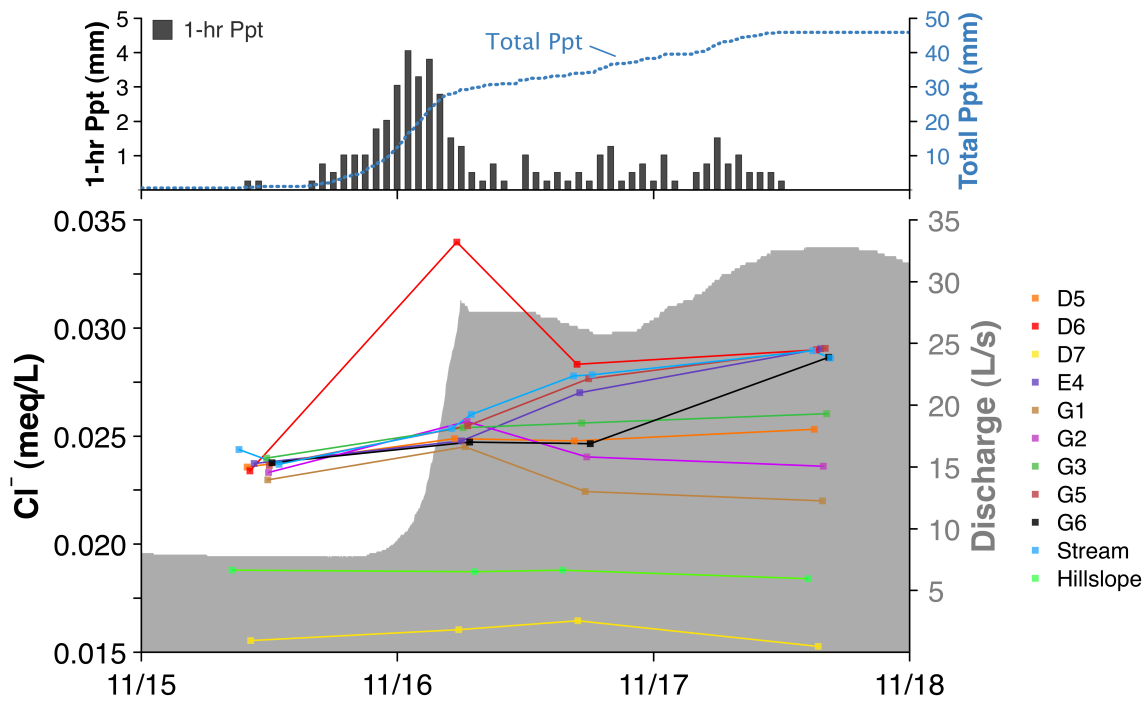


**Figure 3.7 – Hyporheic and stream chloride concentrations from 11/15/13 to 11/17/13.** Discharge is displayed in the background. 1-hour precipitation totals and cumulative precipitation are given in the top panel. Precipitation and discharge data are from the PRIMET meteorological station and WS1 gaging station at the H.J. Andrews Experimental Forest.

### 3.5.5 Ion balance

Ion balances in the stream and wells during the storm were erratic (Figure 3.8).

The ion balances were heavily influenced by low observed pH values. We have some concern that the observed pH values do not reflect actual hydrogen ion concentrations, as the pH meter may have been malfunctioning. However, the pH meter did calibrate well prior to each sampling run and correctly read the pH of calibration buffer solutions even after sampling. If the ion balances are correct, they may suggest increased transport of organic acids into hyporheic and stream waters during storm events.

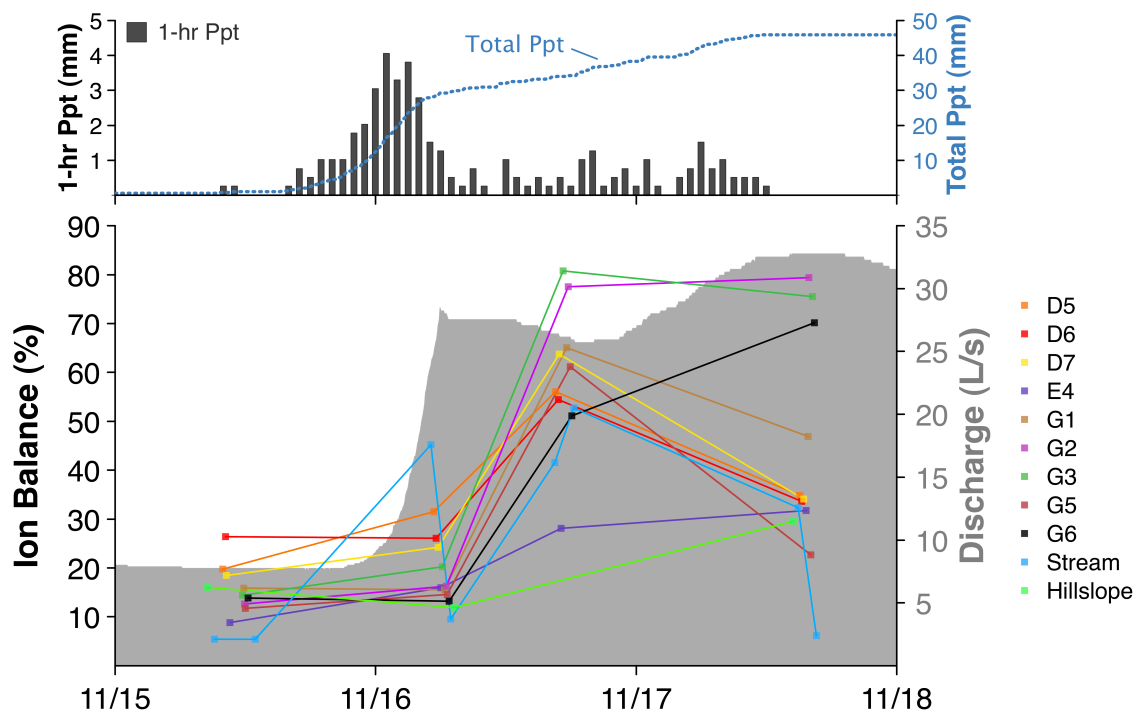


**Figure 3.8** - Hyporheic and stream ion balance from 11/15/13 to 11/17/13. Discharge is displayed in the background. 1-hour precipitation totals and cumulative precipitation are given in the top panel. Precipitation and discharge data are from the PRIMET meteorological station and WS1 gaging station at the H.J. Andrews Experimental Forest.

### **3.6 Discussion**

#### *3.6.1 Stream solute dynamics*

Stream DOC and nitrate concentrations displayed clockwise hysteresis during the storm event (Figures 3.3, 3.4, 3.6). Eight hours after discharge began to increase due to heavy precipitation, stream DOC concentrations reached 260% of pre-storm concentrations and nitrate concentrations reached 678% of pre-storm concentrations. As discharge remained high, however, we observed progressively lower DOC and nitrate concentrations. This pattern is consistent with previous work conducted in WS1 (Hood et al., 2006), elsewhere in the H.J. Andrews Experimental forest (van Verseveld et al., 2008), and in other forested catchments (Buffam et al., 2001; McGlynn and McDonnell, 2003; Bishop et al., 2004; Raymond and Saiers, 2010).

Previous research into nutrient flushing and hillslope hydrology in forested headwater environments has suggested that during the early portion of storm events, DOC-rich riparian water is flushed into the stream, causing high stream DOC concentrations. Later in the storm event, when hillslopes are hydrologically connected to the stream, stream water DOC concentrations are diluted by inputs of more dilute soil water (Hood et al., 2006; van Verseveld et al., 2008; Ward et al., 2013). If we consider only stream solute dynamics during our storm event, the observed increase in stream water DOC and nitrate concentrations during the rising leg and subsequent decrease in stream DOC and nitrate concentrations later in the event are consistent with this mechanistic framework (Figures 3.3, 3.4, 3.6). Furthermore, low DOC and nitrate concentrations observed in the hillslope well throughout the storm suggest that hillslopes

within WS1, once connected, would have contributed comparatively diluted water to the stream, as suggested. However, if we also consider observations from the riparian well network – located near the mouth of the watershed – the data suggest that this framework may not in fact explain patterns observed during the November storm in WS1, because solute patterns observed in the hyporheic zone do not parallel those observed in the well network.

Stream DOC concentrations were higher than hyporheic DOC concentrations in all but one well (G3) throughout the storm (Figure 3.4). This suggests that hyporheic water was not a source of DOC to the stream during this November storm event. It is possible that the reaction rate of DOC in the stream decreased during the storm due to biofilm disruption. Alternatively, DOC-rich water may have entered the stream as a result of canopy throughfall or via lateral flow through surface soil horizons. However, previous research in WS1 has shown that flow through unsaturated WS1 soils is vertical, not horizontal, so we do not expect that lateral soil water movement is a likely source of DOC to the stream (van Verseveld et al., 2008). Additional DOC could also have been generated within the stream itself, as increased discharge may have scoured the streambed of leaf mats or other organic debris accumulations within the wetted channel. Although two larger storms with higher peak discharge occurred in early November, prior to the storm we sampled (Figure 3.2), it is possible that two weeks would be sufficient time to re-accumulate organic matter in the streambed.

Although both nitrate and DOC concentrations displayed hysteresis during the storm event, the dynamic between hyporheic and stream nitrate concentrations was different than for DOC. Stream nitrate concentrations were lower than nitrate

concentrations in the majority of the hyporheic wells. This could suggest that the riparian zone was the source of nitrate to the stream during this storm event (Figure 3.6). If this were the case, this would conflict with the mechanistic relationship suggested by DOC. However, the nitrate concentrations observed in the hyporheic zone during the second sampling run were markedly elevated in comparison to stream concentrations. It is possible that we should have observed higher stream nitrate concentrations if the hyporheic zone was in fact the source of solutes to the stream during the storm. Therefore, the nitrate and DOC concentration patterns observed in the hyporheic zone may in fact be consistent, and together could suggest that the hyporheic zone was not a critical source of water and solutes to the stream during this small storm.

Patterns in DIC neither support nor refute this hypothesis. During the November storm event, hyporheic water consistently had higher DIC concentrations than stream water. If, during the storm, riparian zones contributed this high DIC water to the stream throughout the watershed, we might expect DIC concentrations in the stream to increase over the storm. However, we observed a decrease in stream DIC. This could suggest that the hyporheic zone was not a source of DIC to the stream during the storm. Alternatively, inputs of DIC-rich hyporheic water may have been diluted by increased stream discharge and inputs of low-DIC hillslope water. In addition, DIC as CO<sub>2</sub> is rapidly evaded from the stream, especially during high flows when the water is more turbulent (Raymond et al., 2012).

The chloride concentration of the WS1 stream water increased steadily over the course of the storm event, and by the end of the storm was 120% of the pre-storm concentration (Figure 3.7). Chloride concentrations in the stream were higher than those

observed in the well network or the hillslope well, suggesting that neither the hyporheic zone nor hillslope water (nor, potentially, groundwater – as represented by well D7) was the source of chloride to the stream during this storm. Precipitation may have been a source of chloride, although three-week bulk precipitation chemistry from the PRIMET station at the H.J. Andrews Experimental Forest indicates that rainwater chloride concentrations during this time period were too low to account for the observed stream concentrations.

Overall, the temporal patterns in solute concentrations observed in the stream during this small storm must integrate processes occurring in the watershed as a whole. Observations within our well network do not appear to support a hyporheic explanation for the changes in solute concentrations. Our well network is located in a reach with a relatively wide valley floor. However, over much of the WS1 stream network, the valley floor is narrow, so that connectivity between hillslopes and the stream may be much different than in our well network. A more extensive measurement campaign that examines the watershed more holistically would likely be necessary to understand the processes driving the observed changes. In any event, our results show that watershed responses are likely to be complex, and that simple explanations based solely on a time-sequence of samples collected at the mouth of the watershed (e.g. Hood et al., 2006), may be insufficient to clearly understand the specific sources and mechanisms determining whole watershed response.

### *3.6.2 Hyporheic solute dynamics*

Several distinct patterns in solute concentrations emerged in the hyporheic zone.

Chloride concentrations in hyporheic wells generally increased, but this increase only persisted throughout the storm in a handful of short travel time wells. Overall, chloride concentrations did not display a clear pattern.

Travel time appeared to be strongly associated with nitrate and DOC response patterns in the hyporheic zone. In wells with long travel times, DOC and nitrate concentrations showed a clockwise hysteresis pattern that mimicked and even exceeded that observed in the stream. However, in wells with short travel times, we observed only a shallow peak in DOC and nitrate concentrations during the storm.

The timeframe in which we observed a nitrate and DOC response in long residence time wells in the hyporheic zone was too short for the solute pulse to be explained by stream water infiltration into the well network. Instead, we hypothesize that DOC- and nitrate- rich soil water was delivered to hyporheic flowpaths via vertical infiltration. Given that soils in the H.J. Andrews are highly porous and transmit water rapidly (Rothacher et al., 1967; Dyrness, 1969; Harr, 1976; Jones, 2000), we expect that rainwater could vertically infiltrate soils, mobilize DOC and nitrate that had accumulated in soils under dry conditions, and reach hyporheic flowpaths within hours. Vertical flow in unsaturated zones in WS1 soils has been observed during storm events (van Verseveld et al., 2008). Amongst wells that displayed the strongest hysteresis pattern (G1, G2, G3, D6), DOC concentrations during the second sampling run on the rising leg of the storm hydrograph were negatively related to pre-storm depth to water in these wells (Table 3.1; Corson-Rikert, 2014). This suggests that DOC- and nitrate-rich water, if transported via

vertical infiltration, reached wells located in regions with high pre-storm water tables before it reached wells with deeper initial water tables. If this were the case, DOC and nitrate would have accumulated over a longer period in the wells with shallow initial water tables, leading to higher total concentrations. In all wells, if DOC and nitrate concentrations in overlying soils were depleted, hyporheic concentrations of these solutes would have been diluted by continued vertical infiltration, potentially leading to the observed hysteresis concentration-discharge pattern (Figures 3.3, 3.4, 3.6). Nitrate concentrations could also be influenced by the location of individual alder trees, as dying alders may release nitrogen into surrounding soils. This might explain the late strong response in well D7, which is located downslope of a cluster of alders.

In contrast, we hypothesize that the broader concentration peaks observed in short travel time wells (Figures 3.4, 3.6) were the result of two processes – the vertical infiltration of solutes described above, as well as the lateral infiltration of stream water into the hyporheic zone. By the third and fourth sampling runs, stream water from early in the hydrograph with moderately elevated DOC and nitrate concentrations could potentially have reached short travel-time wells, prolonging the DOC and nitrate peaks that we suggest were produced due to vertical infiltration.

The DIC response in the hyporheic zone was not as clearly associated with travel time, although in wells with very short travel times, DIC concentrations decreased throughout the storm event, as in the stream. In the majority of the hyporheic wells we observed a decrease in and then slight recovery of DIC concentrations that coincided with a reduction in precipitation and discharge. In two hyporheic wells, this recovery continued even after additional precipitation caused streamflow to again increase. It is

possible that in the majority of wells, our sampling period was too short to capture any microbial response to the pulsed input of DOC.

Overall, during the small November storm event, we hypothesize that hyporheic solute concentrations in short residence time wells were influenced by both stream water and vertical leaching, while concentration patterns in intermediate and long residence time wells were influenced by vertical leaching alone.

### **3.7 *Conclusions***

We sampled a small headwater stream, a hillslope well, and nine hyporheic wells during a small November storm event in the Western Cascades of Oregon. In the stream, DOC and nitrate concentrations displayed clockwise hysteresis, and we observed a decrease in DIC concentrations and a steady increase in chloride concentrations.

Stream DOC concentrations were higher than hyporheic DOC concentrations in all but one well throughout the storm. In contrast, stream nitrate concentrations were lower than those observed in much of the well network. These patterns suggest that observed changes in stream solute concentrations are not explained by export from the distal ends of hyporheic flowpaths.

Several distinct patterns in solute concentrations emerged in the hyporheic zone. Travel time appeared be strongly associated with nitrate and DOC response patterns in the hyporheic zone. In wells with long travel times, DOC and nitrate concentrations showed a clockwise hysteresis pattern that mimicked and even exceeded that observed in the stream. We hypothesize that these solutes were flushed from overlying soils into the hyporheic zone via vertically infiltrating rainwater. In wells with short travel times, we

observed only a small peak in DOC and nitrate concentrations during the storm, which we suggest was due to the combined influence of stream water and vertical infiltration on short residence time wells. The DIC response in the hyporheic zone was not as clearly associated with travel time, although in wells with very short travel times DIC concentrations decreased throughout the storm event, as in the stream. In the majority of the hyporheic wells we observed a decrease in and then slight recovery of DIC concentrations that coincided with a modest reduction in precipitation and streamflow. In two hyporheic wells, this recovery continued even after additional precipitation caused streamflow to again increase. It is possible that in the majority of wells, our sampling period was too short to capture any microbial response to the pulsed input of DOC.

During this small November storm event, temporal patterns in stream water chemistry differed from patterns we observed in the well network. This suggests that whole-watershed processes that controlled stream water chemistry during this storm event were different than those that controlled solute concentrations in the hyporheic zone. Nonetheless, the hyporheic zone must have been linked to the stream. That measurements in our well network reveal a very different response between the stream and the hyporheic zone suggests that: 1) Our hyporheic zone is not representative of stream-hyporheic riparian processes that occur within the larger watershed, or 2) Hillslope-stream or within-stream processes dominate during storms, and at these times the influence of the hyporheic zone on the stream is much weaker than during baseflow.

### 3.8 References

- Benjamin, M. M. (2010) *Water Chemistry*. Waveland, Long Grove, IL.
- Bishop, K., J. Seibert, S. Köhler, and H. Laudon (2004), Resolving the Double Paradox of rapidly mobilized old water with highly variable responses in runoff chemistry, *Hydrological Processes*, 18, 185–189, doi:10.1002/hyp.5209.
- Buffam, I., J. N. Galloway, L. K. Blum, and K. J. McGlathery (2001), A stormflow / baseflow comparison of dissolved organic matter concentrations and bioavailability in an Appalachian stream, *Biogeochemistry*, 53, 269–306.
- CCAL (2013) CCAL Water Analysis Laboratory Quality Assurance Plan. Oregon State University and United States Forest Service Cooperative Chemical Analytical Laboratory.  
<http://www.ccal.oregonstate.edu/sites/ccal/files/pdf/QAP%20Rev%203%202013.pdf>
- Corson-Rikert, H. A. (2014), Carbon dynamics in the hyporheic zone of a headwater mountain stream in the Cascade Mountains, Oregon. M.S. Thesis. Oregon State University.
- Dyrness, C. T. (1969), Hydrologic properties of soils on three small watersheds in the western Cascades of Oregon, PNW-111, 17 pp., Pacific Northwest Forest and Range Experiment Station, U.S.D.A. Forest Service, Corvallis, Oregon.
- Halpern, C. B., and J. F. Franklin (1990), Physiognomic development of Pseudotsuga forests in relation to initial structure and disturbance intensity, *Journal of Vegetation Science*, 1, 475–482.
- Harr, R. D. (1976), Hydrology of small forest streams in western Oregon, PNW-55, 19 pp., Pacific Northwest Forest and Range Experiment Station, U.S.D.A. Forest Service, Corvallis, Oregon.
- Hinton, M. J., S. L. Schiff, and M. C. English (1998), Sources and flowpaths of dissolved organic carbon during storms in two forested watersheds of the Precambrian Shield, *Biogeochemistry*, 41, 175–197.
- Hood, E., D. M. McKnight, and M. W. Williams (2003), Sources and chemical character of dissolved organic carbon across an alpine/subalpine ecotone, Green Lakes Valley, Colorado Front Range, United States, *Water Resources Research*, 39(7), doi:10.1029/2002WR001738.

- Hood, E., M. N. Gooseff, and S. L. Johnson (2006), Changes in the character of stream water dissolved organic carbon during flushing in three small watersheds, Oregon, *Journal of Geophysical Research*, 111, G01007, doi:10.1029/2005JG000082.
- Hornberger, G. M., K. E. Bencala, and D. M. McKnight (1994), Hydrological controls on dissolved organic carbon during snowmelt in the Snake River near Montezuma , Colorado, *Biogeochemistry*, 25, 147–165.
- Johnson, S. L., and J. A. Jones (2000), Stream temperature responses to forest harvest and debris flows in western Cascades, Oregon, *Canadian Journal of Fisheries and Aquatic Sciences*, 57(S2), 30–39, doi:10.1139/cjfas-57-S2-30.
- Jones, J. A. (2000), Hydrologic processes and peak discharge response to forest removal, regrowth, and roads in 10 small experimental basins, Western Cascades, Oregon, *Water Resources Research*, 36(9), 2621–2642, doi:10.1029/2000WR900105.
- McGlynn, B. L., and J. J. McDonnell (2003), Role of discrete landscape units in controlling catchment dissolved organic carbon dynamics, *Water Resources Research*, 39(4), doi:10.1029/2002WR001525.
- Millero, F. J., T. B. Graham, F. Huang, H. Bustos-Serrano, and D. Pierrot (2006), Dissociation constants of carbonic acid in seawater as a function of salinity and temperature, *Marine Chemistry*, 100, 80–94, doi:10.1016/j.marchem.2005.12.001.
- Pacific, V. J., K. G. Jencso, and B. L. McGlynn (2010), Variable flushing mechanisms and landscape structure control stream DOC export during snowmelt in a set of nested catchments, *Biogeochemistry*, 99, 193–211, doi:10.1007/s10533-009-9401-1.
- Raymond, P. A., and J. E. Saiers (2010), Event controlled DOC export from forested watersheds, *Biogeochemistry*, 100(1-3), 197–209, doi:10.1007/s10533-010-9416-7.
- Raymond, P. A., C. J. Zappa, D. Butman, T. L. Bott, J. Potter, P. Mulholland, A. E. Laursen, W. H. McDowell, and D. Newbold (2012), Scaling the gas transfer velocity and hydraulic geometry in streams and small rivers, *Limnology & Oceanography: Fluids & Environments*, 2, 41–53, doi:10.1215/21573689-1597669.
- Rothacher, J., C. T. Dyrness, and R.L. Fredriksen (1967), Hydrologic and related characteristics of three small watersheds in the Oregon Cascades, report, 54 pp., Pacific Northwest Forest and Range Experiment Station, U.S.D.A. Forest Service, Corvallis, Oregon.

- Van Verseveld, W. J., J. J. McDonnell, and K. Lajtha (2008), A mechanistic assessment of nutrient flushing at the catchment scale, *Journal of Hydrology*, 358, 268–287, doi:10.1016/j.jhydrol.2008.06.009.
- Ward, A. S., M. Fitzgerald, M. N. Gooseff, T. J. Voltz, A. M. Binley, and K. Singha (2012), Hydrologic and geomorphic controls on hyporheic exchange during base flow recession in a headwater mountain stream, *Water Resources Research*, 48(4), n/a–n/a, doi:10.1029/2011WR011461.
- Wilson, H. F., J. E. Saiers, P. A. Raymond, and W. V. Sobczak (2013), Hydrologic Drivers and Seasonality of Dissolved Organic Carbon Concentration, Nitrogen Content, Bioavailability, and Export in a Forested New England Stream, *Ecosystems*, 16(4), 604–616, doi:10.1007/s10021-013-9635-6.
- Wondzell, S. M. (2006), Effect of morphology and discharge on hyporheic exchange flows in two small streams in the Cascade Mountains of Oregon, USA, *Hydrological Processes*, 20(2), 267–287, doi:10.1002/hyp.5902.

#### 4 Conclusions

We studied carbon dynamics in the hyporheic zone of a headwater mountain stream located within the H.J. Andrews Experimental Forest. We sampled under baseflow conditions during seven months, capturing a seasonal shift from dry summer conditions to the wet fall and winter months. We also sampled during one fall storm event, collecting pre-storm, rising leg, and extended high flow samples.

The hydrology of this system is complex – hyporheic exchange flows follow extended, non-linear flow paths through a heterogeneous subsurface and may be augmented by lateral inflows of groundwater and, during storms, vertical infiltration of soil water. As a result, the dynamics of carbon processing that we observed within the well network are exceptionally difficult to interpret. Each observed concentration is the sum of numerous biogeochemical processes – which may amplify or negate one another – as well as physical processes – which lead water from a variety of sources to mix in unknown portions and control the rate at which water moves through the subsurface. At the network scale, the end result is a composite signal, the layers of which are difficult to tease apart. Despite the physical complexity of our site and the temporal span of our investigation, patterns in carbon dynamics did emerge:

During baseflow periods, hyporheic DOC decreased with median travel time through the subsurface. DIC concentrations increased with travel time, but the magnitude of this increase in DIC was too large to be explained by metabolism of stream water DOC. This suggests that there are additional sources of DIC and/or DOC in the subsurface, and that hyporheic DIC concentrations are not well linked to stream-source DOC. The most likely supplemental sources of DIC to hyporheic water are soil CO<sub>2</sub> and

microbial respiration of DOC leached from buried particulate organic matter and from overlying soils. Overall, the hyporheic zone appears to be a source of DIC to the stream.

In summer, the hyporheic zone is likely isolated from vertical infiltration or lateral inflow of soil water, and particulate organic carbon is not present in stream water. Thus, spatial patterns in hyporheic zone biogeochemistry must result from underlying spatial patterns in hyporheic flowpaths, groundwater inputs, and buried particulate organic carbon. With the transition to the rainy season throughout the fall and early winter, vertical infiltration and leaching of accumulated solutes from the overlying soil appear to become important sources of carbon that help explain patterns in hyporheic zone biogeochemistry.

During a small November storm event, DOC and nitrate concentrations in the stream displayed clockwise hysteresis, and we observed a decrease in DIC concentrations and a steady increase in chloride concentrations. DOC concentrations in the hyporheic zone were lower than those observed in the stream, while nitrate and DIC concentrations in the hyporheic zone were higher than those observed in the stream. Travel time appeared to be associated with both nitrate and DOC response patterns in the hyporheic zone. In wells with long travel times, DOC and nitrate concentrations showed a clockwise hysteresis pattern that mimicked and even exceeded that observed in the stream. We hypothesize that these solutes were flushed from overlying soils into the hyporheic zone via vertically infiltrating rainwater. In wells with short travel times, we observed only a small peak in DOC and nitrate concentrations during the storm, potentially due to lateral infiltration of stream water later in the event. The DIC response in the hyporheic zone was not as clearly associated with travel time, although in wells

with very short travel times, DIC concentrations decreased throughout the storm event, as in the stream. In the majority of the hyporheic wells we observed a decrease in and then slight recovery of DIC concentrations that coincided with a modest reduction in precipitation and streamflow. In two hyporheic wells, this recovery continued even after additional precipitation caused streamflow to again increase.

Overall, temporal patterns in stream water chemistry during the November storm differed from patterns we observed in the well network. This suggests that whole-watershed processes that controlled stream water chemistry during this storm event were different than those that controlled solute concentrations in the hyporheic zone. Nonetheless, the hyporheic zone must have been linked to the stream. That measurements in our well network reveal a very different response between the stream and the hyporheic zone suggests that: 1) Our hyporheic zone is not representative of stream-hyporheic riparian processes that occur within the larger watershed, or 2) Hillslope-stream or within-stream processes dominate during storms, and at these times the influence of the hyporheic zone on the stream is much weaker than during baseflow.

Results from both baseflow and storm sampling suggest that a complex set of physical mechanisms and biogeochemical processes influence carbon transport and transformation within this hyporheic environment. Future work, through conservative tracer injections, reactive transport modeling, additional instrumentation of the well network, and continued monthly sampling, will seek to better understand how carbon is delivered to and transported through the well network, and will identify the biogeochemical processes that drive the consumption of DOC and production of DIC in this hyporheic environment.

## BIBLIOGRAPHY

- Aufdenkampe, A. K., E. Mayorga, P. A. Raymond, J. M. Melack, S. C. Doney, S. R. Alin, R. E. Aalto, and K. Yoo (2011), Riverine coupling of biogeochemical cycles between land, oceans, and atmosphere, *Frontiers in Ecology and the Environment*, 9(1), 53–60, doi:10.1890/100014.
- Baker, M. A., C. N. Dahm, and H. M. Valett (1999), Acetate retention and metabolism in the hyporheic zone of a mountain stream, *Limnology and Oceanography*, 44(6), 1530–1539, doi:10.4319/lo.1999.44.6.1530.
- Battin, T. J. (1999), Hydrologic flow paths control dissolved organic carbon fluxes and metabolism in an alpine stream hyporheic zone, *Water Resources Research*, 35(10), 3159–3169.
- Battin, T. J. (2000), Hydrodynamics is a major determinant of streambed biofilm activity : From the sediment to the reach scale, *Limnology and Oceanography*, 45(6), 1308–1319.
- Battin, T. J., L. A. Kaplan, D. J. Newbold, and S. P. Hendricks (2003), A mixing model analysis of stream solute dynamics and the contribution of a hyporheic zone to ecosystem function, *Freshwater Biology*, 48, 995–1014.
- Battin, T. J., L. A. Kaplan, S. Findlay, C. S. Hopkinson, E. Marti, A. I. Packman, J. D. Newbold, and F. Sabater (2008), Biophysical controls on organic carbon fluxes in fluvial networks, *Nature Geoscience*, 1, 95–100, doi:10.1038/ngeo602.
- Benjamin, M. M. (2010) *Water Chemistry*. Waveland, Long Grove, IL.
- Benstead, J. P., and D. S. Leigh (2012), An expanded role for river networks, *Nature Geoscience*, 5, 678–679, doi:10.1038/ngeo1593.
- Bishop, K., J. Seibert, S. Köhler, and H. Laudon (2004), Resolving the Double Paradox of rapidly mobilized old water with highly variable responses in runoff chemistry, *Hydrological Processes*, 18, 185–189, doi:10.1002/hyp.5209.
- Boulton, A. J., and J. G. Foster (1998), Effects of buried leaf litter and vertical hydrologic exchange on hyporheic water chemistry and fauna in a gravel-bed river in northern New South Wales, Australia, *Freshwater Biology*, (40), 229–243.
- Buffam, I., J. N. Galloway, L. K. Blum, and K. J. McGlathery (2001), A stormflow / baseflow comparison of dissolved organic matter concentrations and bioavailability in an Appalachian stream, *Biogeochemistry*, 53, 269–306.

- Butman, D., and P. A. Raymond (2011), Significant efflux of carbon dioxide from streams and rivers in the United States, *Nature Geoscience*, 4, 839–842, doi:10.1038/ngeo1294.
- CCAL (2013) CCAL Water Analysis Laboratory Quality Assurance Plan. Oregon State University and United States Forest Service Cooperative Chemical Analytical Laboratory.  
<http://www.ccal.oregonstate.edu/sites/ccal/files/pdf/QAP%20Rev%203%202013.pdf>
- Chestnut, T. J., and W. H. McDowell (2000), C and N dynamics in the riparian and hyporheic zones of a tropical stream, Luquillo Mountains, Puerto Rico, *Journal of the North American Benthological Society*, 19(2), 199–214.
- Cole, J. J., Y. T. Prairie, N. F. Caraco, W. H. McDowell, L. J. Tranvik, R. G. Striegl, C. M. Duarte, P. Kortelainen, J. A. Downing, J. J. Middelburg, and J. Melack (2007), Plumbing the Global Carbon Cycle: Integrating Inland Waters into the Terrestrial Carbon Budget, *Ecosystems*, 10, 171–184, doi:10.1007/s10021-006-9013-8.
- Corson-Rikert, H. A. (2014), Carbon dynamics in the hyporheic zone of a headwater mountain stream in the Cascade Mountains, Oregon. M.S. Thesis. Oregon State University.
- Crawford, J. T., R. G. Striegl, K. P. Wickland, M. M. Dornblaser, and E. H. Stanley (2013), Emissions of carbon dioxide and methane from a headwater stream network of interior Alaska, *Journal of Geophysical Research: Biogeosciences*, 118(2), 482–494, doi:10.1002/jgrg.20034.
- Crocker, M. T., and J. L. Meyer (2014), Stream Interstitial dissolved organic carbon in sediments of a southern Appalachian headwater stream, *Journal of the North American Benthological Society*, 6(3), 159–167.
- Downing, J., J. J. Cole, C. M. Duarte, J. J. Middelburg, J. M. Melack, Y. T. Prairie, P. Kortelainen, R. G. Striegl, W. H. McDowell, and L. J. Tranvik (2012), Global abundance and size distribution of streams and rivers, *Inland Waters*, 2, 229–236, doi:10.5268/IW-2.4.502.
- Dyrness, C. T. (1969), Hydrologic properties of soils on three small watersheds in the western Cascades of Oregon, PNW-111, 17 pp., Pacific Northwest Forest and Range Experiment Station, U.S.D.A. Forest Service, Corvallis, Oregon.
- Findlay, S. (1995), Importance of surface-subsurface exchange in stream exchange ecosystems: The hyporheic zone, *Limnology and Oceanography*, 40(1), 159–164.

- Findlay, S., and W. V Sobczak (1996), Variability in removal of dissolved organic carbon in hyporheic sediments, *Journal of the North American Benthological Society*, 15(1), 35–41.
- Findlay, S., D. Strayer, C. Goumbala, and K. Gould (1993), Metabolism of streamwater dissolved organic carbon in the shallow hyporheic zone, *Limnology and Oceanography*, 38(7), 1493–1499, doi:10.4319/lo.1993.38.7.1493.
- Grimm, N. B., and S. G. Fisher (1984), Exchange between interstitial and surface water : Implications for stream metabolism and nutrient cycling, *Hydrobiologia*, 111, 219–228.
- Gurwick, N. P., D. M. McCorkle, P. M. Groffman, A. J. Gold, D. Q. Kellogg, and P. Seitz-Rundlett (2008), Mineralization of ancient carbon in the subsurface of riparian forests, *Journal of Geophysical Research*, 113, G02021, doi:10.1029/2007JG000482.
- Halpern, C. B., and J. F. Franklin (1990), Physiognomic development of *Pseudotsuga* forests in relation to initial structure and disturbance intensity, *Journal of Vegetation Science*, 1, 475–482.
- Harr, R. D. (1976), Hydrology of small forest streams in western Oregon, PNW-55, 19 pp., Pacific Northwest Forest and Range Experiment Station, U.S.D.A. Forest Service, Corvallis, Oregon.
- Hedin, L. O. (1990), Factors controlling sediment community respiration in woodland stream ecosystems, *Oikos*, 57, 94–105.
- Hinton, M. J., S. L. Schiff, and M. C. English (1998), Sources and flowpaths of dissolved organic carbon during storms in two forested watersheds of the Precambrian Shield, *Biogeochemistry*, 41, 175–197.
- Hood, E., D. M. McKnight, and M. W. Williams (2003), Sources and chemical character of dissolved organic carbon across an alpine/subalpine ecotone, Green Lakes Valley, Colorado Front Range, United States, *Water Resources Research*, 39(7), doi:10.1029/2002WR001738.
- Hood, E., M. N. Gooseff, and S. L. Johnson (2006), Changes in the character of stream water dissolved organic carbon during flushing in three small watersheds, Oregon, *Journal of Geophysical Research*, 111, G01007, doi:10.1029/2005JG000082.
- Hornberger, G. M., K. E. Bencala, and D. M. McKnight (1994), Hydrological controls on dissolved organic carbon during snowmelt in the Snake River near Montezuma , Colorado, *Biogeochemistry*, 25, 147–165.

- Jencso, K. G., B. L. McGlynn, M. N. Gooseff, K. E. Bencala, and S. M. Wondzell (2010), Hillslope hydrologic connectivity controls riparian groundwater turnover: Implications of catchment structure for riparian buffering and stream water sources, *Water Resources Research*, 46(10), doi:10.1029/2009WR008818.
- Johnson, S. L., and J. A. Jones (2000), Stream temperature responses to forest harvest and debris flows in western Cascades, Oregon, *Canadian Journal of Fisheries and Aquatic Sciences*, 57(S2), 30–39, doi:10.1139/cjfas-57-S2-30.
- Jones, J. A. (2000), Hydrologic processes and peak discharge response to forest removal, regrowth, and roads in 10 small experimental basins, Western Cascades, Oregon, *Water Resources Research*, 36(9), 2621–2642, doi:10.1029/2000WR900105.
- Kasahara, T., and S. M. Wondzell (2003), Geomorphic controls on hyporheic exchange flow in mountain streams, *Water Resources Research*, 39(1), 1–14, doi:10.1029/2002WR001386.
- Khadka, M. B., J. B. Martin, and J. Jin (2014), Transport of dissolved carbon and CO<sub>2</sub> degassing from a river system in a mixed silicate and carbonate catchment, *Journal of Hydrology*, 513, 391–402, doi:10.1016/j.jhydrol.2014.03.070.
- Levno, A., and J. Rothacher (1969), Increases in maximum stream temperatures after slash burning in a small experimental watershed, PNW-11, 7 pp., Pacific Northwest Forest and Range Experiment Station, U.S.D.A. Forest Service, Corvallis, Oregon.
- Liu, W., X. Xu, N. M. McGoff, J. M. Eaton, P. Leahy, N. Foley, and G. Kiely (2014), Spatial and Seasonal Variation of dissolved organic carbon (DOC) concentrations in Irish streams: importance of soil and topography characteristics., *Environmental management*, 53(5), 959–67, doi:10.1007/s00267-014-0259-1.
- McDowell, W. H. (1985), Kinetics and Mechanisms of Dissolved Organic Carbon Retention in a Headwater Stream, *Biogeochemistry*, 1(4), 329–352.
- McGlynn, B. L., and J. J. McDonnell (2003), Role of discrete landscape units in controlling catchment dissolved organic carbon dynamics, *Water Resources Research*, 39(4), doi:10.1029/2002WR001525.
- Millero, F. J., T. B. Graham, F. Huang, H. Bustos-Serrano, and D. Pierrot (2006), Dissociation constants of carbonic acid in seawater as a function of salinity and temperature, *Marine Chemistry*, 100, 80–94, doi:10.1016/j.marchem.2005.12.001.
- Mulholland, P. J., E. R. Marzolf, J. R. Webster, D. R. Hart, and S. P. Hendricks (1997), Evidence that hyporheic zones increase heterotrophic metabolism and phosphorus uptake in forest streams, *Limnology and Oceanography*, 42(3), 443–451.

- Öquist, M. G., M. Wallin, J. Seibert, K. Bishop, and H. Laudon (2009), Dissolved inorganic carbon export across the soil/stream interface and its fate in a boreal headwater stream., *Environmental science & technology*, 43(19), 7364–9.
- Pacific, V. J., K. G. Jencso, and B. L. McGlynn (2010), Variable flushing mechanisms and landscape structure control stream DOC export during snowmelt in a set of nested catchments, *Biogeochemistry*, 99, 193–211, doi:10.1007/s10533-009-9401-1.
- Poole, G. C., S. J. O'Daniel, K. L. Jones, W. W. Woessner, E. S. Bernhardt, A. M. Helton, J. A. Stanford, B. R. Boer, and T. J. Beechie (2008), Hydrologic spiralling: the role of multiple interactive flow paths in stream ecosystems, *River research and applications*, 14 pp, doi:10.1002/rra.1099.
- Pusch, M. (1996), The metabolism of organic matter in the hyporheic zone of a mountain stream , and its spatial distribution, *Hydrobiologia*, 107–118.
- Pusch, M., and J. Schwoerbel (1994), Community respiration in hyporheic sediments of a mountain stream (Steina, Black Forest), *Archiv fur Hydrobiologie*, 130(1), 35–52.
- Raymond, P. A., and J. E. Bauer (2001), Riverine export of aged terrestrial organic matter to the North Atlantic Ocean., *Nature*, 409, 497–500.
- Raymond, P. A., and J. E. Saiers (2010), Event controlled DOC export from forested watersheds, *Biogeochemistry*, 100(1-3), 197–209, doi:10.1007/s10533-010-9416-7.
- Raymond, P. A., C. J. Zappa, D. Butman, T. L. Bott, J. Potter, P. Mulholland, A. E. Laursen, W. H. McDowell, and D. Newbold (2012), Scaling the gas transfer velocity and hydraulic geometry in streams and small rivers, *Limnology & Oceanography: Fluids & Environments*, 2, 41–53, doi:10.1215/21573689-1597669.
- Robbins, L. L., M. E. Hansen, J. A. Kleypas, and S. C. Meylan (2010), *CO2calc: A User-Friendly Seawater Carbon Calculator for Windows, Mac OS X, and iOS (iPhone)*.
- Rothacher, J., C. T. Dyrness, and R.L. Fredriksen (1967), Hydrologic and related characteristics of three small watersheds in the Oregon Cascades, report, 54 pp., Pacific Northwest Forest and Range Experiment Station, U.S.D.A. Forest Service, Corvallis, Oregon.
- Schindler, J. E., and D. P. Krabbenhoft (1998), The hyporheic zone as a source of dissolved organic carbon and carbon gases to a temperate forested stream, *Biogeochemistry*, 43(2), 157–174.

- Sobczak, W. V., and S. Findlay (2002), Variation in bioavailability of dissolved organic carbon among stream hyporheic flowpaths, *Ecology*, 83(11), 3194–3209.
- Stumm, W., and J. J. Morgan (1996), Aquatic Chemistry, Chemical Equilibria and Rates in Natural Waters, 3rd ed., John Wiley, New York.
- Swanson, F.J., and M.E. James (1975), Geology and geomorphology of the H.J. Andrews Experimental Forest, Western Cascades, Oregon, PNW-188, 15 pp., Pacific Northwest Forest and Range Experiment Station, U.S.D.A. Forest Service, Corvallis, Oregon.
- Tsyplkin, M., and G. L. Macpherson (2012), The effect of precipitation events on inorganic carbon in soil and shallow groundwater, Konza Prairie LTER Site, NE Kansas, USA, *Applied Geochemistry*, 27, 2356–2369, doi:10.1016/j.apgeochem.2012.07.008.
- Van Verseveld, W. J., J. J. McDonnell, and K. Lajtha (2008), A mechanistic assessment of nutrient flushing at the catchment scale, *Journal of Hydrology*, 358, 268–287, doi:10.1016/j.jhydrol.2008.06.009.
- Voltz, T., M. Gooseff, A. S. Ward, K. Singha, M. Fitzgerald, and T. Wagener (2013), Riparian hydraulic gradient and stream-groundwater exchange dynamics in steep headwater valleys, *Journal of Geophysical Research: Earth Surface*, 118(2), 953–969, doi:10.1002/jgrf.20074.
- Ward, A. S., M. Fitzgerald, M. N. Gooseff, T. J. Voltz, A. M. Binley, and K. Singha (2012), Hydrologic and geomorphic controls on hyporheic exchange during base flow recession in a headwater mountain stream, *Water Resources Research*, 48(4), n/a–n/a, doi:10.1029/2011WR011461.
- Wilson, H. F., J. E. Saiers, P. A. Raymond, and W. V. Sobczak (2013), Hydrologic Drivers and Seasonality of Dissolved Organic Carbon Concentration, Nitrogen Content, Bioavailability, and Export in a Forested New England Stream, *Ecosystems*, 16(4), 604–616, doi:10.1007/s10021-013-9635-6.
- Wondzell, S. M. (2006), Effect of morphology and discharge on hyporheic exchange flows in two small streams in the Cascade Mountains of Oregon, USA, *Hydrological Processes*, 20(2), 267–287, doi:10.1002/hyp.5902.
- Wondzell, S. M. (2011), The role of the hyporheic zone across stream networks, *Hydrological Processes*, 25(22), 3525–3532, doi:10.1002/hyp.8119.
- Wondzell, S. M. (2012), Hyporheic Zones in Mountain Streams: Physical Processes and Ecosystem Functions, *Rocky Mountain Research Station - Stream Notes*.

Wondzell, S. M., J. LaNier, and R. Haggerty (2009), Evaluation of alternative groundwater flow models for simulating hyporheic exchange in a small mountain stream, *Journal of Hydrology*, 364(1-2), 142–151,  
doi:10.1016/j.jhydrol.2008.10.011.

Yvon-Durocher, G., J. M. Caffrey, A. Cescatti, M. Dossena, P. del Giorgio, J. M. Gasol, J. M. Montoya, J. Pumpanen, P. A. Staehr, M. Trimmer, G. Woodward, and A. P. Allen (2012), Reconciling the temperature dependence of respiration across timescales and ecosystem types., *Nature Letters*, 487(7408), 472–6,  
doi:10.1038/nature11205.

Zarnetske, J. P., R. Haggerty, S. M. Wondzell, and M. A. Baker (2011), Dynamics of nitrate production and removal as a function of residence time in the hyporheic zone, *Journal of Geophysical Research*, 116, G01025,  
doi:10.1029/2010JG001356

## **APPENDICES**

## Appendix A Complete model lists

### Appendix A.1 Complete list of September DOC models

**Table A.1** - A full list of DOC models for September. Models are ranked based on the associated AIC values. Adjusted  $r^2$  are given since the models include three terms.

Rank	Variables	lm AIC	$r^2a$	Need Spatial Correlation Structure?
1	$\text{PO}_4^{3-}$ , pH, $\text{Ca}^{+2}$	-202.20	0.769	no
2	$\text{PO}_4^{3-}$ , Total Alk., $\text{Mg}^{+2}$	-201.11	0.760	no
3	$\text{PO}_4^{3-}$ , $\text{Ca}^{+2}$ , Travel Time	-200.64	0.756	no
4	$\text{PO}_4^{3-}$ , $\text{Ca}^{+2}$ , $\text{Mg}^{+2}$	-200.30	0.753	no
5	$\text{PO}_4^{3-}$ , $\text{Ca}^{+2}$ , $\text{NO}_3^-$	-199.76	0.747	no
6	$\text{PO}_4^{3-}$ , Dist. from stream, $\text{NO}_3^-$	-199.67	0.747	no
7	$\text{PO}_4^{3-}$ , $\text{Ca}^{+2}$ , $\text{K}^+$	-199.62	0.746	no
8	$\text{PO}_4^{3-}$ , $\text{Ca}^{+2}$ , Anion Def.	-199.42	0.744	no
9	$\text{PO}_4^{3-}$ , $\text{NO}_3^-$ , $\text{SO}_4^{-2}$	-197.95	0.730	no
10	$\text{PO}_4^{3-}$ , Travel Time, Total Alk.	-197.83	0.729	no
11	$\text{NO}_3^-$ , Dist. from stream, $\text{SO}_4^{-2}$	-189.69	0.633	no
12	$\text{NO}_3^-$ , Temp., Dist. from stream	-187.09	0.596	no
13	Travel Time, $\text{SO}_4^{-2}$ , $\text{Ca}^{+2}$	-185.49	0.572	no
14	$\text{K}^+$ , Total Alk., $\text{Mg}^{+2}$	-183.82	0.544	no
15	Travel Time, $\text{SO}_4^{-2}$ , Total Alk.	-182.03	0.513	no
16	Travel Time, $\text{SO}_4^{-2}$ , $\text{NO}_3^-$	-179.77	0.470	no

### Appendix A.2 Complete list of November DOC models

**Table A.2** - A full list of DOC models for November. Models are ranked based on the associated AIC values. Adjusted  $r^2$  are given since the models include three terms.

Rank	Variables	November DOC Models				Best gls AIC with Spatial Corr. Structure	Spatial Corr. Type
		lm AIC	$r^2a$	Need Spatial Corr. Structure?	gls model AIC		
1	Temp., Cl <sup>-</sup> , K <sup>+</sup>	-171.2	0.74	?	-156.9	-159.6	Ratio
2	Temp., K <sup>+</sup> , Anion Def.	-170.9	0.74	no			
3	Temp., PO <sub>4</sub> <sup>-3</sup> , Dist. from stream	-170.3	0.74	no			
4	K <sup>+</sup> , SO <sub>4</sub> <sup>-2</sup> , Cl <sup>-</sup>	-169.5	0.73	no			
5	PO <sub>4</sub> <sup>-3</sup> , SO <sub>4</sub> <sup>-2</sup> , K <sup>+</sup>	-168.8	0.72	no			
6	pH, Cl <sup>-</sup> , K <sup>+</sup>	-168.4	0.72	no			
7	PO <sub>4</sub> <sup>-3</sup> , NO <sub>3</sub> <sup>-</sup> , Na <sup>+</sup>	-168.0	0.71	no			
8	PO <sub>4</sub> <sup>-3</sup> , NO <sub>3</sub> <sup>-</sup> , SO <sub>4</sub> <sup>-2</sup>	-166.2	0.69	no			
9	Cl <sup>-</sup> , Mg <sup>+2</sup> , K <sup>+</sup>	-165.4	0.68	no			
10	pH, PO <sub>4</sub> <sup>-3</sup> , NO <sub>3</sub> <sup>-</sup>	-165.4	0.68	no			
11	Cl <sup>-</sup> , Anion Def., K <sup>+</sup>	-165.3	0.68	no			
12	NO <sub>3</sub> <sup>-</sup> , Cl <sup>-</sup>	-165.2	0.67	no			
13	PO <sub>4</sub> <sup>-3</sup> , Mg <sup>+2</sup> , Cl <sup>-</sup>	-164.2	0.67	no			
14	PO <sub>4</sub> <sup>-3</sup> , Mg <sup>+2</sup> , Na <sup>+</sup>	-162.3	0.64	no			
15	NO <sub>3</sub> <sup>-</sup> , Na <sup>+</sup> , K <sup>+</sup>	-161.5	0.63	no			
16	PO <sub>4</sub> <sup>-3</sup> , NO <sub>3</sub> <sup>-</sup> , Ca <sup>+2</sup>	-161.3	0.63	no			
17	PO <sub>4</sub> <sup>-3</sup> , Anion Def., Dist. from stream	-160.5	0.62	no			
18	Na <sup>+</sup> , K <sup>+</sup> , Mg <sup>+2</sup>	-160.4	0.61	no			
19	PO <sub>4</sub> <sup>-3</sup> , Anion Def., NO <sub>3</sub> <sup>-</sup>	-160.2	0.61	no			
20	PO <sub>4</sub> <sup>-3</sup> , Mg <sup>+2</sup> , Dist. from stream	-160.1	0.61	no			
21	PO <sub>4</sub> <sup>-3</sup> , Dist. from stream, NO <sub>3</sub> <sup>-</sup>	-159.0	0.59	no			
22	PO <sub>4</sub> <sup>-3</sup> , NO <sub>3</sub> <sup>-</sup> , Total Alk.	-158.8	0.59	no			
23	K <sup>+</sup> , Mg <sup>+2</sup> , Dist. from stream	-155.9	0.54	no			
24	PO <sub>4</sub> <sup>-3</sup> , Mg <sup>+2</sup> , Total Alk.	-155.9	0.54	no			
25	PO <sub>4</sub> <sup>-3</sup> , Depth to Water, Na <sup>+</sup>	-151.4	0.45	?	-129.8	-131.5	Ratio

### Appendix A.3 Initial list of September DIC models

**Table A.3** – An initial list of DIC models for November, before the stepwise regression was re-done to include a spatial autocorrelation structure. Models are ranked based on the associated AIC values. Adjusted  $r^2$  are given since the models include three terms.

September DIC models							
(WITHOUT a spatial autocorrelation structure)							
Rank	Variables	lm AIC	$r^2a$	Need Spatial Corr. Structure?	Orig. model AIC	Best gls AIC with Spatial Corr. Structure	Spatial Corr. Type
1	pH, Total Alk., Anion Def.	-84.6	0.94	no			
2	pH, Total Alk, $\text{SO}_4^{2-}$	-82.2	0.94	no			
3	pH, Depth to Water, $\text{Mg}^{+2}$	-80.5	0.93	no			
4	pH, $\text{Mg}^{+2}$ , Anion Def.	-79.2	0.93	no			
5	pH, Total Alk., $\text{Ca}^{+2}$	-77.0	0.92	no			
6	pH, Sampling Depth, Total Alk.	-76.8	0.92	no			
7	pH, $\text{Mg}^{+2}$ , $\text{SO}_4^{2-}$	-75.5	0.92	?	-72.4	-73.9	Gaus
8	pH, Sampling Depth, $\text{Mg}^{+2}$	-75.4	0.92	no			
9	pH, Total Alk., $\text{PO}_4^{-3}$	-75.1	0.92	no			
10	pH, Sampling Depth, Temp.	-74.6	0.92	no			
11	$\text{SO}_4^{2-}$ , Total Alk., DOC	-50.0	0.79	?	-53.9	-57.2	Gaus
12	$\text{SO}_4^{2-}$ , $\text{NO}_3^-$ , $\text{Mg}^{+2}$	-48.7	0.78	yes	-58.7	-63.2	Gaus
13	$\text{SO}_4^{2-}$ , $\text{Mg}^{+2}$ , DOC	-47.7	0.77	yes	-54.4	-58.8	Gaus
14	$\text{SO}_4^{2-}$ , $\text{K}^+$ , $\text{Mg}^{+2}$	-44.5	0.74	yes	-56.6	-60.6	Gaus
15	$\text{SO}_4^{2-}$ , $\text{PO}_4^{-3}$ , $\text{Mg}^{+2}$	-44.2	0.74	yes	-58.3	-62.5	Gaus
16	$\text{SO}_4^{2-}$ , Dist. from stream, Total Alk.	-42.9	0.73	yes	-37.2	-40.9	Gaus
17	$\text{SO}_4^{2-}$ , Total Alk., $\text{NO}_3^-$	-41.7	0.72	yes	-50.4	-55.1	Gaus
18	$\text{SO}_4^{2-}$ , DOC, $\text{Ca}^{+2}$	-41.6	0.71	yes	-47.4	-51.8	Gaus
19	$\text{Ca}^{+2}$ , Total Alk., Travel Time	-41.4	0.71	no			
20	$\text{SO}_4^{2-}$ , Total Alk., $\text{PO}_4^{-3}$	-40.6	0.70	?	-52.8	-53.8	Gaus
21	$\text{Mg}^{+2}$ , $\text{Ca}^{+2}$ , Travel Time	-40.5	0.70	no			
22	$\text{SO}_4^{2-}$ , $\text{NO}_3^-$ , Temp.	-37.5	0.67	yes	-40.7	-45.1	Ratio
23	$\text{SO}_4^{2-}$ , Total Alk., $\text{Ca}^{+2}$	-37.1	0.66	yes	-43.3	-48.7	Gaus
24	$\text{Mg}^{+2}$ , $\text{Ca}^{+2}$ , $\ln K_{\text{sat}}$	-36.0	0.65	?	-29.8	-30.8	Gaus
25	$\text{Ca}^{+2}$ , Total Alk., $\ln K_{\text{sat}}$	-35.8	0.64	?	-28.4	-29.1	Gaus
26	$\text{Mg}^{+2}$ , Total Alk., Travel Time	-35.5	0.64	no			
27	$\text{Mg}^{+2}$ , $\text{PO}_4^{-3}$ , DOC	-30.4	0.57	no			
28	$\text{Ca}^{+2}$ , Total Alk., Anion Def.	-29.3	0.55	no			
29	$\text{Mg}^{+2}$ , $\text{PO}_4^{-3}$ , Dist. from stream	-28.9	0.54	yes	-30.4	-34.2	Gaus
30	$\text{Mg}^{+2}$ , $\text{Na}^+$ , $\text{K}^+$	-26.8	0.51	no			
31	$\text{Mg}^{+2}$ , $\text{PO}_4^{-3}$ , $\text{Na}^+$	-26.5	0.50	?	-40.6	-43.2	Gaus
32	$\text{Mg}^{+2}$ , $\text{PO}_4^{-3}$ , $\text{NO}_3^-$	-24.9	0.47	yes	-41.3	-47.1	Gaus
33	$\text{Mg}^{+2}$ , $\ln K_{\text{sat}}$ , $\text{K}^+$	-23.6	0.44	yes	-25.3	-39.0	Gaus
34	$\text{Ca}^{+2}$ , $\ln K_{\text{sat}}$ , $\text{Na}^+$	-23.3	0.44	yes	-19.9	-27.3	Gaus
35	$\text{Mg}^{+2}$ , $\text{PO}_4^{-3}$ , $\ln K_{\text{sat}}$	-23.0	0.43	yes	-26.5	-31.5	Gaus

#### Appendix A.4 Final list of September DIC models

**Table A.4** – A full list of DIC models for September, with the Gaussian spatial autocorrelation structure. Models are ranked based on the associated AIC values.  $r^2$  cannot be computed for general linear models fit with the 'nlme' package in R.

September DIC Models (with Gaussian spatial autocorrelation structure)		
Rank	Variables	gls AIC
1	pH, Mg <sup>+2</sup> , SO <sub>4</sub> <sup>-2</sup>	-73.9
2	pH, Mg <sup>+2</sup> , PO <sub>4</sub> <sup>-3</sup>	-73.0
3	SO <sub>4</sub> <sup>-2</sup> , Total Alk., pH	-72.7
4	pH, Anion Def., Total Alk.	-67.9
5	pH, Mg <sup>+2</sup> , Anion Def.	-66.3
6	Ca <sup>+2</sup> , Total Alk., pH	-64.2
7	pH, Anion Def., Ca <sup>+2</sup>	-62.6
8	SO <sub>4</sub> <sup>-2</sup> , DOC, Cl <sup>-</sup>	-62.0
9	Depth to Water, pH, SO <sub>4</sub> <sup>-2</sup>	-58.4
10	SO <sub>4</sub> <sup>-2</sup> , Cl <sup>-</sup> , PO <sub>4</sub> <sup>-3</sup>	-58.0
11	SO <sub>4</sub> <sup>-2</sup> , Total Alk., DOC	-57.2
12	PO <sub>4</sub> <sup>-3</sup> , Travel Time, pH	-55.1
13	SO <sub>4</sub> <sup>-2</sup> , Total Alk., NO <sub>3</sub> <sup>-</sup>	-55.1
14	Depth to Water, pH, Mg <sup>+2</sup>	-54.2
15	SO <sub>4</sub> <sup>-2</sup> , Travel Time, pH	-52.6
16	Depth to Water, pH, Anion Def.	-51.8
17	SO <sub>4</sub> <sup>-2</sup> , DOC, Ca <sup>+2</sup>	-51.8
18	SO <sub>4</sub> <sup>-2</sup> , Total Alk., Na <sup>+</sup>	-51.6
19	PO <sub>4</sub> <sup>-3</sup> , Mg <sup>+2</sup> , Cl <sup>-</sup>	-49.9
20	pH, Sampling Depth, Total Alk.	-49.1
21	pH, Sampling Depth, Anion Def.	-48.4
22	PO <sub>4</sub> <sup>-3</sup> , NO <sub>3</sub> <sup>-</sup> , Mg <sup>+2</sup>	-47.1
23	Depth to Water, pH, lnK <sub>sat</sub>	-44.6
24	SO <sub>4</sub> <sup>-2</sup> , NO <sub>3</sub> <sup>-</sup> , Temp	-43.4
25	PO <sub>4</sub> <sup>-3</sup> , Mg <sup>+2</sup> , Total Alk.	-42.3
26	PO <sub>4</sub> <sup>-3</sup> , Mg <sup>+2</sup> , Ca <sup>+2</sup>	-42.1
27	PO <sub>4</sub> <sup>-3</sup> , Mg <sup>+2</sup> , DOC	-41.8
28	SO <sub>4</sub> <sup>-2</sup> , lnK <sub>sat</sub> , DOC	-41.5
29	pH, Sampling Depth, lnK <sub>sat</sub>	-41.3
30	SO <sub>4</sub> <sup>-2</sup> , Total Alk., Dist	-40.9
31	PO <sub>4</sub> <sup>-3</sup> , NO <sub>3</sub> <sup>-</sup> , Ca <sup>+2</sup>	-39.0
32	Mg <sup>+2</sup> , Na <sup>+</sup> , K <sup>+</sup>	-38.0
33	PO <sub>4</sub> <sup>-3</sup> , Travel Time, Ca <sup>+2</sup>	-37.5
34	PO <sub>4</sub> <sup>-3</sup> , NO <sub>3</sub> <sup>-</sup> , Temp	-37.4
35	Travel Time, K <sup>+</sup> , Na <sup>+</sup>	-37.3
36	Ca <sup>+2</sup> , Total Alk., PO <sub>4</sub> <sup>-3</sup>	-34.8
37	Mg <sup>+2</sup> , Na <sup>+</sup> , DOC	-32.9
38	lnK <sub>sat</sub> , K <sup>+</sup> , NO <sub>3</sub> <sup>-</sup>	-32.7
39	Mg <sup>+2</sup> , Total Alk., DOC	-32.2
40	Ca <sup>+2</sup> , Travel Time, Cl <sup>-</sup>	-31.8
41	Mg <sup>+2</sup> , Ca <sup>+2</sup> , lnK <sub>sat</sub>	-30.8
42	Ca <sup>+2</sup> , Total Alk., lnK <sub>sat</sub>	-29.1
43	Travel Time, K <sup>+</sup> , lnK <sub>sat</sub>	-28.9
44	Ca <sup>+2</sup> , Total Alk., Anion Def.	-27.0
45	Ca <sup>+2</sup> , Total Alk., Travel Time	-24.4
46	Mg <sup>+2</sup> , Total Alk., lnK <sub>sat</sub>	-24.2
47	Ca <sup>+2</sup> , Travel Time, lnK <sub>sat</sub>	-19.4
48	Travel Time, Total Alk., lnK <sub>sat</sub>	-13.8

### Appendix A.5 Initial list of November DIC models

**Table A.5** - An initial list of DIC models for November, before the stepwise regression was re-done to include a spatial autocorrelation structure. Models are ranked based on the associated AIC values. Adjusted  $r^2$  are given since the models include three terms.

November DIC Models								
(WITHOUT a spatial autocorrelation structure)								
Rank	Variables	lm AIC	$r^2a$	Need Spatial Corr. Structure ?	Orig. model	Best gls AIC with Spatial Corr. Structure	Spatial Corr. Type	
1	pH, Anion Def., Total Alk.	-80.4	0.85	?	-68.1	-68.3	Gaus	
2	pH, Anion Def., Ca <sup>+2</sup>	-75.5	0.82	yes	-64.3	-69.1	Ratio	
3	pH, Temp., Anion Def.	-73.1	0.80	yes	-55.9	-63.1	Ratio	
4	pH, Anion Def., Dist. from stream	-72.3	0.80	yes	-51.3	-61.5	Gaus	
5	pH, Anion Def., Mg <sup>+2</sup>	-71.9	0.79	yes	-63.8	-70.0	Gaus	
6	pH, Temp., Dist. from stream	-68.9	0.77					
7	Depth to Water, Temp., Dist. from stream	-68.1	0.76					
8	NO <sub>3</sub> <sup>-</sup> , Na <sup>+</sup> , K <sup>+</sup>	-50.8	0.53					
9	NO <sub>3</sub> <sup>-</sup> , K <sup>+</sup> , Travel Time	-49.1	0.50					
10	Anion Def., PO <sub>4</sub> <sup>-3</sup> , Travel Time	-47.5	0.47					
11	NO <sub>3</sub> <sup>-</sup> , K <sup>+</sup> , Cl <sup>-</sup>	-47.5	0.47	We did not investigate whether these models needed a spatial autocorrelation structure, because of the clear need for a spatial autocorrelation structure amongst the top models				
12	NO <sub>3</sub> <sup>-</sup> , Ca <sup>+2</sup> , Dist. from stream	-46.8	0.45					
13	NO <sub>3</sub> <sup>-</sup> , PO <sub>4</sub> <sup>-3</sup> , Na <sup>+</sup>	-46.8	0.45					
14	NO <sub>3</sub> <sup>-</sup> , Total Alk., K <sup>+</sup>	-46.2	0.44					
15	NO <sub>3</sub> <sup>-</sup> , Ca <sup>+2</sup> , K <sup>+</sup>	-46.1	0.44					
16	NO <sub>3</sub> <sup>-</sup> , PO <sub>4</sub> <sup>-3</sup> , Cl <sup>-</sup>	-45.4	0.42					
17	NO <sub>3</sub> <sup>-</sup> , Na <sup>+</sup> , Dist. from stream	-44.4	0.40					
18	NO <sub>3</sub> <sup>-</sup> , PO <sub>4</sub> <sup>-3</sup> , Travel Time	-43.9	0.39					
19	NO <sub>3</sub> <sup>-</sup> , Total Alk., Dist. from stream	-42.2	0.35					

### **Appendix A.6 Final list of November DIC models**

**Table A.6** - A full list of DIC models for September, with the Gaussian spatial autocorrelation structure. Models are ranked based on the associated AIC values.  $r^2$  cannot be computed for general linear models fit with the 'nlme' package in R.

<b>November DIC Models</b>		
(with Gaussian spatial autocorrelation structure)		
<i>Rank</i>	<i>Variables</i>	<i>gls AIC</i>
1	$\text{SO}_4^{-2}$ , $\text{Mg}^{+2}$ , $\text{Cl}^-$	-74.8
2	pH, Anion Def., Total Alk.	-68.3
3	$\text{SO}_4^{-2}$ , $\text{Mg}^{+2}$ , Temp.	-64.8
4	pH, Anion Def., Dist. from stream	-61.5
5	pH, Temp., Anion Def.	-56.3
6	$\text{K}^+$ , $\text{Cl}^-$ , $\ln K_{\text{sat}}$	-55.2
7	pH, Temp., $\text{Mg}^{+2}$	-53.7
8	$\text{K}^+$ , $\text{Cl}^-$ , Travel Time	-53.6
9	$\text{K}^+$ , $\text{Cl}^-$ , Depth to Water	-49.8
10	$\text{K}^+$ , Travel Time, DOC	-49.5
11	$\text{K}^+$ , $\text{Cl}^-$ , Sampling Depth	-49.1
12	Total Alk., Dist. from stream, $\text{SO}_4^{-2}$	-47.8
13	Total Alk., Dist. from stream, Temp.	-44.9
14	$\text{K}^+$ , Travel Time, Temp.	-44.6
15	pH, Temp., Dist. from stream	-42.6
16	$\text{Ca}^{+2}$ , Dist. from stream, Travel Time	-26.6

## Appendix B Detailed field methods

### Day 1

- Calibrate the pH meter
- Measure pH and temperature in all of the wells (for quality control purposes). If water level is too low, use the graduated cylinder
- Measure and record depth to water in all of the wells, using the metric tape measurer, the wet erase marker, and the rag.
- Purge ~ 700 mL (at least 5 syringe-fulls) from each of the wells, using the DI-rinsed 140 mL syringes, and the DI-rinsed purge tubing, as well as one stopcock per syringe.
- Make a note in your field notebook if any wells are dry or could not be fully purged.
- That night, label all of the bottles and syringes and attach stopcocks to the syringes. Make sure to include field duplicates (1 per 10 wells). Prepare tables in field notebook.
- Put the ice packs in the freezer to cool overnight.

### Day 2

- Prepare two coolers with icepacks
- Pack up your sample equipment, separating bottles and syringes into transects.
- Calibrate the pH meter
- Keep the bottle and syringe for the hillslope well separate, and include the graduated cylinder, for measuring pH and T in the hillslope well.
- For each well:
  - Using tweezers put one clean GFF filter into the filter apparatus. GRIDDED SIDE DOWN.
  - Uncap the well and insert the sample tubing – attach one stopcock to the tubing.
  - Attach the syringe and its stopcock to the tubing stopcock, so that there are two stopcocks stacked on each other.
  - Pull water up using the syringe, and rinse the 60 mL syringe 3 times, or until the water is fairly clear, purging the water out the side of one of the stopcocks.
  - Pull 60 mL of fresh water and LOCK the sample tubing by turning the bottom stopcock.
  - Separate the syringe and its stopcock from the bottom stopcock. Attach the syringe and its stopcock to the filter apparatus. Use the 60 mL of water to flush the filter and the 250 mL bottle, dispensing it in 3 aliquots. Make sure that the bottle and lid are thoroughly rinsed, including the threads.
  - Re-attach the syringe and stopcock to the sample tubing, and use ~ 5-syringe fulls to fill the 250 mL bottle until an inverted meniscus is formed, FILTERING the water through the filter apparatus. Pull water at a steady pace, not rapidly, so that air bubbles do not enter the sample tubing. Each time, be sure to lock the sample tubing before separating the syringe and attaching it to the filter apparatus. If the

filter becomes clogged, change the filter and flush it with a bit of sample water before proceeding. Once you have 250mL, cap the bottle immediately.

- Once the bottle is filled, re-attach the syringe and fill it one last time, making sure that there are as few bubbles as possible in the syringe. This time LOCK the TOP stopcock, so that the syringe itself is locked. This prevents atmospheric exposure. Place the locked syringe in a Ziploc bag.
  - Record the time of sampling in the field notebook.
  - Put the syringe into one of the sample coolers (for syringes only)
  - Put the bottle into the other sample cooler (for bottles only)
  - Remove the sample tubing and replace the cap on the well
- Once you have sampled a well, place the pH meter in it, and record pH and temperature.
  - Then place the dO meter in the well, and record dO.
  - Note anything unusual in the field notebook
  - Transport all samples back to the lab in a cooler, being gentle with the syringes. Keep the samples cold until analysis.

## Appendix C Detailed laboratory methods

### *Appendix C.1 Detailed methods for DIC analysis*

*Note:* Perform DIC analysis on a Shimadzu TOC-VSCH Combustion Carbon Analyzer within 72 hours according to CCAL operating procedure 21A.0. In summer 2013, Kathy Motter and Hayley Corson-Rikert decided to modify the procedure slightly in order to account for higher concentrations of DIC in hyporheic water by using ten standards ranging in concentration from 0 to 20 ppm and including both 1 and 10 ppm check standards (method detection limit: 0.05 mgC/L).

1. Turn on the Shimadzu TOC-VSCH Combustion Carbon Analyzer according to the instructions given in the TOC Analysis Quick Guide, located below the computer monitor in the IWW Collaboratory. When you turn on the gas, open it all the way and then back it off a bit.
2. Before opening the sample table editor, open the software control panel and make sure that the furnace is off. If necessary, you can open the lid above the furnace on the analyzer so that it cools more rapidly
3. Check system run conditions per the guide (e.g. rinse water, humidifier level, drain pot level, etc.). Use NANOPURE water in all cases.
4. Make sure that there is enough reagent for the analysis (phosphoric acid) and enough room in the waste container.
5. Lay all filled 60 mL syringes out in the alphanumerical order (i.e. C2, C3, C6 ..... H6, S1, UHH2/3, etc.) that will be used to design the sample template for analysis.
6. Write out a list of samples and standards according to the sample template on the computer. Begin the run with a rinse and then the standards (0, 0.2, 0.5, 1, 2, 5, 7.5, 10, 15, 20), inserting a high and low check standard and a blank after the 5 mg/L standard. Make sure to insert a high and low check standard and blank every 10 samples. For example, after the first high and low check standard and blank, you have the remaining 4 standards and then your first 6 samples, then another high check, low check, and blank, then 10 samples, then high check, low check, and blank, etc. Be sure to end your run with a high check standard, a low check standard, and a blank, even if they follow fewer than 10 samples.
7. Enter your list into the excel sample template on the computer.
8. Count the total number of standards and samples and write down your name, the date, the analysis type, and this total in the provided logbook.
9. Using gloves, place the appropriate number of clean, acid washed carbon vials into the plastic racks, then label the vials with a Sharpie according to the sample template list.

10. Return to the machine and follow the instructions for warming up the machine using the ic-startup file.
11. Once the machine is warming up, get out the 0.45 µm filters for the syringes and the acid-washed vial caps.
12. Wearing gloves, fill the rinse vial and the blank vials with DI water until an inverted meniscus is formed, and then cap them.
13. Open the bag of filters and lay it on the counter so that you can squeeze out clean filters without reaching your hand (even when gloved) into the bag.
14. Filter your syringe samples into the appropriate vials. Make sure you are wearing gloves. For each sample, shake the syringe thoroughly and then remove the stopcock and screw on a clean filter. Rinse the filter by pressing ~10 mL of the sample through the filter into the sink. Then, filter the sample at an angle into the appropriate vial. Use one hand to support the vial at an angle AND support both the syringe and the filter, so that neither cracks from the pressure. Use the heel of your palm of your other hand to press the syringe and push the sample water through the syringe. Make sure that the filtered water runs down the inner side of the vial, so that atmospheric exposure is minimized. Work quickly, but do not rush. As soon as an inverted meniscus is formed, cap the vial with a clean vial cap. Place the vial back in the plastic rack in the correct spot. Unscrew the filter from the syringe and throw it away. Screw the stopcock back on the syringe. Repeat with next sample until all are filtered.
15. Retrieve the fresh DIC standards from Kathy and fill all of the standard vials with the appropriate standards/check standards, filling each until an inverted meniscus is formed and capping each immediately. Invert the standards to mix them before pouring.
16. Prepare the sample run template as outlined in the machine guide. Be sure to follow the instructions for DIC analysis, not the ones for DOC analysis.
17. Check the results of the start-up run and make sure the peaks look good and are consistent. Make sure that the system run conditions are met.
18. Load filled vials into the autosampler rack. Make sure that the tops of all the vials are level. Place the filled rack in the machine, and replace the rack cover.
19. Start sample analysis according to directions on sheet.
20. The next day, when the run is complete, remove the vials from the autosampler, and set them aside to be acid washed. Shut down the machine and turn off the gas.
21. Review data through software, checking to see if peaks were good and consistent.
22. Export data and analyze in DIC template. Make sure check standards came out well.

### ***Appendix C.2 Detailed methods for DOC analysis***

**Note:** Perform DOC analysis on a Shimadzu TOC-VSCH Combustion Carbon Analyzer within 2 weeks (or ideally as soon as possible) according to CCAL operating procedure 20A.2 (method detection limit: 0.05 mgC/L).

1. Turn on the Shimadzu TOC-VSCH Combustion Carbon Analyzer according to the instructions given in the TOC Analysis Quick Guide, located below the computer monitor in the IWW Collaboratory. When you turn on the gas, open it all the way and then back off a bit.
2. Before opening the sample table editor, open the software control panel and make sure that the furnace is ON (680 °C). Allow it to warm up for 30 minutes before beginning the start-up.
3. Check system run conditions per the guide (e.g. rinse water, humidifier level, drain pot level, etc.). Use NANOPURE water in all cases.
4. Make sure that there is enough reagent for the analysis (2N HCL) and enough room in the waste container.
5. Arrange all the 250 mL sample bottles in the alphanumerical order (i.e. C2, C3, C6 ..... H6, S1, UHH2/3, etc.) that will be used to design the sample template for analysis.
6. Write out a list of samples and standards according to the sample template on the computer. Begin the run with a rinse and then the standards (0, 0.2, 0.5, 1, 2, 5), inserting a check standard and a blank after the 5 mg/L standard. As you build your list, make sure to insert a check standard and blank every 10 samples. For example, after the first check standard and blank, you have your first 10 samples, then another check and blank, then 10 samples, then a check and blank, etc. Be sure to end your run with a check standard and a blank, even if they follow fewer than 10 samples. Don't forget to include 3 lab duplicates in addition to the field duplicates.
7. Enter your list into the excel sample template on the computer.
8. Count the total number of standards and samples and write down your name, the date, the analysis type, and this total in the provided logbook.
9. Using gloves, set out the appropriate number of clean, acid washed and ASHED carbon vials into the plastic racks, then label the vials with a Sharpie according to the sample template list.
10. Return to the machine and follow the instructions for warming up the machine using the test.t32 startup file.
11. Make sure you are wearing gloves. Retrieve the DOC standards from the fridge and fill the standard and check standard vials with approximately 25 mL of the appropriate standards (~ half-way full). Use NANOPURE water for the rinse, the 0 standard, and all of the blanks. Cap the vials with acid-washed vial caps.

12. For each sample, shake the 250 mL bottle, uncap it, and fill the appropriate vial with ~ 25 mL of the sample water. Cap the vials with acid-washed vial caps.
13. Prepare the sample run template as outlined in the machine guide. Be sure to follow the instructions for DOC analysis, not the ones for DIC analysis (e.g. use “kat cal 0706.2006”)
14. Check the results of the start-up run and make sure the peaks look good and are consistent. Make sure the system run conditions are met.
15. Load filled vials into the autosampler rack. Make sure that the tops of all vials are level. Place the filled rack in the machine, and replace the rack cover.
16. Start sample analysis according to directions on sheet.
17. The next day, when the run is complete, remove the vials from the autosampler, and set them aside to be acid washed. Shut down the machine and turn off the gas.
18. Review data through software, checking to see if peaks were good and consistent and if the machine excluded the correct peaks. Check to makes sure lab duplicates were good.
19. Export the data and analyze it in the DOC template. Make sure check standards came out well and that no dilutions are necessary. Don’t forget to adjust for the background carbon in the standards by adding back in the intercept for all SAMPLES.

### ***Appendix C.3 Detailed methods for anion analysis***

**Note:** Concentrations of major anions NO<sub>3</sub>, SO<sub>4</sub>, Cl, and PO<sub>4</sub> are determined on a Dionex 1500 Ion Chromatograph according to CCAL procedure 50B.1 (Method detection limit 0.01 mg/L). Results (mg/L) are in terms of the whole compound, not the element (NO<sub>3</sub>, not N)

1. Follow the IC Analysis Quick Guide provided in the IWW Collaboratory to start up the machine, prepare the eluent, and prime the system.
2. Follow the instructions to stabilize the system. It will take up to a few hours to stabilize, depending on how recently it has been run.
3. Retrieve the 250 mL samples from the cold room and set them out in the alphanumerical order (i.e. C2, C3, C6 ..... H6, S1, UHH2/3, etc.) that will be used to design the sample template for analysis.
4. Write out a list of samples and standards according to the sample template on the computer. Begin the run with a rinse and then the standards (0, 0.2, 1, 2, 5), inserting a check standard and a blank after the 5 mg/L standard. As you build your list, make sure to insert a check standard and blank every 10 samples. For example, after the

first check standard and blank, you have your first 10 samples, then another check standard and blank, then 10 samples, then a check standard and blank, etc. Be sure to end your run with a check standard and a blank, even if they follow fewer than 10 samples. Do not forget to include 3 LAB duplicates in addition to the field duplicates.

5. Enter your list into the excel sample template on the computer. Count the total number of standards and samples and write down your name, the date, the analysis type, and this total in the provided logbook.
6. Using gloves, insert the appropriate number of clean poly vials into the autosampler plastic racks, then label the vials with a Sharpie according to the sample template list. Make sure you are labeling in the correct direction (see numbers on top of rack).
7. Retrieve the anion standards from the fridge, and fill the appropriate vials with the standards to the level indicated on the plastic racks. Use DI water for the rinse and all blanks. Cap the vials with the filter caps, using the provided tools. Put the standards back in the fridge.
8. For each sample, shake the 250 mL bottle, uncap it, and pour the sample into the appropriate poly vial until the water reaches the correct level. Cap the poly vials with the filter caps as you go. Don't forget to pour the lab duplicates when you pour the corresponding sample. Once all vials are filled and capped, make sure all the caps are level with the top of the racks.
9. Prepare the sample run template according to the directions in the guide.
10. Once the system is stabilized, load the racks into the autosampler and press run. Start the analysis according to the guide directions
11. The next day, shut down the instrument according to the guide instructions. Turn off the gas. Throw away your used vials and filter caps.
12. Analyze the data from your run in the Chromeleon software, checking to make sure the peaks are correctly defined and that there is a clean baseline curve. Export the data to an Excel spreadsheet. Make sure check standards and lab duplicates came out well.

#### ***Appendix C.4 Detailed methods for cation analysis***

**Note:** Concentrations of major cations K, Na, Mg, and Ca are determined on a Perkin-Elmer Atomic Absorption Spectrometer, a Perkin-Elmer AAnalyst-100, according to CCAL procedure 60B.1 (Method detection limits: K - 0.03 mg L<sup>-1</sup>, Na - 0.01 mg L<sup>-1</sup>, Mg - 0.02 mg L<sup>-1</sup>, Ca - 0.06 mg L<sup>-1</sup>).

1. Start up the FAAS according to the Perkin Elmer AAnalyst 100 Atomic Absorption Spectrometer User Quick Guide provided in the IWW Collaboratory. Make sure there is enough space in the waste container, and lift it off the shelf. Check the ventilation.
2. Select the lamp and load the method for the cation you want to run. If Ca, you may need to enter in the lamp current, wavelength, and slit height. See the book in the drawer to the left of the instrument. Use the business card provided in the drawer to make sure that the burner head is well-aligned. Press [Cont] and autozero [A/Z]. Allow the lamp to warm up for at least 45 minutes, longer if Ca. Autozero the lamp every 10 minutes or so.
3. Write out a list of samples and standards. Begin each run with a blank and your standards, and follow these with a check standard (check 1) and blank. As you build your list, make sure to insert a check standard and blank every 10 samples. For example, after the first check standard and blank, you have your first 10 samples, then another check (check 2) and blank, then 10 samples, then a check (check 3) and blank, 10 samples, then a check (check 1) and blank, etc. Be sure to end your run with a check standard and a blank, even if they follow fewer than 10 samples. Don't forget to include 3 lab duplicates in addition to the field duplicates.
4. Prepare your samples as follows:
  - Na/K:
    - Make sure you are wearing gloves.
    - Retrieve the bin of clean plastic mini cups from the drawer to the left of the machine and fill the plastic racks with the correct number of cups. Label the cups (or tape and label the rack) according to your list. Use a separate rack for the first blank and the standard cups.
    - Fill the cups for the blanks with DI water.
    - Retrieve the cation standards from the fridge, and fill the standard and check standard cups with the appropriate Na/K standards/check standards.
    - For each sample, shake the 250 mL bottle, uncap it, and pour a small amount into the correct cup. Don't forget the lab duplicates.
    - NOTE: these poured samples (and standards) can be used for both the Na and the K analysis.

- Mg/Ca:
  - Make sure you are wearing gloves, a lab coat, and safety glasses.
  - Retrieve the bin of clean plastic mini cups from the drawer to the left of the machine and fill the plastic racks with the correct number of cups. Label the cups (or tape and label the rack) according to your list. Do not include cups for the Ca and Mg standards.
  - Fill two large beakers with DI water. One will serve as a coarse rinse and the other as a fine rinse.
  - Using a pipette, fill the cups for the blanks with 10 mL DI water.
  - Label 8 beakers (4 Mg standards, 3 Ca standards, one blank).
  - Pipette 30 mL of DI water into the beaker for the blank.
  - Retrieve the cation standards from the fridge, and pipette 30 mL of the standards into the appropriate beakers. Be sure to rinse the pipette 3 times (1 coarse, 2 fine) between each standard.
  - Pipette 10 mL of the check standards into the appropriate check standard cups.
  - For each sample, shake the 250 mL bottle, uncap it, and pipette 10 mL into the correct cup. Don't forget the lab duplicates. Be sure to rinse the pipette 3 times (1 coarse, 2 fine) between each sample.
  - Retrieve the Lanthanum from the hood, making sure you are wearing gloves, a lab coat, and safety glasses.
  - Pipette 3 mL of Lanthanum into each of the standard beakers and the blank beaker. Pipette 1 mL of Lanthanum into each of the sample cups, check standard cups, and blank cups. (The ratio is always 1 mL Lanthanum:10 mL standard/sample/check standard).
  - Note: these acidified samples can be used for both Ca and Mg runs.
- 5. Approximately 20 minutes before you are ready to run, turn on the gas and air according to the instructions in the quick guide. To adjust the outlet gauge pressure on the gas, turn the outlet gauge knob clockwise until the correct pressure range is reached. The air outlet gauge pressure does not need to be adjusted. Make sure the gas and air flow to the machine are correct by checking the front of the machine – gas should be 2 units, oxidant 4 units. Ignite the flame, and fill a fresh beaker with DI water so that the flame aspirate DI water while it stabilizes. Press [A/Z] to autozero the machine and monitor it for drift while it warms up.
- 6. When you run the machine, make sure you wear gloves and safety glasses. If you are running Ca and Mg, also wear a lab coat.
- 7. Once the lamp and flame are warmed up and stable, switch to data collection mode by pressing [data]. Make sure that print is on. To calibrate, aspirate your blank and press autozero [A/Z]. Then immediately aspirate your first standard, count to 5, and press [0] then [calibrate]. This clears the previous calibration. Aspirate the rinse water (the big beaker of DI), then aspirate the second standard, count to 5, and press [calibrate]. Aspirate the rinse water, then aspirate the third standard, count to 5, and

press [calibrate]. If there is a fourth standard (Mg), repeat with the fourth standard. The machine will print the calibration curve. Make sure that it has a good correlation coefficient ( $>0.999$ ).

8. If your calibration is good, you can begin your run. Make sure to follow your calibration with a check standard and blank before running your samples. The readings for any set of 10 samples are only valid if the check standards and blanks on either end were good (within the detection limit if below the threshold value (TV) provided on the machine, or within 5% if above the threshold value). Essentially, all samples must be ‘bracketed’ by good check standards.

To run each check standard and sample, aspirate the check/sample, count to 5, and then press [read]. Make sure to rinse the tubing after each sample. Record your results as you go. If your check standards are not good at any point, re-calibrate, and re-run any samples that were not bracketed by good check standards. It is best to run all your samples on one calibration (which is why we let the machine warm up for so long, so that drift is minimized).

9. Once your run is complete, write the names of your check standards and samples on the print out, so that you have a second record of your data. Make sure your duplicates are good.
10. If you are running another cation, press [Param Entry] and select the next lamp you want to run, following the method entry and warm up procedure described above. Be sure to allow sufficient time for each lamp to warm up. You can leave the flame on while the next lamp warms up. Don’t forget to autozero the lamp every 10 minutes or so.
11. When you are completely done for the day, shut down the flame. To do so, follow the directions in the quick guide: Aspirate DI water to rinse the tubing, then remove the tubing from the DI water to clear it out. Press [Flame on/off] to turn off the flame. Close the air valve and turn off the gas tank. Press [Gases on/off] to bleed the gas lines. Do so until the indicator tubes on the front of the machine show no air or gas pressure (this usually means pressing [Gases on/off] 6 times or so). After the gas lines are bled, the outlet gage pressure on the gas should read zero. However, you STILL NEED to depressurize the outlet gage pressure by turning the outlet gage knob counter-clockwise until it is barely screwed in. This way, the outlet gage will not be pressurized the next time someone else turns on the gas.
12. Turn off the machine. Place the waste container back on the shelf.
13. Pour your samples and standards down the sink and rinse all your cups and beakers 4 times with DI water. Place them to dry. Return to put them away the next day.

